J. Fluid Mech. (1986), *vol.* 165, *pp.* 1–60
Printed in Great Britain

Instability and chaotic behaviour in a free-surface flow

By W. G. PRITCHARD†

Mathematics Research Center, University of Wisconsin – Madison,
610 Walnut Street, Madison, WI 53705

(Received 29 May 1985 and in revised form 23 September 1985)

This paper describes some experimental observations of free-surface flows arising when fluid is poured over the end of a flat plate into a reservoir well below the plate. This class of flows was found to be highly unstable with over seven hundred qualitatively different flows being observed in the experiment. At very small values of the flux the liquid fell from the plate into the reservoir in the form of droplets which devcloped periodically at a number of sites on the underside of the plate. As the flux was increased these 'sites' were able to sustain continuous, unbroken streams, and combinations of drip sites and continuous streams were possible. At still larger values of the flux there was a tendency for the liquid to fall in 'sheets' and several combinations of 'sheet flows' and continuous streams were observed, some of which flows exhibited a rather chaotic temporal behaviour. At even larger flux values the flow resembled that of the classic waterfall, but here there were also some unexpected instabilities where the attachment line of the free surface of the liquid with the plate developed corrugations.

1. Introduction

A description is given of experimental observations of a free-surface flow that was highly unstable, exhibiting a wide range of different motions (over seven hundred), some of which were steady, some nearly periodic in time and some of which had a less regular, almost chaotic, behaviour in time. The particular situation to be studied resembled that of a 'waterfall', where fluid flowed down the bed of a uniform channel and poured over the end of a plate into a reservoir. It was the nature of the flow in the region near the end of the plate that was of special interest here, with the falling liquid having the propensity to develop many different flow structures. Because the Reynolds numbers for these experiments were not large, ranging between 0.05 and 37, it would appear that the non-uniqueness was controlled mainly through the nonlinearities at the free surface.

Although a specification of the flow conditions depended on at least nine dimensionless-parameter groupings, only one quantity, namely the flux, was systematically varied in these experiments. At very small values of the flux the flow consisted basically of a number of sites from which droplets of liquid fell into the reservoir. As the flux was increased continuous streams became possible and at larger values of the flux the liquid had a tendency to fall in the form of sheets rather than in the

† Permanent address: Department of Mathematics, University of Essex, Colchester CO4 3SQ, UK.

form of streams. Various combinations of drops and streams or streams and sheet-flows were possible, leading to the large multiplicity referred to above. Some of the observed flow structures, such as the (2T + C) and the (2T + 2C) flows described below, had a rather complicated dependence on time. In these cases the temporal dependence was not reminiscent of a nearly periodic motion but was of a more chaotic nature, with the flow differing markedly from 'cycle' to 'cycle'.

The paper has a second purpose, concerning the position at which the free surface of the liquid attached to the plate. There have been many attempts in recent years to simulate, by numerical computation, certain free-surface flows that arise in so-called die-swell problems and in the coating of solid surfaces with liquid films. It is common in such calculations (e.g. see Nickell, Tanner & Caswell 1974, Silliman & Scriven 1978, Omodei 1980, Cuvelier 1981, Saito & Scriven 1981, Dutta & Ryan 1982) to specify *a priori* the attachment point of the free boundary to the rigid surface; usually a sharp corner of the rigid surface is chosen for the attachment point. However, Jean & Pritchard (1980) questioned the validity of this assumption and demonstrated in laboratory experiments that it does not hold in general. It is the thesis of Jean & Pritchard that, without the means of pinning the free-surface attachment at some particular place through the application of 'external' point forces, the attachment position of the free surface needs to be determined as part of the overall solution of the flow problem. Thus, assuming the free surface attaches to the solid at a sufficiently smooth part of the boundary, both Jean (1980) and Solonnikov (1980) were able to demonstrate the existence of a unique solution, in two dimensions, to a mathematical problem representing a certain class of flows of the above kind. An important feature of these theories is that there should be a surface tension acting at the free boundary of the liquid phase for, in the absence of surface tension, the basic estimates deriving from the theory for elliptic equations were not strong enough to allow an existence theory to be established.

On the other hand, numerical calculations made in the absence of surface tension (e.g. see Nickell *et al.* 1974) suggest there is in fact a 'smooth' solution to the associated continuous problem when no surface tension acts at the free boundary. Thus, there remains an important gap in the mathematical theory, especially with regard to the regularity that can be expected at the free surface of these viscosity-dominated flows.

In the present paper empirical evidence will be given to support the hypothesis that the location at which a free surface contacts a rigid boundary is, in general, determined by the overall flow conditions. In particular, examples will be given showing that, for given flow parameters, more than one stable, steady flow was possible, and that these flows were distinguishable by the locations of the attachment points of the free boundaries to the rigid surfaces. The attachment points were not, in general, seen to coincide with a corner of the rigid boundary. So, it would appear that usually it is the attachment point which adjusts to reflect the global conditions rather than the downstream conditions adjusting in response to a preferred location of the contact point.

Since first preparing this manuscript it has been drawn to my attention that S. Kistler and L. E. Scriven of the University of Minnesota have made a study (see Kistler 1983) relating to the attachment location of the free surface in certain 'film-delivery' flows.

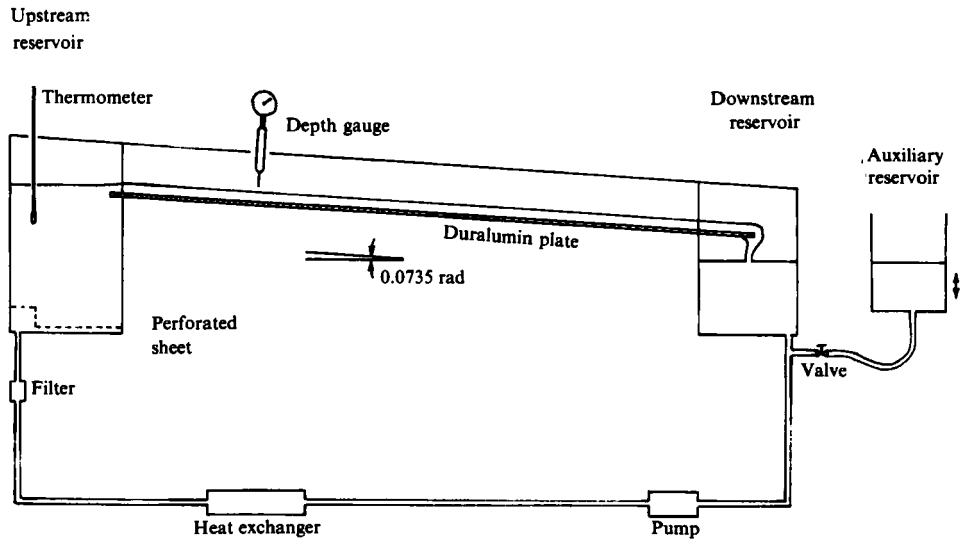

FIGURE 1. Schematic layout of the apparatus.

2. Experimental apparatus

A schematic layout of the apparatus is given in figure 1. The central part of the apparatus was an open channel of uniform section, of width 127 mm and depth 74.5 mm, sloping at an angle 0.0735 rad to the horizontal; it was 1.20 m long. The bed of the channel was made from sheet duralumin plate, of thickness 6.4 mm, resting on an aluminium C-section (not indicated in the diagram). At the upstream end of the channel was an inlet reservoir from which the liquid (an oil) poured into the channel, and at the downstream end was a receiving reservoir. The sidewalls of the channel and of the reservoirs were 10 mm-thick sheet acrylic (Perspex).

The return from the reservoir downstream to the one upstream was basically a 25 mm-bore pipe. A T-joint into this pipe, just below the exit from the downstream reservoir, led through a stopcock to an auxiliary reservoir. This reservoir was seated on a platform that could easily be raised or lowered, conveniently allowing liquid either to be added to or taken from that which was circulating round the main system. The flow was forced by a centrifugal pump, located as shown in the sketch. The pump was driven by a (commercially produced) d.c. motor-tachogenerator with a feedback speed-control system, the speed of the motor nominally being controlled to within 1 part in 10^4. After leaving the pump the oil passed through a heat exchanger and a filter before returning to the upstream tank. The heat-exchange unit consisted of an array of copper tubes through which the oil passed and around which cool water flowed. By carefully adjusting the flow rate of the water past the array of tubes a nicely controlled, stable operating temperature could be achieved for the circulating oil. A perforated plate, which was located just above the inlet to the upstream reservoir, helped even out the flow in the reservoir.

A mercury bulb thermometer was located in the upstream reservoir, as shown in figure 1. The oil temperature, which was noted at frequent intervals, was measured to within an uncertainty of approximately ± 0.01 K. The temperature of the laboratory was maintained at (21 ± 0.5) °C and the oil temperature was usually stabilized at about 21 °C.

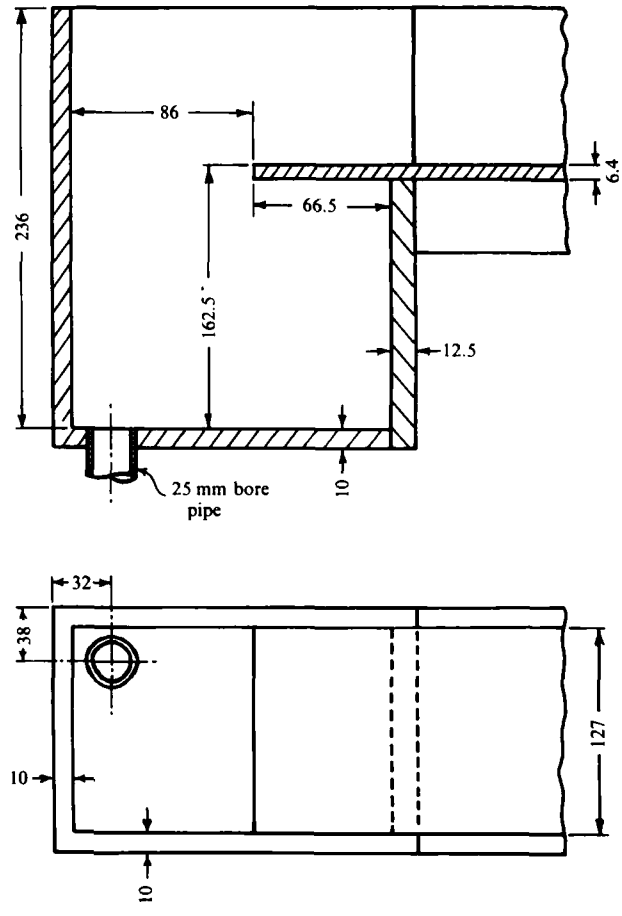

FIGURE 2. The downstream reservoir. The numbers indicate dimensions in mm.

The main unit rested on feet located under each of the reservoirs. Adjustment screws in the feet were carefully set to ensure that the bed of the channel was nearly horizontal in a direction normal to the main axis of the channel (i.e. in a direction normal to the sidewalls). In particular, at the end of the plate that protruded into the downstream reservoir, the bed was horizontal in the cross-channel direction to within 0.02 mm. The slope of the bed in the long-channel direction was determined by direct measurement relative to the surface of a stationary liquid in the channel.

More complete details of many of the experimental techniques are to be reported in a forthcoming paper concerning free-surface flows of liquids in channels at small Reynolds numbers, for which purpose the present apparatus was originally constructed.

2.1. *The downstream reservoir*

The experiment centred around the free-surface patterns observed in the downstream reservoir, the details of which are given in figure 2. The reservoir was basically a Perspex box of rectangular cross-section into which protruded the duralumin plate used to form the bed of the main channel. The end of the plate was carefully milled to be square to its upper and lower surface, and edges. The plate formed an 'airtight' fit with the walls of the reservoir.

2.2. *The working liquid*

The liquid employed in these experiments was a commercial vegetable oil used in the catering industry. This oil was a blended mixture of a variety of vegetable oils, but is believed to have been derived predominantly from oilseed rape. One minor inconvenience of this oil was that its mechanical properties, in particular its shear viscosity, showed small changes with use. This kind of oil has been used for about five years in our laboratory and over this period it has been found that, in normal use, the shear viscosity of the oil increased by roughly 0.04 % per day. Thus, regular monitoring of the viscosity of the oil was needed. This was usually done once a week during periods of experimentation. Some tests also were made to ascertain whether or not the oil showed significant non-Newtonian properties by estimating its primary normal-stress difference for a viscometric flow. These tests were carried out in the laboratory of Professor A. S. Lodge at the University of Wisconsin by Mr H. Vo. The liquid indicated negligible normal-stress effects, even at shear rates several orders of magnitude in excess of those arising in the present experiments. Also, over the same range, the shear viscosity was found to be independent of the shear rate.

Near the usual operating temperatures for the present experiments the (shear) viscosity of the oil was found to change by approximately 3.7 % per degree kelvin, the viscosity decreasing with increasing temperature. Therefore, not only was it important to monitor carefully the temporal properties of the oil, but it was also necessary to determine the operating temperature for each experiment.

The viscosity of the oil was monitored by measuring the time for a given quantity of fluid to discharge through a capillary viscometer. This time was determined to a reproducible accuracy of better than 0.1 %, and so *relative* changes of the viscosity of the oil could be tracked very closely. The *absolute* viscosity was determined by comparison of the viscosity of the oil with that of distilled water, the value of which was taken from international standards. The kinematic viscosity of the oil at the working temperatures of the experiment was approximately 0.8 stokes (or 80×10^{-6} m^2 s^{-1}), which is roughly 80 times the kinematic viscosity of water at the same temperature. The actual viscosity for a given experiment was known to within 1 %.

The surface tension of the oil was determined in two ways. The force exerted on a thin plate whose edge had been brought down to touch the surface of the oil was measured, and this quantity was used to estimate the surface tension. (Measurements were, of course, made with plates of different lengths to allow for the anomalies at the ends of the plate. Also the contact angle of the oil with the plate surface was observed to be very small, if not zero.) The second method consisted of determining the force acting on a circular ring of wire drawn out through the liquid surface.

From these two kinds of measurements the surface tension of the oil (determined at a temperature of 21 °C) was estimated to be 33.0 ± 1.0 dyn cm^{-1}.

The density of the oil was measured using a relative density bottle and was estimated to be 0.922 g cm^{-3} at a temperature of 21 °C.

2.3. *Specification of the flux*

The basic physical quantity being varied in this experiment was the volume flux through the system. A convenient way of monitoring this quantity is to measure the depth of the liquid flowing down the channel.

Consider a viscous fluid flowing, under the action of gravity, down a plane surface inclined at an angle α to the horizontal. Suppose that the thickness of the sheet of

liquid is h and that y measures the normal distance above the plane. Then the Poiseuille velocity distribution $u(y)$ for steady flow down the plane is

$$u = \frac{gh^2 \sin\alpha}{2\nu}\left[2\left(\frac{y}{h}\right)-\left(\frac{y}{h}\right)^2\right], \tag{2.1}$$

where ν is the kinematic viscosity of the fluid and g is the gravity constant. Corresponding to this flow, the volume flux, Q, per unit width is

$$Q = \frac{gh^3 \sin\alpha}{3\nu}, \tag{2.2}$$

and the velocity at the free surface is equal to $(1.5Q/h)$. Thus, the liquid depth in the uniform channel provides a convenient means of specifying the basic flow parameters for the present experiment. That the above distribution (2.1) did indeed give a good description of the flow in the channel was checked by direct measurements of the surface speed which agreed over a range of operating conditions, to within 1.5 % of that predicted from (2.1) using the empirically determined values of h, α and ν.

Measurements of the depth h were made near the central plane about midway along the channel using a pointer gauge. (Except for small regions near the walls and near the entrance and exit of the channel, the depth was found to be very nearly uniform throughout.) This gauge consisted of a fine sewing needle mounted in the end of a piece of 1.2 mm-diameter brass rod which could be raised and lowered in a direction normal to the plane of the channel bed. A dial gauge bearing on the upper end of the brass rod was used to determine the height of the needle point above the bed of the channel. The dial gauge was graduated in units of 0.01 mm and had a range of 25 mm. The position of the free surface was found by carefully lowering the needle until the point broke the surface, an event that was easily recognizable because of surface tension pulling the liquid up the shaft of the needle. The depth measurements were accurate and reproducible to within approximately ± 0.01 mm. Thus, for a depth of 1 mm, corresponding roughly to the smallest flow rate used here, the accuracy of the determination of h corresponds to a 3 % error in the specification of Q (cf. (2.2)). The temperature of the oil was determined to within approximately ± 0.02 °C, corresponding to an uncertainty of ± 0.2 % in the nominal value of ν.

It will be important later to have some idea of how nearly constant Q remained throughout any given experiment. As indicated above, the speed of the pump used to drive the flow was controlled by a feedback system which, on the basis of previous experience in the laboratory, should have provided a very tight control on the flux. Also, to check that the depth measurements did, indeed, give an accurate representation of the flux, some direct measurements were made of surface speeds in the channel. These measurements showed less than ± 0.5 % variation in surface speed at each of a number of pump settings, suggesting that the flux was, in fact, held very nearly constant. On the other hand, depth measurements made under ostensibly steady flow conditions showed occasional deviations of up to 0.02 mm. Measured depth variations of this magnitude were significant and correspond, in a depth of say 3 mm, to a 2 % change in Q. I do not know how such variations came about as small effects of this kind could arise from many possible sources: for example, the sensitivity of the system to small effects is illustrated by the feature that a change of temperature of $\frac{1}{4}$ °C would have brought about a depth change of approximately 0.3 % (or approximately 0.01 mm in a depth of 3 mm), not even allowing for any changes in the pump characteristics; also, there is a potential long-wave instability of the free surface when the Reynolds number exceeds a critical value $R_c = \frac{5}{6}\cot\alpha$ (e.g. see Yih 1969, p. 502)

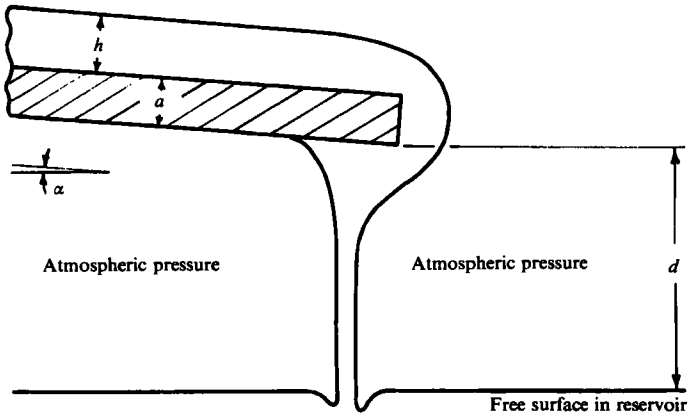

FIGURE 3. Schematic representation of flow near the end of the plate. The flow occurs in a channel of width b.

but, as many of the measurements were made at Reynolds numbers well below the value of 11.3 for R_c obtaining in the present experiment, this effect would not appear to provide the explanation for the observed depth variations.

3. A parametrization

The aim here is to provide a maximal list of parameters that are needed to specify the flow conditions. Consider a flow in a channel of width b, the bed of which slopes at angle α to the horizontal. We wish to describe the flow field in the region near the end of a plate of thickness a, which protrudes into the downstream reservoir. There the fluid pours off the plate into the reservoir, as depicted schematically in figure 3.

In some of the experiments to be reported there was an unbroken sheet of liquid spanning the reservoir, so that the possibility existed of sustaining a differential in pressure across the liquid sheet. We shall, however, avoid the complicating factor of this parameter in the present experiments by ensuring that atmospheric pressure is maintained on either side of the sheet (cf. figure 3).

Suppose that the lower corner of the end of the plate is at a height d above the free-surface level in the reservoir well away from the zone in which the liquid falls into the reservoir. That d could be defined in this manner in the present experiments means that the end walls of the reservoir were effectively at 'large distances' from the end of the plate. In all the experiments below, d was kept fixed, in the following sense. Because of the fixed volume of liquid circulating in the system d changed, in response to the changed depth of liquid flowing down the channel, whenever the flow rate was changed. Compensation for the consequent changes in d were made by adjustments from the auxiliary reservoir, a process that was easy to carry out in the present experiments. Usually d was set to within about 0.01 mm of a fixed value (by bringing the free-surface level to a mark on the wall of the reservoir) and usually changes to the flow rate were small enough that the adjustments needed to keep d at its prescribed value were less than 0.5 mm. The flow structures described below were apparently very sensitive to changes in d.

Let the depth in the channel, well upstream of the end of the plate, be h.

Then, in summary, it would appear that the parameters a, b, d, α, h suffice to fix the geometric features of the present experiment together with (i) the distances of

the end walls of the reservoir from the end of the plate, (ii) the height of the end of the plate above the floor of the reservoir and (iii) the location and size of the outlet hole in the bottom of the reservoir.

All these quantities, with the exception of h, were kept fixed in the experiments. Values for the parameters mentioned in (i), (ii) and (iii) can be obtained from figure 2, but it is believed they did not play a prominent role in the outcome of the experiments. The values for the other parameters were: $a = 6.4$ mm, $b = 127$ mm, $d = 36$ mm and $\alpha = 0.0735$. Note that, although the actual value of d was not determined very accurately, it was, nevertheless, held fixed relative to a mark on the wall of the reservoir, to much greater accuracy, as described above.

We now determine the parameters that arise from dynamical considerations. The discussions of §2 suggest that the fluid motions should be well described by the incompressible form of the Navier–Stokes equation. Suppose the flow occupies an open domain $\Omega \subset \mathbb{R}^3$ and let $\partial\Omega$ denote the boundary of Ω. Let $\partial\Omega$ be partitioned into disjoint sets Γ_D and Γ_F on which Dirichlet-type conditions and free-surface conditions are to be specified respectively. Note that Ω, and, in the present case, Γ_F may depend on time.

The lengthscale which most appropriately characterizes Ω would appear to be h, and a representative velocity scale would appear to be $U := (Q/h)$, with Q specified by (2.2). Using these scales we shall henceforth consider all variables to be in dimensionless form.

Let $\boldsymbol{u}(\boldsymbol{x})$ denote the fluid velocity at each position $\boldsymbol{x} \in \Omega$ and let $p(\boldsymbol{x})$ denote the pressure. Then the dynamical equations governing the fluid motion in Ω are

$$R\left(\frac{\partial \boldsymbol{u}}{\partial t} + (\boldsymbol{u}\cdot\nabla)\boldsymbol{u}\right) = -\nabla p + \Delta \boldsymbol{u} - G\boldsymbol{j}, \tag{3.1}$$

and

$$\nabla\cdot\boldsymbol{u} = 0, \tag{3.2}$$

where t denotes time, $\boldsymbol{j}$ is the unit vector in the vertically upwards direction, $R := Uh/\nu$ ($= Q/\nu$ here) and $G := gh^2/\nu U$ ($= 3/\sin\alpha$ here). In these definitions ν is the kinematic viscosity of the fluid and g is the gravity constant. The quantity R, the Reynolds number, characterizes the relative importance of inertial and viscous stresses, and G is the gravity parameter, typifying the relative importance of the body forces due to gravity and the viscous stress field. Note that $(R/G)^{\frac{1}{2}} = U/(gh)^{\frac{1}{2}}$ is the parameter usually referred to as the Froude number. (The gravity parameter G took the value 40.9 in the experiments, F ranged between 0.04 and 0.95 and the Reynolds number between 0.05 and 37.)

The stress tensor $\boldsymbol{\sigma}(\boldsymbol{x})$, which is scaled by $(\rho\nu U/h)$, where ρ is the fluid density, is given, in rectangular Cartesian coordinates, by

$$\sigma_{ij} := -p\delta_{ij} + (u_{j,i} + u_{i,j}). \tag{3.3}$$

The boundary conditions applying to (3.1) are as follows.

(i) $$\boldsymbol{u}(\boldsymbol{x}) = \boldsymbol{q} \quad \text{for} \quad \boldsymbol{x} \in \Gamma_D, \tag{3.4}$$

where $\boldsymbol{q}$ is some prescribed velocity field (compatible with (3.2)).

(ii) Let us suppose that the set Γ_F representing the free surface is specified implicitly by the equation

$$f(\boldsymbol{x}, t) = 0,$$

where f is a suitable smooth function constrained by the fact that points in the free surface remain there for all time. This leads to the kinematic condition on f:

$$f_t + \boldsymbol{u}\cdot\nabla f = 0 \quad \text{for} \quad \boldsymbol{x}\in\Gamma_{\mathrm{D}}. \tag{3.5}$$

Let $\boldsymbol{n}(\boldsymbol{x})$ and $\boldsymbol{t}(\boldsymbol{x})$ be mutually orthogonal unit vectors at each point $\boldsymbol{x}\in\Gamma_{\mathrm{F}}$, with $\boldsymbol{n}$ normal to the surface and directed out of Ω. Then the boundary conditions at the free surface arising from dynamical considerations are:

(a) a shear-stress condition, namely

$$\sigma_{ij}\, n_i\, t_j = 0; \tag{3.6}$$

(b) the normal-stress condition,

$$\sigma_{ij}\, n_i\, n_j = \left(\frac{T}{\rho\nu U}\right)\left(\frac{1}{r_1}+\frac{1}{r_2}\right), \tag{3.7}$$

where r_1 and r_2 are the principal radii of curvature of the surface, reckoned positive when directed into Ω, and T is the surface tension. Define $S := (T/\rho\nu U)$, which we shall refer to as the surface-tension parameter (in the experiments S ranged between 109 and 1.6);

(c) a 'contact angle' γ_1 at the attachment points of the free surface of the liquid to the plate, and an angle γ_2 at the attachment points on the sidewalls of the reservoir. In the present experiments both γ_1 and γ_2 were very small. For unsteady motions additional parameters may be needed to characterize moving contact lines, but the controlling parameters for such flows are not currently well understood.

In summary, therefore, we have that any dependent variable can be written as a function of the following dimensionless parameters:

$$\frac{a}{h},\ \frac{b}{h},\ \frac{d}{h},\ \alpha,\ R,\ G,\ S,\ \gamma_1,\ \gamma_2.$$

In the experiments described below all the geometric parameters a, b, d, α, γ_1 and γ_2 were held constant. The depth h of the approaching stream was, however, varied and so, in the above parameterization, the only parameters to remain fixed were α, γ_1, γ_2 and G. The reason h was chosen as the lengthscale was that it seemed the scale most relevant to the balances associated with R, S and G. In describing the experiments we shall therefore quote only R, S, h and ν, from which all other parameter values can be deduced, including the velocity scale, if required.

4. Experimental results

The discussion of the experimental observations will be centred around photographs showing the main features of the visible flow properties. The photographs were taken from one of two aspects. The first was an end elevation, looking upstream along the channel. For these photographs the camera was aimed slightly downwards, thus rendering visible the free surface of the oil in the reservoir (and sometimes reflections in that surface are evident in the photographs). A lengthscale can be taken approximately from the plate thickness a, but note that the plate was photographed through a curved liquid surface which acted as a lens. The significance of this effect can be seen by the apparent distortion in some photographs of the plate near the walls of the channel. Alternatively, a lengthscale is obtainable from the channel width b, though this can be difficult to discern accurately in some of the photographs. The field was illuminated from the right (for all photographs) and, in order to provide

adequate illumination to the entire field, the stream on the right-hand wall was sometimes over-exposed in the photographs. Near the top of the photographs showing the end elevation, just above the plate, is a 'horizontal' line: this is a reflection from the curved surface of the liquid pouring over the end of the plate. The blurred images in the background of these photographs are some screws (used in the construction of the reservoir) and the end of the aluminium C-section used to support the channel.

In the experiments there was a distinct stream, or rivulet, on the side walls of the reservoir, one edge of which connected with the edge of the meniscus on the wall of the channel, the other edge forming part of the meniscus line on the wall of the reservoir under the plate.

Photographs were also taken of a side elevation of the experiment, the illumination for which was the same as for the end-elevation photographs. Thus, bright regions of the photographs indicate that light rays have passed through the channel to the camera lens, whereas the dark regions indicate that rays from the source had either been reflected or refracted away from the camera at a surface of the liquid sheet. The complex structures associated with the stream running down the wall of the channel and with the flow near the reservoir walls will be evident from some of these photographs.

Before describing the different flows that have been observed in these experiments we shall first illustrate the importance for theoretical models of not specifying *a priori* the attachment point of the free surface.

4.1. *The attachment of the free surface to the plate*

In figure 4 (a, b) are shown side elevations of two flows made under essentially the same operating conditions. These are representative of two branches of flows in which a sheet of liquid spanned the width of the channel and was attached to the plate on its underside. The flows in figures 4 (a, b), at $R \approx 9.2$, can be distinguished by the distance of the attachment point from the corner of the plate. For the flow shown in figure 4 (a) this distance was approximately $1.13a$ whereas, for the flow shown in figure 4 (b), the attachment point was only about $0.32a$ from the corner.

Another example of the same kind of phenomenon is shown in figures 4 (c, d). The flow of figure 4 (c) was from the same branch of flows as the one shown in figure 4 (b), but with $R \approx 23.1$. In this case the attachment point on the underside of the plate was approximately $0.15a$ from the corner. The photograph of figure 4 (d) at $R \approx 23.3$ was, however, representative of a branch of flows in which the attachment point of the free surface was on the end face of the plate, roughly in the middle of this face.

More complete details of these flows will be given below (in particular, the end evaluation relating to figure 4 (d) reveals additional structure), but the photographs of figure 4 suffice for the present to illustrate the importance of allowing the attachment point to adjust itself according to the global flow properties.

4.2. *The overall picture*

There was such a large variety of possible flows in this experiment that a description of the overall picture is quite complex. For this reason I shall introduce special terminology, as the description unfolds, to be able to refer easily to the various flow structures.

4.2.1. *Five-site flows*

At the smallest flow rates that could be maintained in these experiments, the flow over the end of the plate settled into a form indicated by the photographs of

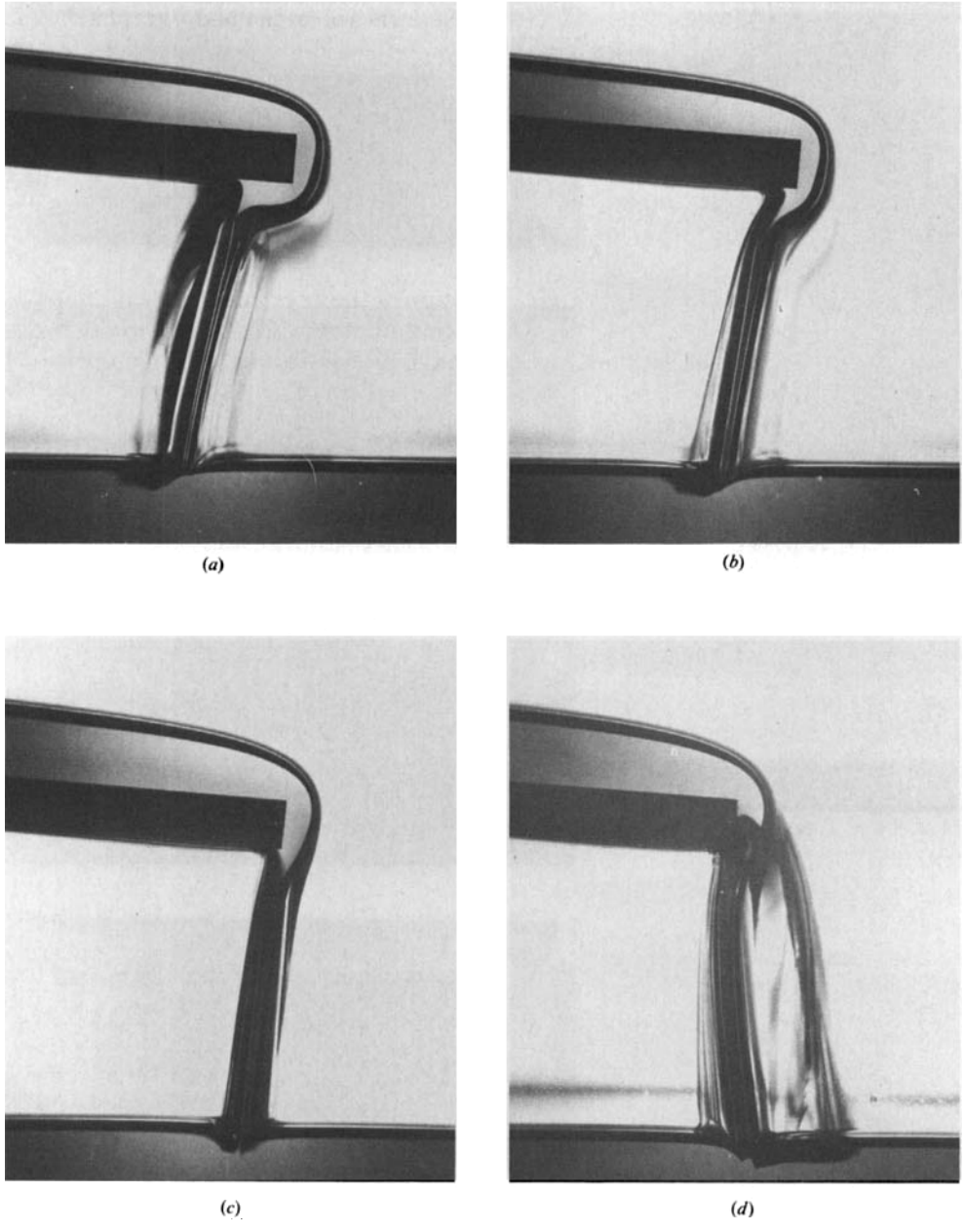

FIGURE 4. Examples of different attachment points of the free surface to the plate. (*a*) $R = 9.23$, $S = 4.15$, $h = 5.99$ mm, $\nu = 0.748$ St; (*b*) $R = 9.22$, $S = 4.20$, $h = 5.95$ mm, $\nu = 0.742$ St; (*c*) $R = 23.1$, $S = 2.29$, $h = 8.05$ mm, $\nu = 0.737$ St; (*d*) $R = 23.27$, $S = 2.29$, $h = 8.05$ mm, $\nu = 0.735$ St.

figure 5. The oil flowed round the end of the plate to the underside, where a row of droplets formed. Eventually the droplets would acquire too much liquid to remain attached to the plate and would fall into the main reservoir, at which stage a new droplet would develop at the site just vacated by the old droplet. For this particular branch of flows the droplets formed at five sites. We shall refer to such a flow as a (5D)

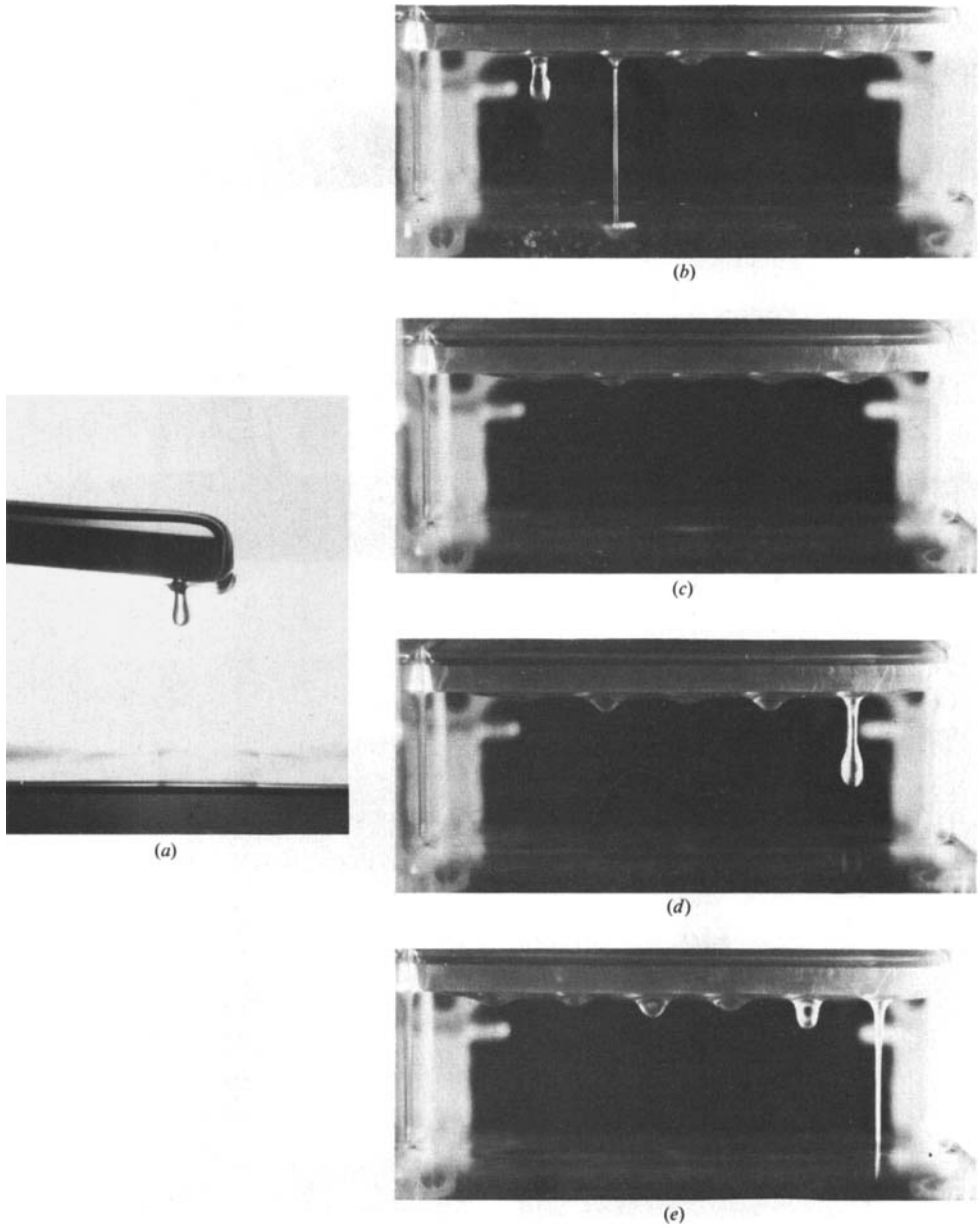

FIGURE 5. Five-site flows. (*a*) Side view: $R = 0.0583$, $S = 121$, $h = 1.11$ mm, $\nu = 0.752$ St; (*b*)–(*e*) are end views: (*b*) $R = 0.0642$, $S = 105$, $h = 1.19$ mm, $\nu = 0.795$ St; (*c*) $R = 0.0897$, $S = 84.0$, $h = 1.33$ mm, $\nu = 0.795$ St; (*d*) $R = 0.114$, $S = 71.7$, $h = 1.44$ mm, $\nu = 0.795$ St; (*e*) the (5D) flow depicted in (*a*)–(*d*) lost stability to this ((5D)C) flow at $R = 0.187$, $S = 51.4$, $h = 1.70$ mm, $\nu = 0.795$ St.

(or (DDDDD)) flow, to indicate that, at each of the 'sites' from which liquid fell from the plate, the motion consisted of the periodic formation of droplets, where the above sequence of Ds corresponds to the sites as viewed from left to right in the photographs.

The shutter speed for these photographs was usually $\frac{1}{120}$ s, during which time the droplets could fall a significant distance, accounting for their blurred outline in some

of the photographs. The side elevation in figure 5(*a*) provides another view of the structure of this branch of flows, and it can be seen that the droplets formed at a distance of roughly 0.7*a* from the lower corner of the plate. The photograph captured a droplet just at the beginning of its fall; the oil level in the reservoir can be seen near the bottom of the photograph.

The end-elevation photographs shown in figures 5(*b–d*) are representative of this branch of flows. The photograph in figure 5(*b*), for which $R \approx 0.06$, was taken at one of the smaller flow rates obtainable in the current apparatus. Although it may appear from the photograph not to be the case, this was in fact at (5D) flow: the second site (from the left) shows the residual string of liquid after the droplet had fallen: this string would have 'nipped' itself at the neck, just under the plate, shortly after the photograph was taken. A circular pattern of waves, emanating from the entry of the droplet, can be seen in the liquid surface in the reservoir. (The small air bubbles visible in the reservoir were formed by the falling droplets.) The (5D) branch of flows depicted in figures 5(*b–d*) lost stability, at a flow rate equivalent to $R \approx 0.19$, to the ((5D)C) flow shown in figure 5(*e*) – a flow consisting of 5 drip sites and one site on the extreme right-hand side that was a continuous (C) stream. (Note the visual difference between the continuous stream in figure 5(*c*) and the dripping flow at site 2 in figure 5(*b*).)

For the flows at the 'D' sites, the droplets formed at very nearly regular intervals, the period of which decreased as the flow rate increased. For example, in one sequence of experiments the formation period of the droplets was approximately 1.0 s at $R = 0.072$, decreasing to 0.81 s at $R = 0.083$, to 0.68 s at $R = 0.095$ and to 0.52 s at $R = 0.144$. (In that particular experiment the (5D) flow lost stability to a ((5D)CC) flow, i.e. a seven-site flow, at $R \approx 0.173$.) Although the droplet formation was very nearly a periodic process it was not, in fact, *exactly* periodic in time, a feature that was apparent because the phase of formation of the drops relative to one another could be seen to change gradually with time. This raises a general theoretical question of whether, in the absence of the inevitable imperfections in a laboratory experiment, the flow would have been strictly periodic in time. Certainly it was my impression from observing the motions that a strictly periodic flow was being 'spoiled' by imperfections, resulting in a motion that was just nearly-periodic in time.

The (5D) flow described above was the most stable flow observed at very small flow rates. Indeed, at the very smallest flow rates used it was the only flow observed in these experiments, though whether or not this branch of flows would have extended down to the limit of zero flow rate, or whether it formed a unique branch at small flow rates is, of course, not known. The particular flow to which the (5D) flow lost stability, as the flow rate was increased, was quite sensitive to the 'local' conditions. Thus, in three different experiments (two of which are mentioned above) the (5D) flow lost stability as follows: (i) at $R \approx 0.17$ to a ((5D)CC) flow; (ii) at $R \approx 0.18$ to a ((5D)C) flow; and (iii) at $R \approx 0.13$ to a (6D) flow. In a separate experiment a (5D) flow was established when a six-site flow lost stability at $R \approx 0.07$.

4.2.2. *Six-site flows*

At flow rates equivalent to Reynolds numbers between approximately 0.068 and 0.250, branches of motions characterized by six sites of attachment at the plate were possible. An example of one such motion was given in figure 5(*e*), where a (5D) flow lost stability to a ((5D)C) flow, the latter consisting of five drip sites and one site that was a continuous, unbroken stream. I was not able to induce the formation of such unbroken streams with five-site flows, but they could easily be sustained with the

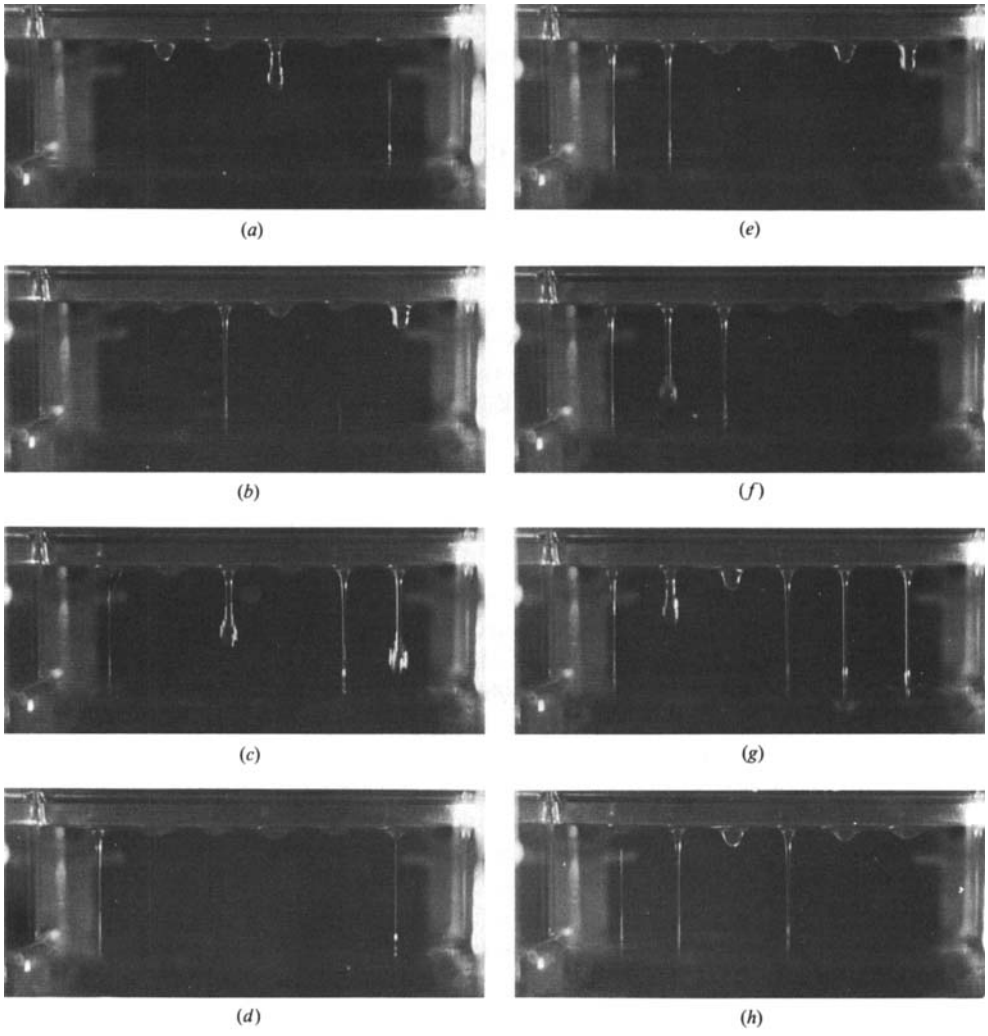

FIGURE 6. Examples of six-site flows. (*a*) (6D) flow at $R = 0.136$, $S = 65.2$, $h = 1.51$ mm, $\nu = 0.780$ St. The conditions for (*b*)–(*h*) were: $R = 0.162$, $S = 58.1$, $h = 1.60$ mm, $\nu = 0.781$ St; (*b*) (DDC(3D)) flow; (*c*) ((4D)CD) flow; (*d*) (C(5D)) flow; (*e*) (CC(4D)) flow; (*f*) (CDC(3D)) flow; (*g*) (CDDCDD) flow; (*h*) (DCDCDD) flow.

six-site flows. For example, in one experiment a (5D) flow lost stability at $R \approx 0.13$ to the (6D) flow shown in figure 6(*a*). Then at $R = 0.162$ a variety of six-site flows, typified by figures 6(*b–h*), were induced. Thus, at these operating conditions, flows comprising one unbroken stream and five drip sites could be established with the unbroken stream at any of the six sites. Examples are shown in figures 5(*b–d*), where the 'C' stream was at sites 3, 5 and 1 respectively. Similarly, flows with two unbroken streams were stable possibilities at these conditions, as shown by figures 6(*e–h*). (Note that, in figure 6(*g*), sites 5 and 6 were, in fact, drip sites.) These examples show, respectively, (CC(4D)), (CDC(3D)), (CDDCDD) and (DCDCDD) flows, but all combinations with two unbroken streams seemed to be viable states. Attempts to establish a flow under these conditions with three unbroken streams were, however, unsuccessful, leading in all cases to a loss of stability of the six-site

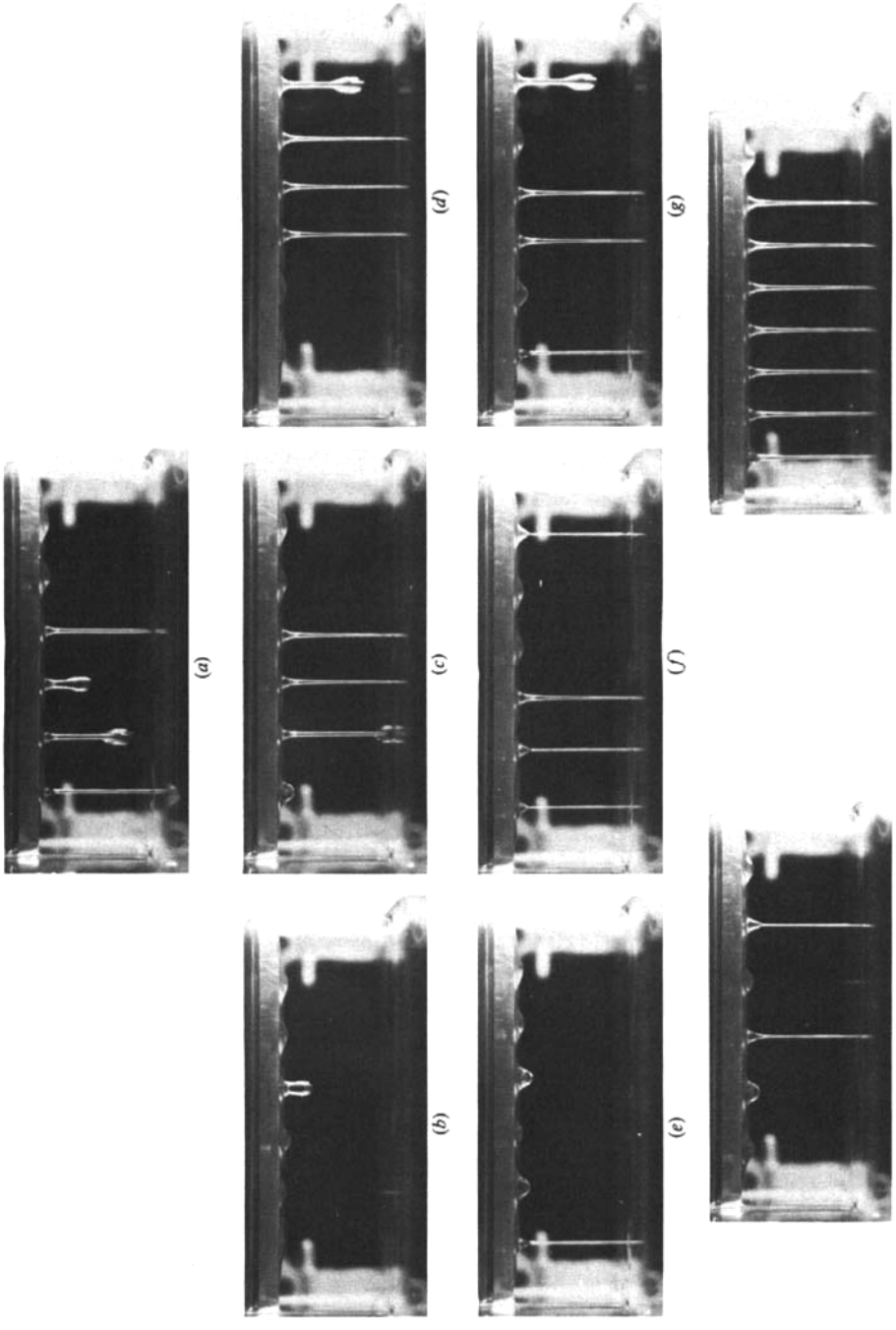

FIGURE 7. Six-site flows. (*a*) (6D) flow at $R = 0.142$, $S = 61.9$, $h = 1.55$ mm, $\nu = 0.795$ St. For (*b*), (*c*), (*d*): $R = 0.150$, $S = 59.5$, $h = 1.58$ mm, $\nu = 0.795$ St; (*b*) (6D) flow; (*c*) (DDCCDD) flow; (*d*) (DD(3C)D) flow. For (*e*), (*f*), (*g*): $R = 0.169$, $S = 55.3$, $h = 1.64$ mm, $\nu = 0.794$ St; (*e*) (6D) flow; (*f*) (DDC(3D)) flow; (*g*) (DDCCDD) flow. (*h*) (6D) flow at $R = 0.195$, $S = 50.2$, $h = 1.72$ mm, $\nu = 0.793$ St; (*i*) ((7C)D) flow at $R = 0.251$, $S = 42.5$, $h = 1.87$ mm, $\nu = 0.792$ St.

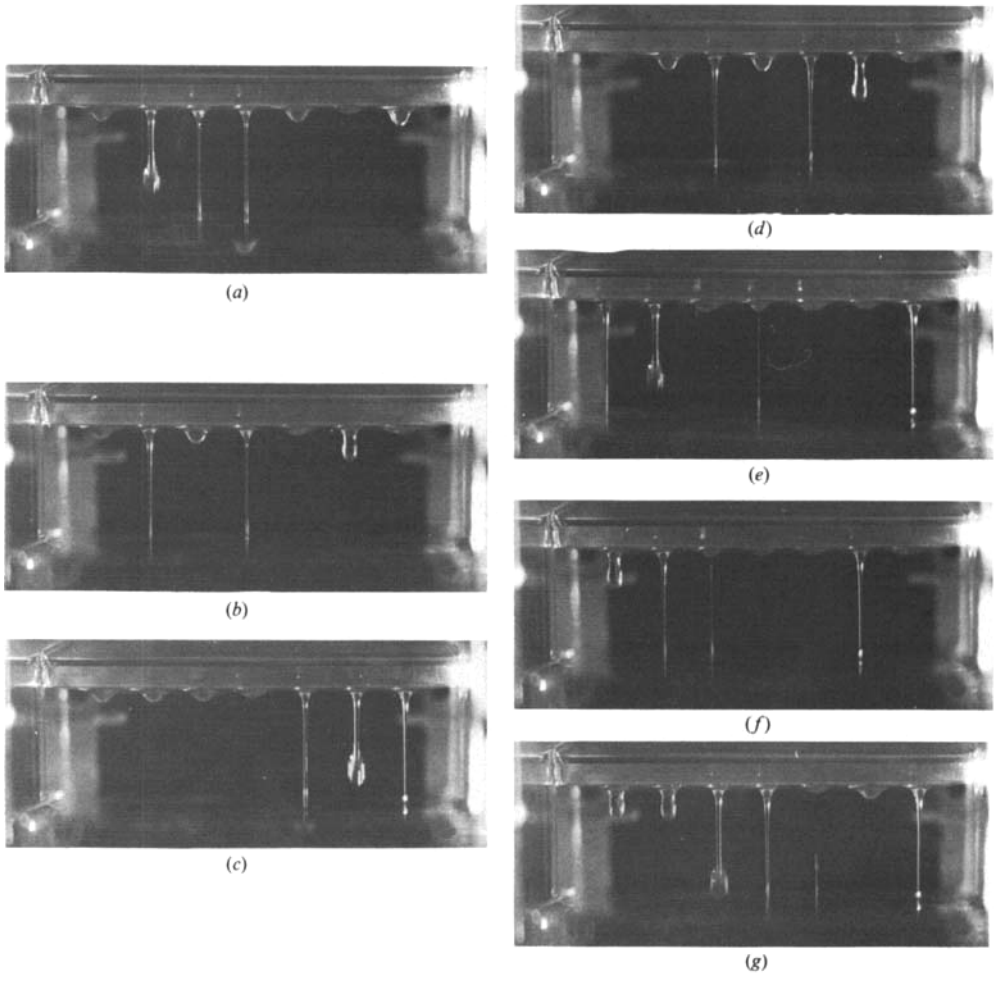

FIGURE 8(*a–g*). For description see facing page.

flows to a seven-site flow. In the experiments it was very easy to transform a dripping site into a continuous stream, and vice versa, by simply disturbing the flow in the zone on the upper side of the plate immediately above the site in question. This was usually done by dipping a glass rod of about 4 mm diameter into the stream.

Another sequence of observations concerning six-site flows is shown in figure 7. This sequence began with the formation of the ((5D)C) flow shown in figure 5(*e*) arising, at $R = 0.187$, from an exchange of stabilities with a (5D) flow. The flow rate was then reduced to a value equivalent to $R = 0.150$, under which conditions a (6D) pattern (see figure 7*b*) was stable, as were patterns comprising one 'C' stream, two 'C' streams (see figure 7*c*) and three 'C' streams (see figure 7*d*). The only pattern with three 'C' streams I established here was the one shown in figure 7(*d*), and these seemed to have a rather small domain of stability. I was unable to establish a six-site flow with four 'C' streams. Some of the stability properties of these flows may, however, have been associated with the features that here the flux Q (and hence R) seemed, from the depth measurements, to vary by about 1 or 2 % over a two- to three-minute interval. In the process of adjusting the flow rate from a value equivalent to $R = 0.187$ to $R = 0.142$ a stable (DDCCDD) flow changed to the (6D) flow shown in figure 7(*a*).

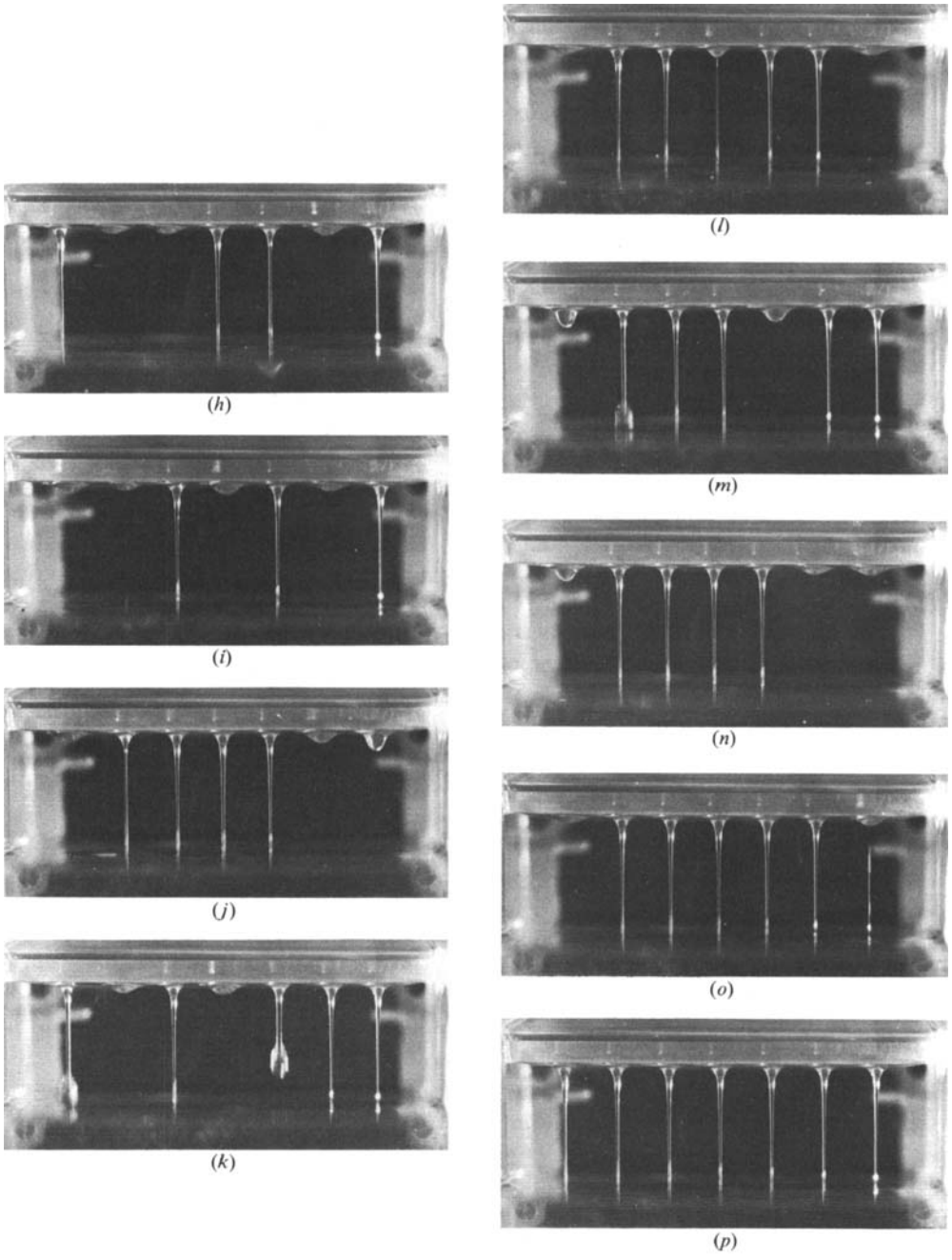

FIGURE 8. Seven-site flows at $R = 0.162$, $S = 58.1$, $h = 1.60$ mm, $\nu = 0.781$ St. (*a*) (7D); (*b*) (DC(5D)); (*c*) ((6D)C); (*d*) (DDCDCDD); (*e*) (C(5D)C); (*f*) (DC(3D)CD); (*g*) ((3D)CDDC); (*h*) (CDDCDDC); (*i*) (DDCDCDC); (*j*) (DD(3C)DD); (*k*) (DDCDDCC); (*l*) (DCCDCCD); (*m*) (DDCCDCC); (*n*) (D(4C)DD); (*o*) (D(5C)D); (*p*) (7C).

The (6D) branch of flows held stability down to a flow rate equivalent to $R \approx 0.067$, at which point a (5D) flow established itself. The flow rate was then readjusted such that $R = 0.162$ and a six-site flow was re-established. At these conditions I induced the (6D) flow and the 'one-C' and 'two-C' flows shown in figure 7(*e–g*), but I was unable to induce a stable pattern with more than two continuous streams. Among the possible six-site flows at $R = 0.202$, only a (6D) pattern (see figure 7*h*) appeared to be a stable possibility, with attempts to induce any 'C' streams leading to a loss of stability of the six-site flow. The (6D) pattern naturally lost stability at $R \approx 0.251$ to the ((7C)D) flow shown in figure 7(*i*).

All the six-site flows observed were nearly periodic in time, in the same sense as described for the five-site flows. There appeared to be at least 23 different six-site flows possible in this experiment.

4.2.3. *Seven-site flows*

A class of flows emanating from seven sites on the underside of the plate were observed at flow rates equivalent to R ranging between approximately 0.12 and 1.8. Examples of some of the flows possible under these conditions are given in figures 8(*a–p*), all of which were obtained under the same operating conditions; many more such flows were also stable under the same conditions. Shown in figure 8(*a*) is a flow in which all seven sites were drip sites (sites 3 and 4 were, in fact, drip sites), whereas (*b*) and (*c*) give examples in which one of the sites was a continuous stream (namely site 2 in figure 8(*b*) and site 7 in (*c*)) but the C stream could be established at any of the seven sites. Examples of flows involving two C sites are shown in figures 8(*d–g*). Again, all combinations involving five D sites and two C sites seemed to be possible. It also seemed possible to generate any combination involving three C sites and four D sites (some examples of which are shown in figures 8(*h–k*)), four C sites and three D sites (see figures 8*l–n*) or those with five C sites and two D sites (e.g. see figure 8*o*). I am not sure if flows with one drip site and six C sites were stable possibilities under these operating conditions but I would suspect this to have been the case for, as shown in figure 8(*p*), a *steady* flow with seven C sites was a stable possibility. The latter is the first steady motion so far encountered in this experiment, all the other flows being nearly periodic in time, as discussed above. Although a flow with one drip site had not specifically been induced under the conditions obtaining for figure 8, such a flow was observed under the conditions $R = 0.200$, $S = 52.7$, $h = 1.68$ mm, $\nu = 0.755$ St; I was, however, unable to induce the steady (7C) flow under those conditions. The flows involving either six or seven C streams seemed to have quite small domains of stability, though no specific attempt was made to delineate these particular domains in the experiments. But estimates were obtained for the stability limits of seven-site flows in general. So, for example, on carefully reducing the flow rate it was found that a (D(5C)D) flow lost stability to a (6D) flow at $R = 0.128$, $S = 65.2$, $h = 1.51$ mm, $\nu = 0.804$ St, and other seven-site flows seemed not to be stable possibilities at these conditions. Near the upper limit it was found that the (D(5C)D) flow lost stability to an eight-stream flow when $R = 0.265$, $S = 40.3$, $h = 1.92$ mm, $\nu = 0.803$ St, under which conditions I was unable to re-establish any of the seven-site flows by disturbing the flow near the end of the plate.

As the flow rate was further increased beyond the stability range of the above flows, a different kind of unsteady motion involving seven sites was observed. This particular flow arose when I was attempting to establish a nine-site flow from an eight-site flow and, as shown in figure 9, it consisted of a D site together with six

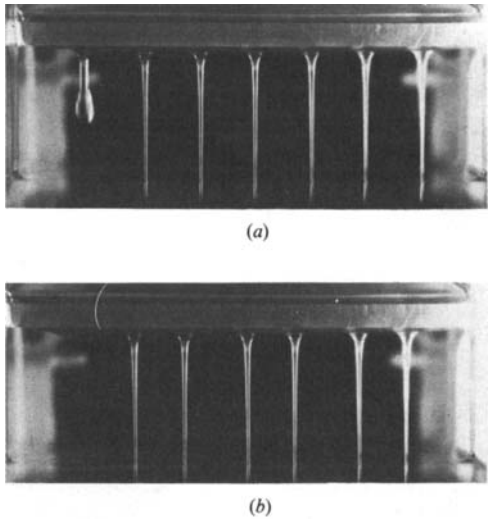

FIGURE 9. An unsteady (D(6C)) flow at $R = 0.294$, $S = 37.2$, $h = 2.00$ mm, $\nu = 0.809$ St. (*a*) and (*b*) are photographs of the same flow at two different times.

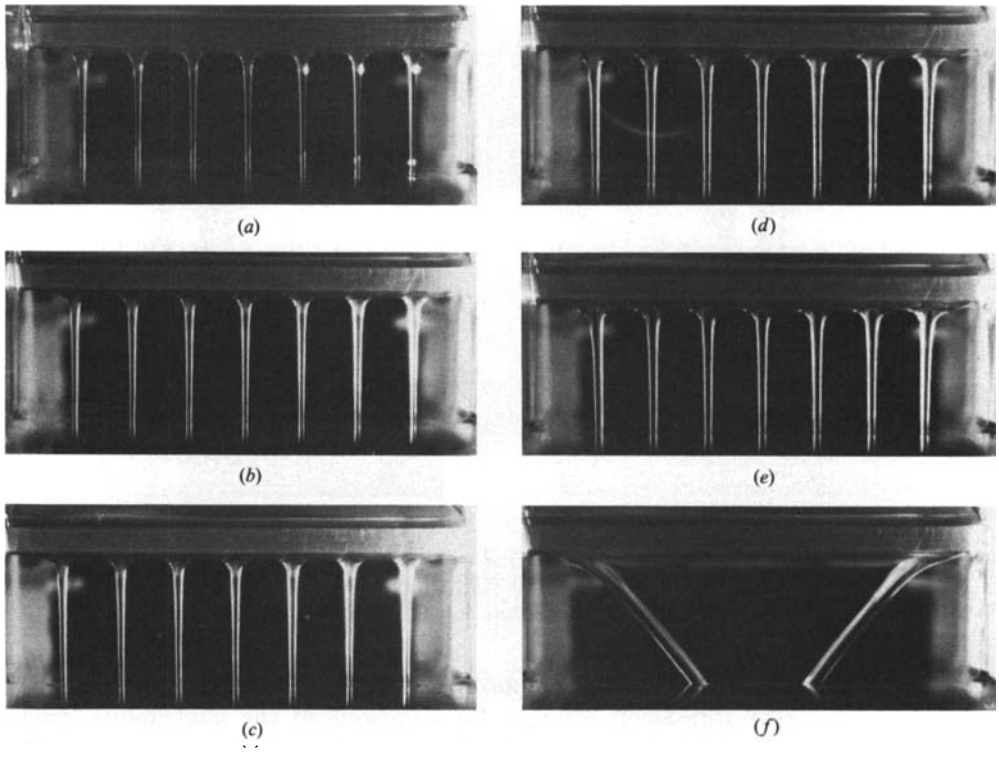

FIGURE 10. Steady (7C) flows: (*a*) $R = 0.794$, $S = 19.4$, $h = 2.77$ mm, $\nu = 0.803$ St; (*b*) $R = 0.863$, $S = 18.3$, $h = 2.85$ mm, $\nu = 0.804$ St; (*c*) $R = 0.937$, $S = 17.6$, $h = 2.91$ mm, $\nu = 0.796$ St; (*d*) $R = 1.48$, $S = 13.0$, $h = 3.38$ mm, $\nu = 0.792$ St; (*e*) $R = 1.79$, $S = 11.5$, $h = 3.60$ mm, $\nu = 0.792$ St. (*f*) The (7C) branch lost stability to this steady (T) flow: $R = 1.81$, $S = 11.4$, $h = 3.61$ mm, $\nu = 0.792$ St.

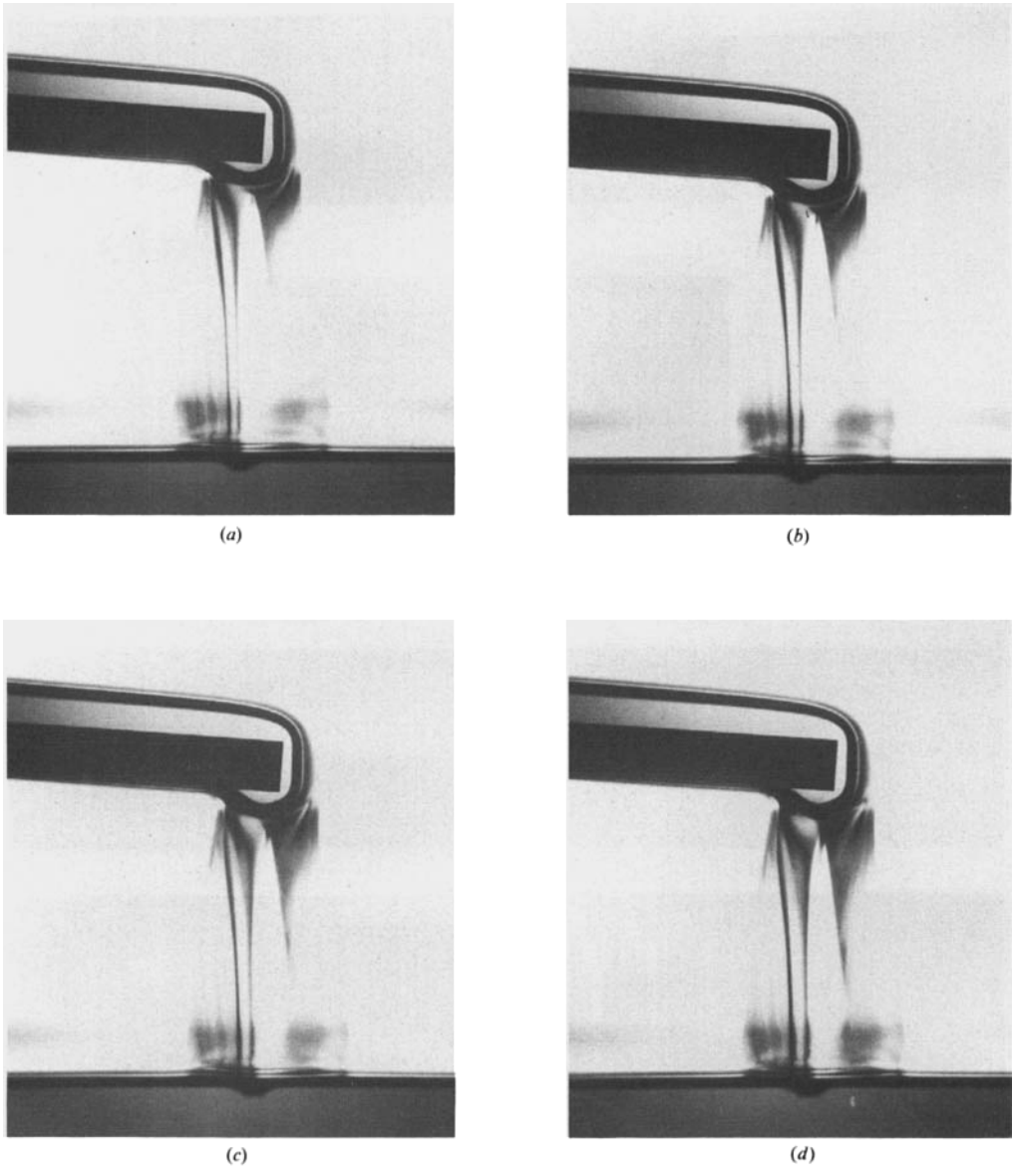

FIGURE 11. Side views of steady (7C) flows. (*a*) $R = 0.976$, $S = 18.3$, $h = 2.85$ mm, $\nu = 0.756$ St; (*b*) $R = 1.21$, $S = 15.9$, $h = 3.06$ mm, $\nu = 0.757$ St; (*c*) $R = 1.58$, $S = 13.4$, $h = 3.33$ mm, $\nu = 0.751$ St; (*d*) $R = 1.80$, $S = 12.2$, $h = 3.49$ mm, $\nu = 0.752$ St.

C sites. A distinguishing feature of this motion was that, as well as being unsteady by virtue of the drip-formation process, the locations of the continuous streams continually changed with time, as indicated by the differences between figures 9(*a*) and (*b*). Note that, in the previous examples involving both D and C sites, a small adjustment of the locations of the C streams near a D site would take place as the droplet grew and then broke off. In the present case, however, the roughly periodic, large-scale excursions of the C streams seemed to take place on a timescale unrelated to, and much larger than, the period for the formation of the droplets. The

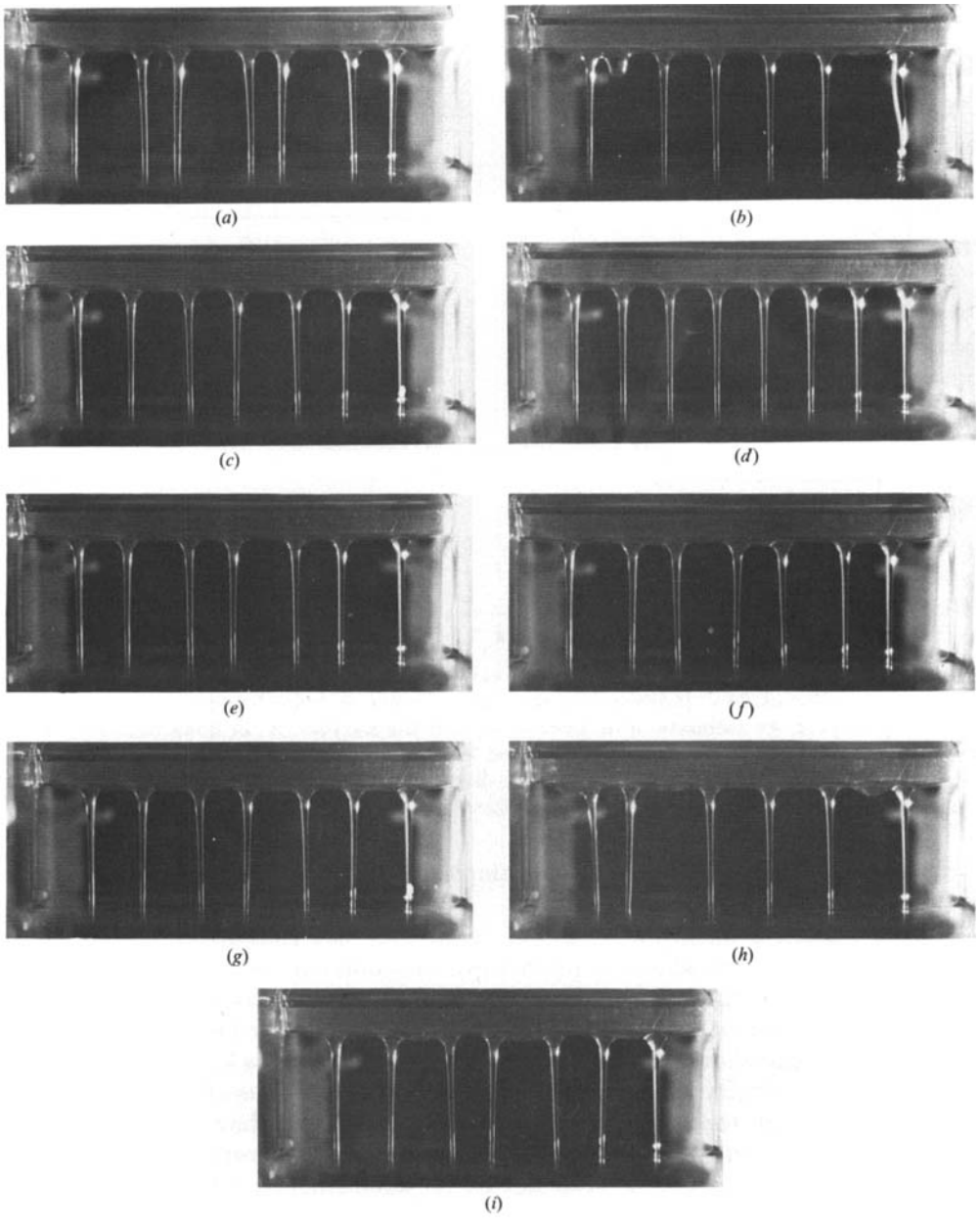

FIGURE 12. Unsteady (7C) flows. (*a*)–(*d*): $R = 0.790$, $S = 19.4$, $h = 2.77$ mm, $\nu = 0.803$ St. (Note: the unsteady motion lost stability to the steady (8C) flow shown in (*d*).) (*e*)–(*i*): $R = 0.764$, $S = 19.9$, $h = 2.73$ mm, $\nu = 0.801$ St.

impression given of this flow was that a 'conventional' (D(6C)) flow was nearly stable, but not quite, and so there was a readjustment of the streams to allow the formation of a new stream; however, this new stream did not eventuate and the flow tried to equilibrate itself, through the influence of surface-tension forces, so that the spacing of the streams was nearly uniform. And so the process repeated itself. This motion was observed for over 16 minutes and, as it appeared to be quite stable, the operating

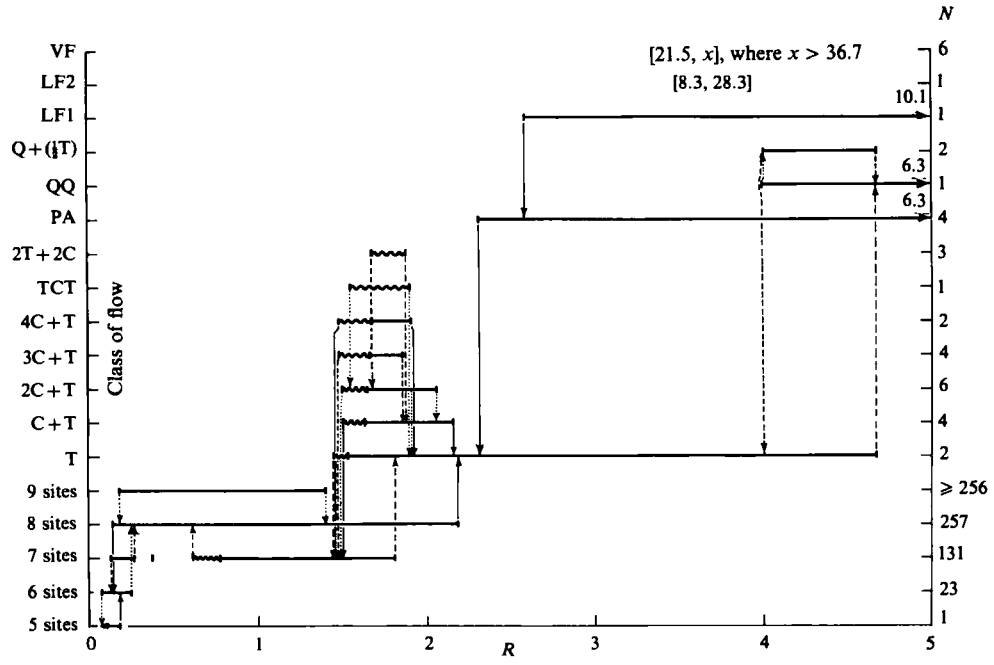

FIGURE 13. A schematic representation of the various flows observed, in terms of the Reynolds number. The 'class of flow' indicated on the left-hand side is defined under the corresponding subheading of §4.2. An estimate of (a lower bound of) the number, N, of flows realizable within each class is indicated on the right. The crinkled lines depict unsteady, chaotic types of motion. The vertical lines indicate the losses of stability described in the text. (But note that they do not give a comprehensive picture of all the possibilities.)

conditions were then changed. Other examples of this kind of phenomenon will be described below.

Another branch of steady (7C) flows, apparently not connected to the branch corresponding to the flow shown in figure 8(p), was found at flow rates corresponding to values of R ranging between $R \approx 0.79$ and $R \approx 1.80$. Examples of the flows observed in this branch are shown in figures 10(a–e), the flow losing stability near $R = 1.80$ to the one shown in figure 10(f), to be referred to as a (T) flow. The way this branch lost stability at the lower end of the range is discussed below.

Remark. Although the two branches of steady (7C) flows shown above were not connected in the particular region of parameter space investigated here, these branches may, of course, have been connected via some other path through parameter space.

Some side views of the present branch of steady (7C) flows are given in figure 11. It is seen that the attachment line of the free surface on the underside of the plate was approximately $0.9a$ from the lower corner of the plate. The place at which the jets penetrated the free surface of the reservoir can be located from the 'dimple' visible at the free surface of the reservoir.

The way in which the branch of steady (7C) flows depicted in figures 10 and 11 lost stability, as the flow rate was reduced, was not decisively clear in the experiments. It is, however, my view that stability was exchanged for an unsteady, chaotic type of motion, comprising basically seven continuous streams, examples of which are given in figure 12. The reason for the difficulty in interpreting the experimental

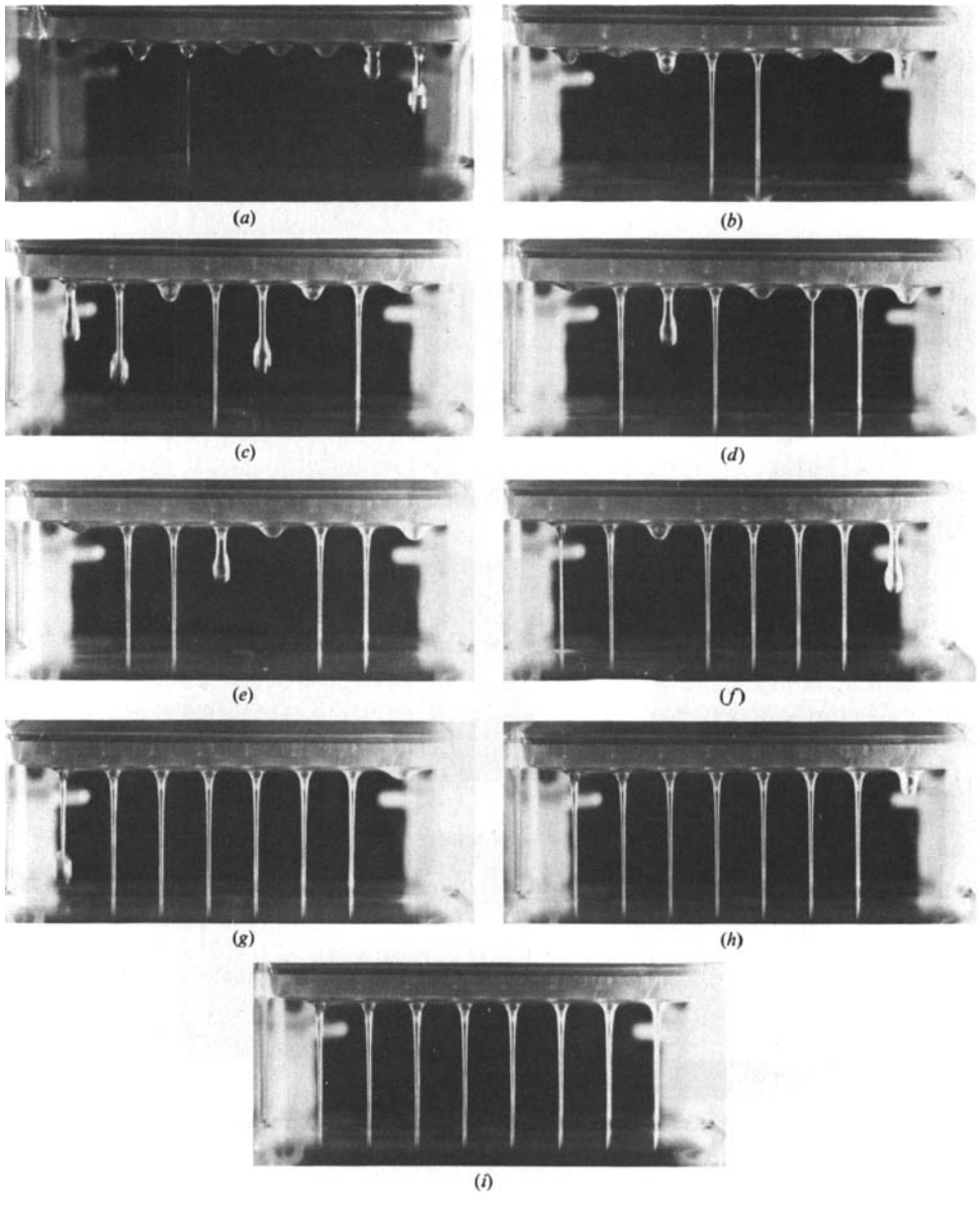

FIGURE 14. Examples of eight-site flows. (*a*) (8D) flow; (*b*) ((3D)C(4D)) flow; (*c*) ((3D)CDDCD) flow; (*d*) (DCDCDDCD) flow; (*e*) (DCCDDCCD) flow; (*f*) (DCD(4C)D) flow; (*g*) (D(6C)D) flow; (*h*) ((7C)D) flow; (*i*) (8C) flow. Experimental conditions. (*a*): $R = 0.254$, $S = 41.2$, $h = 1.90$ mm, $\nu = 0.806$ St; (*b*), (*c*), (*d*), (*f*), (*h*): $R = 0.233$, $S = 44.9$, $h = 1.82$ mm, $\nu = 0.789$ St; (*e*), (*g*): $R = 0.282$, $S = 39.9$, $h = 1.93$ mm, $\nu = 0.784$ St; (*i*): $R = 0.251$, $S = 42.5$, $h = 1.87$ mm, $\nu = 0.792$ St.

observations lies in the possible variations of up to 2% in the flow rate, referred to in §2: it is not clear whether the unsteady motions arose because of inherent variations in the flux or whether there was, in fact, an indefinitely persistent, unsteady motion corresponding to steady operating conditions and which, in the experiments, eventually lost stability to a more stable flow merely because the operating conditions were not held steady enough.

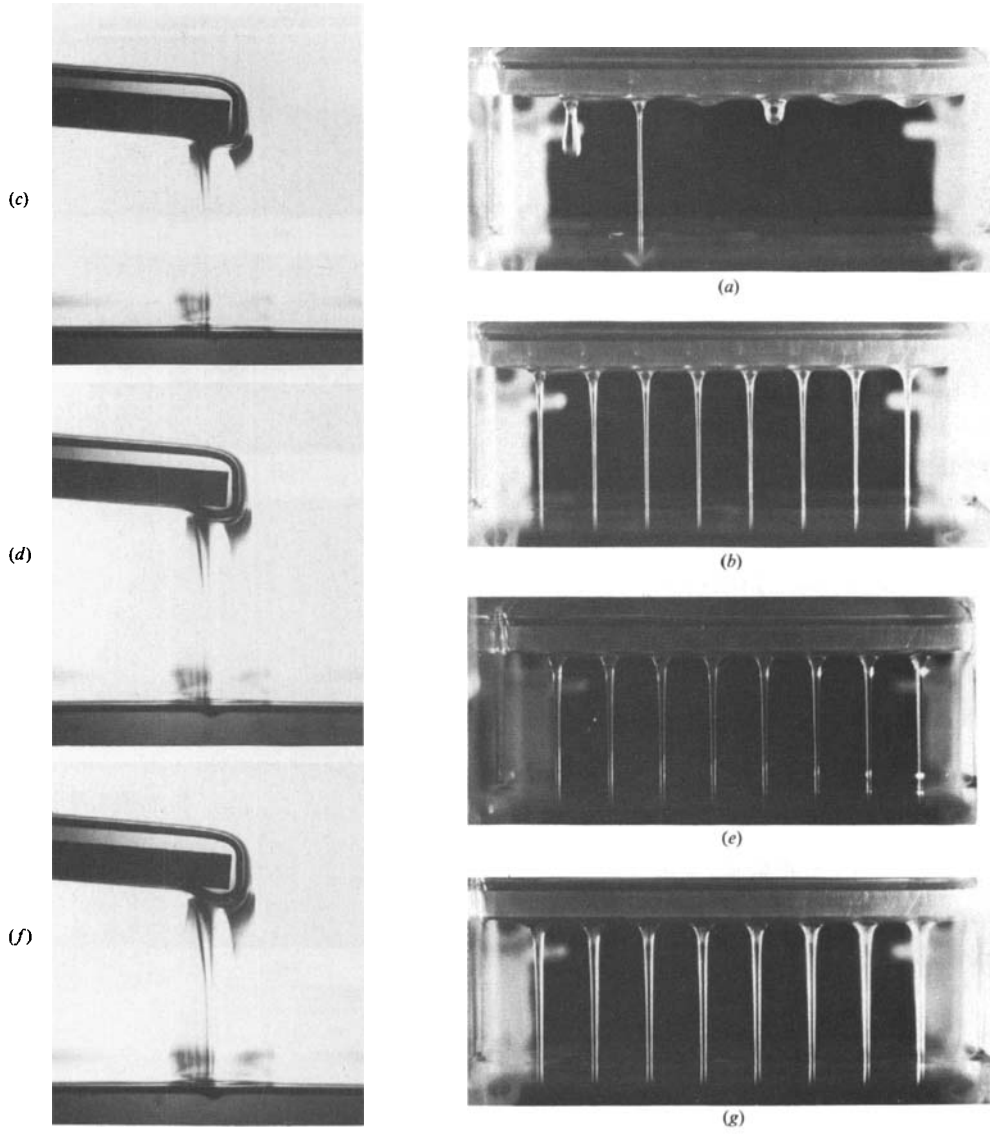

FIGURE 15(*a–g*). For description see facing page.

When the flow rate was reduced below a value equivalent to $R \approx 0.79$ the streams shown in figure 10 started to perform a complicated 'dance' (see the time-sequence of photographs in figures 12(*a–d*), and a sequence under different operating conditions in figures 12(*e–i*)) as though to provide room for an eighth stream to form. This can be seen clearly in figure 12(*h*). However (cf. figure 12*i*) an eighth stream did not develop and the flow settled back towards the uniformly spaced, steady (7C) flow; but this flow was not stable.... A typical period for this chaotic type of motion was about 8 to 10 s, but on some cycles it was as large as 35 or 40 s. The unsteady flow shown in figures 12(*a–c*) was sustained for approximately 30 minutes before collapsing to the steady (8C) flow shown in figure 12(*d*). The unsteady (7C) flow shown in figures 12(*e–i*) was sustained for approximately 50 'cycles' of motion before collapsing to a steady (8C) flow.

Thus, as indicated above, the interpretation of these observations is somewhat

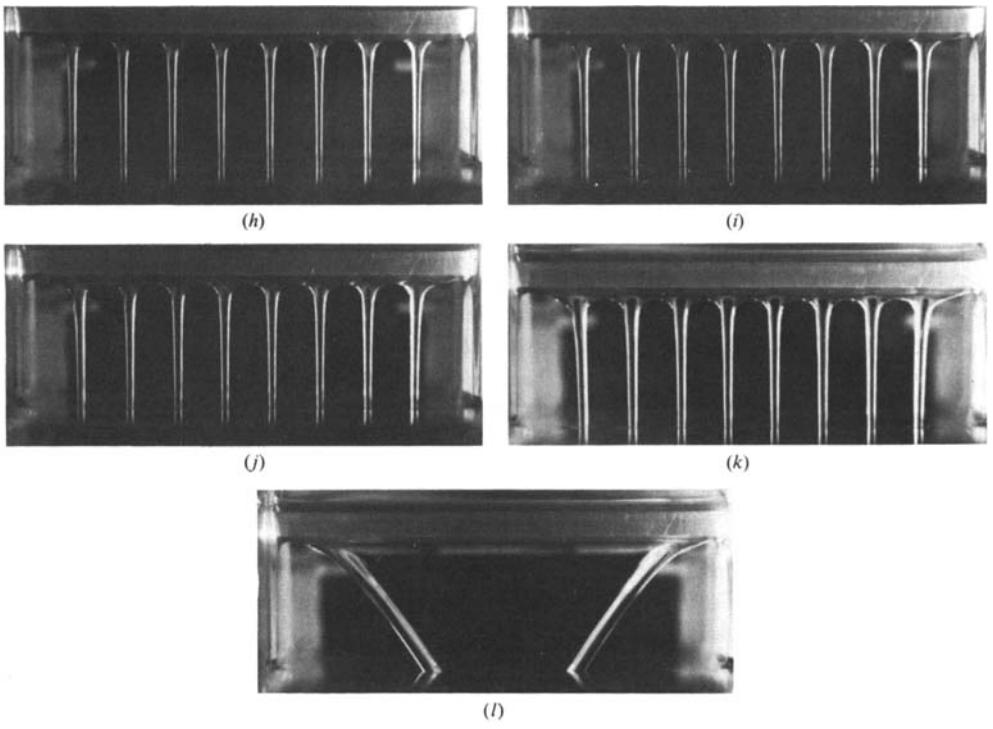

FIGURE 15. Examples from the steady (8C) branch of flows. (*a*) The branch of flows lost stability to this (6D) flow: $R = 0.139$, $S = 63.5$, $h = 1.53$ mm, $\nu = 0.789$ St; (*b*) (8C) flow: $R = 0.174$, $S = 54.6$, $h = 1.65$ mm, $\nu = 0.789$ St; (*c*) (8C) flow, side view: $R = 0.260$, $S = 44.4$, $h = 1.83$ mm, $\nu = 0.754$ St; (*d*) (8C) flow, side view: $R = 0.488$, $S = 29.1$, $h = 2.26$ mm, $\nu = 0.755$ St; (*e*) (8C) flow: $R = 0.559$, $S = 24.4$, $h = 2.47$ mm, $\nu = 0.806$ St; (*f*) (8C) flow, side view: $R = 0.741$, $S = 22.0$, $h = 2.60$ mm, $\nu = 0.756$ St; (*g*) (8C) flow: $R = 0.863$, $S = 18.3$, $h = 2.85$ mm, $\nu = 0.804$ St; (*h*) (8C) flow: $R = 1.22$, $S = 14.7$, $h = 3.18$ mm, $\nu = 0.798$ St; (*i*) (8C) flow: $R = 1.53$, $S = 12.6$, $h = 3.43$ mm, $\nu = 0.797$ St; (*j*) (8C) flow: $R = 1.78$, $S = 11.5$, $h = 3.59$ mm, $\nu = 0.792$ St; (*k*) (8C) flow: $R = 2.09$, $S = 10.4$, $h = 3.79$ mm, $\nu = 0.790$ St. (*l*) The branch of flows lost stability to this (T) flow: $R = 2.19$, $S = 10.1$, $h = 3.84$ mm, $\nu = 0.790$ St.

complicated, but it is my view that an unsteady, chaotic kind of motion would have arisen and persisted indefinitely if the operating conditions had been held more nearly steady. We shall see presently that similar kinds of unsteady flows arose in less ambiguous circumstances in connection with other flow structures. The present observations indicate, on the other hand, the importance of taking into account 'imperfections' in maintaining prescribed operating conditions in a situation in which there are a number of possible flow states.

At this stage it seems worthwhile to attempt a summary of the various flow possibilities correlated to the flux, the quantity that was systematically varied throughout the experiment. This is done in figure 13, where the range of stability of the various flows is shown as a function of R. To keep the diagram relatively uncomplicated, flows have been lumped together in classes, which correspond to the subheadings of §4.2, and an estimate of the number of different possible flows within a given class is indicated on the right-hand side of the figure. Of course figure 13 is a gross simplification of a figure that should be drawn in a five-dimensional parameter space, but it nevertheless gives a rough idea of the various possibilities. The crinkled lines in this figure indicate what I shall refer to as unsteady, chaotic motions.

4.2.4. *Eight-site flows*

Flows emanating from eight sites on the underside of the plate have already been encountered in figures 7 (*i*) and 12 (*d*), and, as indicated by figure 13, flows in this class were observed over a rather wide range of flow rates. It is shown in figure 14 that flows with $(8-j)$ drip sites and (j) C streams, for $j = 0, \ldots, 8$, were stable possibilities and it was my conviction, while carrying out the experiment, that all 256 combinations of such flows could easily be realized. I did not try to delineate the ranges of stability for each of the various kinds of eight-site flows though there were evidently considerable differences between flows. For example, at $R = 0.209$, $S = 47.4$, $h = 1.77$ mm and $\nu = 0.799$ St, all combinations of flows involving zero to six drip sites seemed possible, but I was unable to establish stable flows with either seven or eight drip sites. On the other hand, when the flow rate was increased slightly, such that $R = 0.254$, $S = 41.2$, $h = 1.90$ mm and $\nu = 0.806$ St, all combinations of flows involving zero to eight drip sites seemed to be possible. Then, on changing the operating conditions to $R = 0.282$, $S = 39.9$, $h = 1.93$ mm, $\nu = 0.784$ St, I was unable to establish eight-site flows with more than four drip sites; and, under the conditions $R = 0.294$, $S = 37.2$, $h = 2.00$ mm, $\nu = 0.809$ St, none of the above flows involving a drip site seemed to be a stable possibility. At these latter operating conditions there was, however, one unusual flow which had a drip site near the left-hand wall of the channel and seven C sites. The difference between this and the previous 'D flows' lay in the rhythm of the dripping process, which consisted of a short interval between two drips, followed by a longer interval until the formation of the next drip, whereas normally the interval between successive drips, at a given site, was very nearly uniform. This atypical D-flow seemed to be associated with asymmetries of the apparatus, for I was not able to generate a flow with a D site near the right-hand wall of the channel under the same operating conditions.

Examples spanning the range of flow rates for which the branch of steady (8C) flows were observed are given in figure 15. On reducing the flow rate (cf. figures 15*g*, *e*, *b*) the branch lost stability to the (6D) flow shown in figure 15 (*a*) and, on increasing the flow rate (cf. figures 15*h*–*k*), the (8C) flow eventually lost stability to the (T) flow shown in figure 15 (*l*). Some typical side views of the flow are given in figures 15 (*c*), (*d*), (*f*).

All eight-site flows observed in these experiments were either steady motions (the 8C) branch) or nearly periodic in time, including the atypical (D(7C)) flow.

4.2.5. *Nine-site flows*

Flows emanating from nine sites on the underside of the plate were observed at flow rates corresponding to values of R between approximately 0.18 and 1.4. None of the flows in this class arose naturally from a loss of stability of another flow. They were all established by making suitable perturbations to the stream in the zone above the end of the plate. As with the previous examples, combinations of drip sites and unbroken streams were possible though, in this case, it was slightly more delicate than hitherto to establish the drip sites. In particular, I was able to induce only flows having four or fewer D sites, some examples of which are given in figure 16. It did, however, appear as though all combinations of such flows were stable possibilities and it was my impression that, given more patience, I might have established some flows with five D sites.

I was unable to induce drip sites with this class of flows at flow rates above those corresponding to the conditions obtaining for figure 16 (for which $R = 0.269$), and

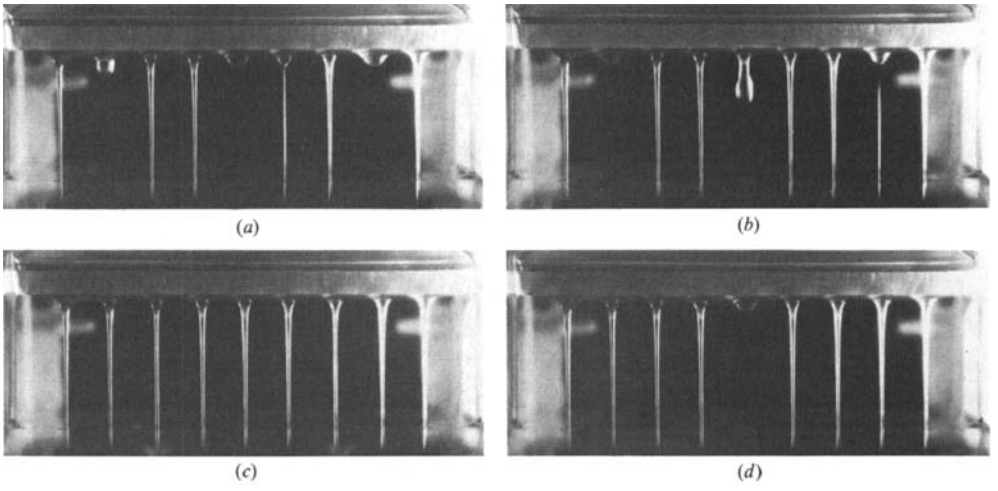

FIGURE 16. Examples of nine-site flows at $R = 0.269$, $S = 40.3$, $h = 1.92$ mm, $\nu = 0.796$ St. (*a*) ((CDCCDDCDC) flow; (*b*) (CDCCDCCDC) flow; (*c*) (CCDCCCDCC) flow; (*d*) ((4C)D(4C)) flow.

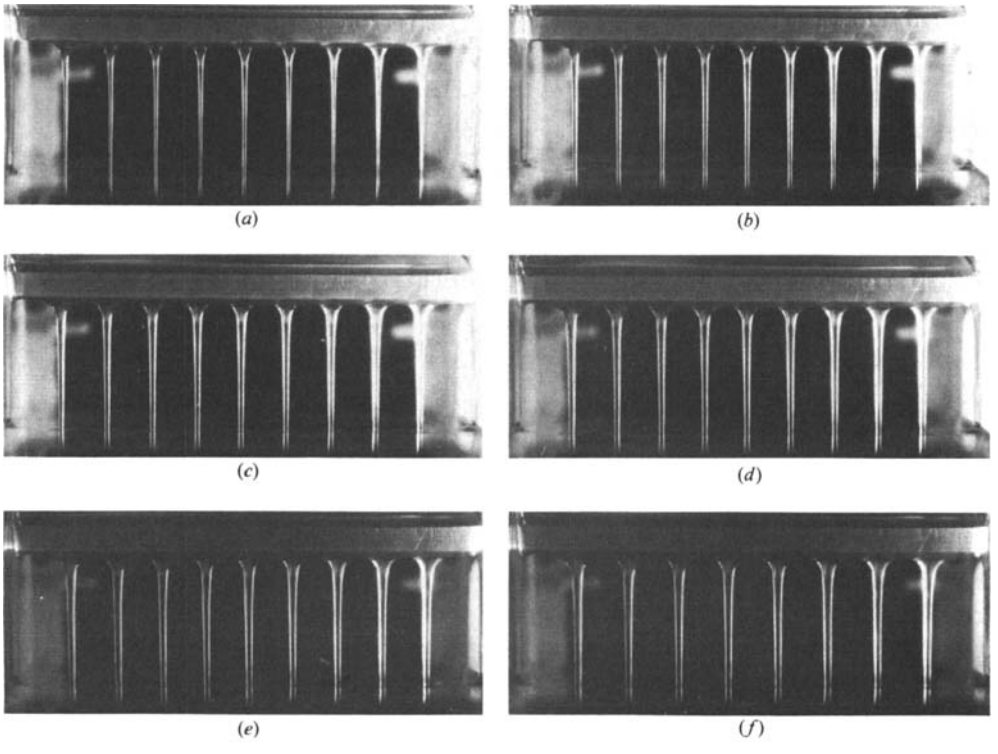

FIGURE 17. Examples from the branch of steady (9C) flows. (*a*) $R = 0.241$, $S = 43.0$, $h = 1.86$ mm, $\nu = 0.802$ St; (*b*) $R = 0.511$, $S = 26.0$, $h = 2.39$ mm, $\nu = 0.802$ St; (*c*) $R = 0.937$, $S = 17.6$, $h = 2.91$ mm, $\nu = 0.796$ St; (*d*) $R = 1.17$, $S = 15.2$, $h = 3.13$ mm, $\nu = 0.795$ St; (*e*) $R = 1.33$, $S = 13.9$, $h = 3.27$ mm, $\nu = 0.795$ St; (*f*) the (9C) flow lost stability to this steady (8C) flow: $R = 1.40$, $S = 13.5$, $h = 3.32$ mm, $\nu = 0.795$ St.

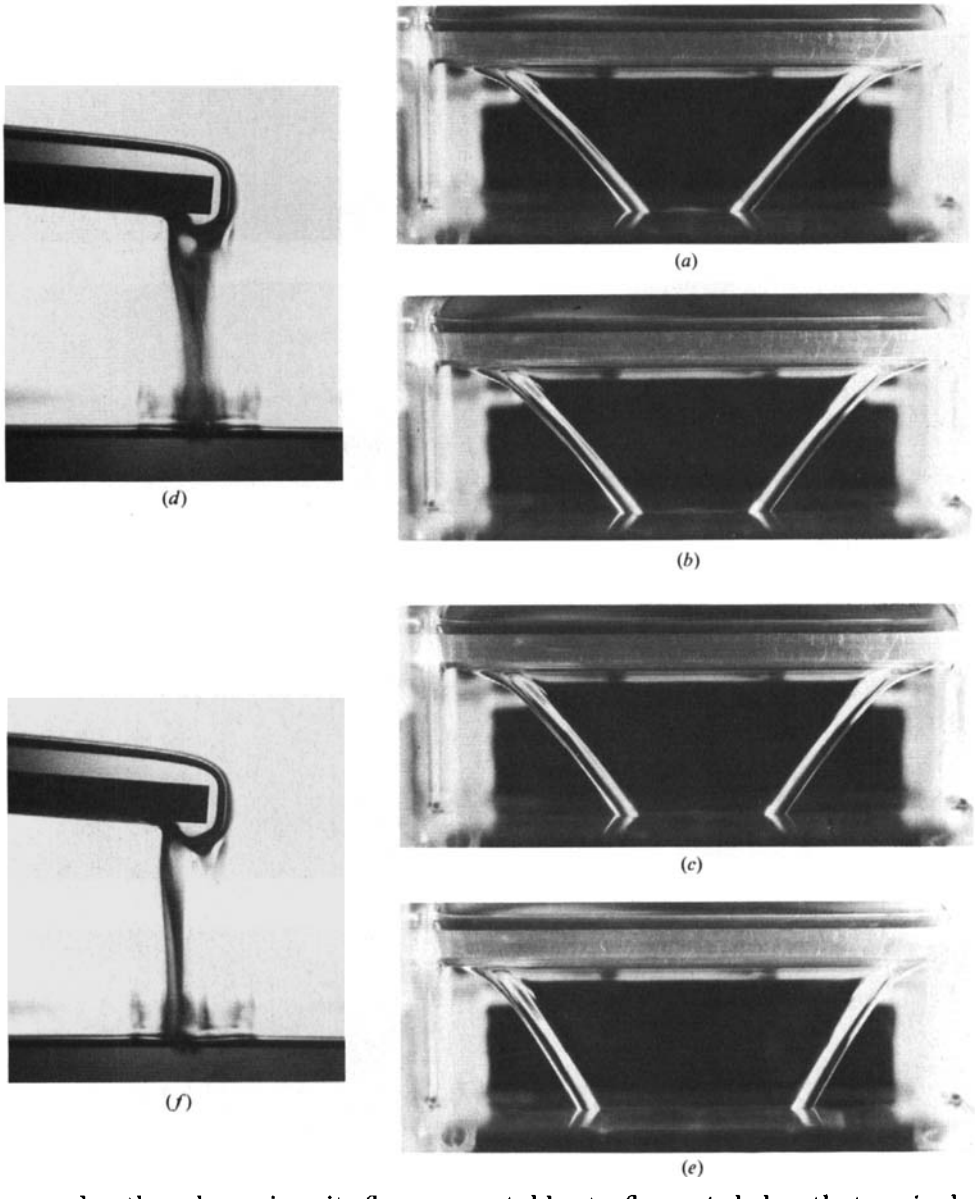

it seemed as though no nine-site flows were stable at a flow rate below that equivalent to $R = 0.178$.

The branch of steady (9C) flows, some examples of which are given in figure 17, was stable over a fairly wide range of flow rates. On reducing the flow rate, stability of the branch was lost at $R = 0.178$, $S = 52.7$, $h = 1.68$ mm, $\nu = 0.802$ St to a steady (8C) flow. The steady (9C) branch of flows also lost stability, on increasing the flow rate, to a steady (8C) flow, as shown in figure 17 (f).

4.2.6. *T flows*

Both the steady (7C) branch of flows and the steady (8C) branch of flows lost stability (cf. figures 10f and 15l) to a branch of steady flows to be referred to as (T)

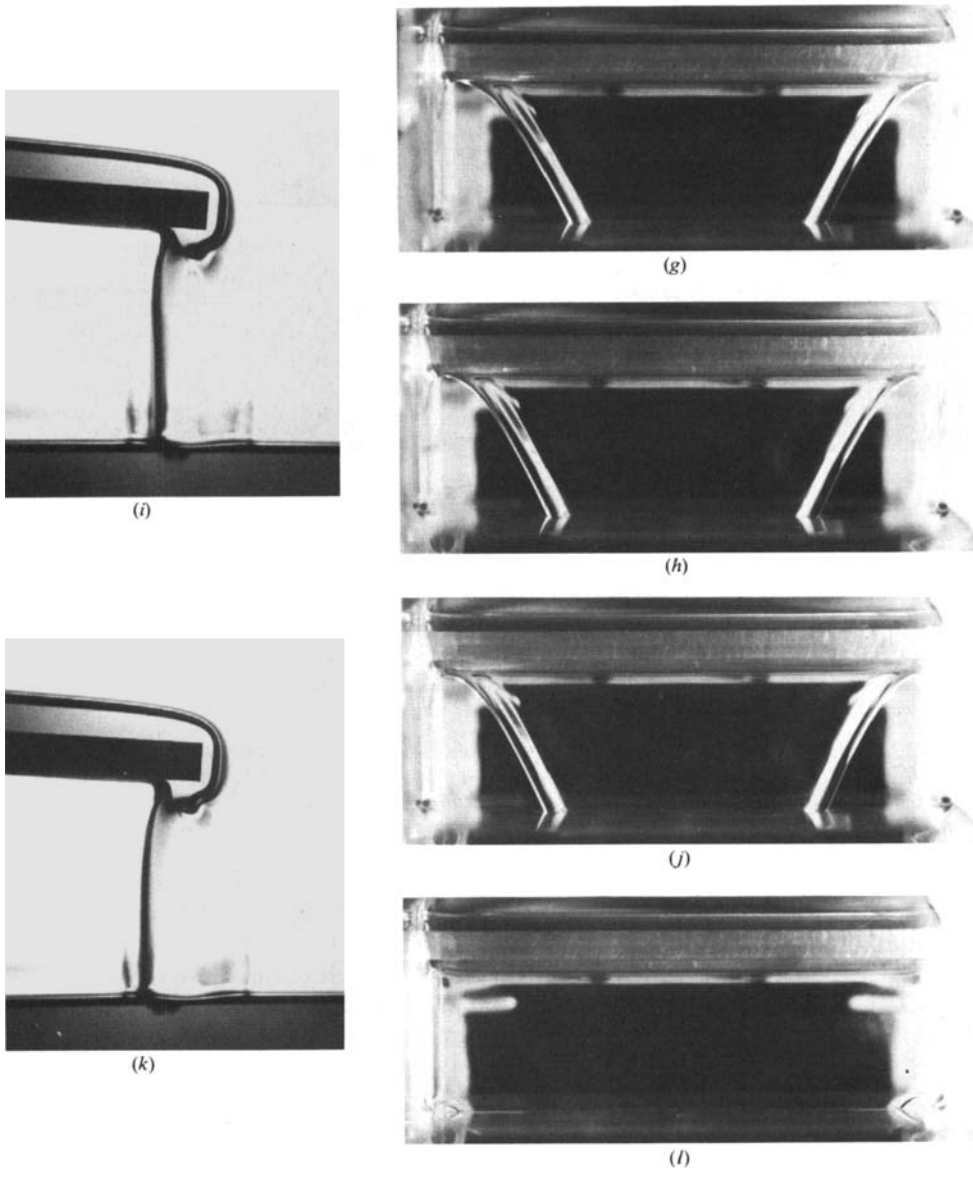

FIGURE 18. Examples from the branch of steady (T) flows. (*a*) $R = 1.61$, $S = 12.3$, $h = 3.47$ mm, $\nu = 0.792$ St; (*b*) $R = 1.80$, $S = 11.4$, $h = 3.61$ mm, $\nu = 0.793$ St; (*c*) $R = 1.96$, $S = 10.8$, $h = 3.71$ mm, $\nu = 0.793$ St; (*d*) side elevation at $R = 2.19$, $S = 10.8$, $h = 3.71$ mm, $\nu = 0.748$ St; (*e*) $R = 2.98$, $S = 8.34$, $h = 4.22$ mm, $\nu = 0.780$ St; (*f*) side view at $R = 3.03$, $S = 8.75$, $h = 4.12$ mm, $\nu = 0.746$ St; (*g*) $R = 3.52$, $S = 7.40$, $h = 4.48$ mm, $\nu = 0.784$ St; (*h*) $R = 4.02$, $S = 6.64$, $h = 4.73$ mm, $\nu = 0.796$ St; (*i*) side view at $R = 4.06$, $S = 7.21$, $h = 4.54$ mm, $\nu = 0.745$ St; (*j*) $R = 4.45$, $S = 6.27$, $h = 4.87$ mm, $\nu = 0.791$ St; (*k*) side view at $R = 4.67$, $S = 6.59$, $h = 4.75$ mm, $\nu = 0.744$ St; (*l*) the branch of (T) flows lost stability to this steady (QQ) flow at $R = 4.65$, $S = 6.09$, $h = 4.94$ mm, $\nu = 0.790$ St.

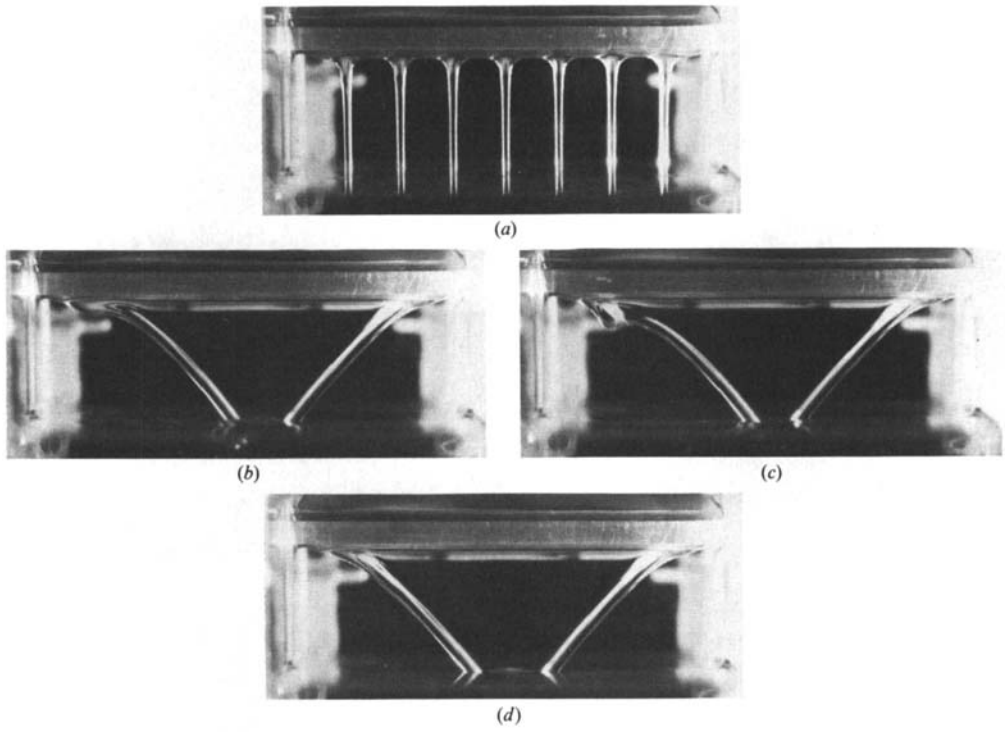

FIGURE 19. Some unsteady (T) flows. (*a*) The unsteady (T) flow lost stability to this steady (7C) flow at $R = 1.45$, $S = 13.2$, $h = 3.35$ mm, $\nu = 0.791$ St; (*b*), (*c*) $R = 1.51$, $S = 12.9$, $h = 3.40$ mm, $\nu = 0.792$ St; (*d*) $R = 1.54$, $S = 12.7$, $h = 3.42$ mm, $\nu = 0.791$ St.

flows. Further examples of these flows, together with some side views, are given in figure 18. The flow, in the region below the plate, consisted of two nearly cylindrical jets of fluid emanating from the underside of the plate and connected by a thin sheet of liquid. These jets, or arms, were pulled towards each other by the tension in the liquid sheet and it can be seen from the figure how the arms became more nearly vertical as they carried a larger volume of liquid. The side elevations (figures 18*d*, *f*, *i*, *k*) show how the attachment line of the free surface on the plate was on the underside of the plate, well behind the lower corner of the plate.

The branch of steady (T) flows lost stability, with increasing flow rate, at $R = 4.65$, $S = 6.09$, $h = 4.94$ mm, $\nu = 0.790$ St to the steady flow shown in figure 18 (*l*), to be referred to as a (QQ) flow, consisting of a sheet of liquid spanning the channel except for two small quadrants missing near the junction of the free surface in the reservoir and the walls. Note that the (T) flow shown in side elevation in figure 18(*k*) was at a slightly larger value of R than that at which the branch lost stability. The reason for this was that the viscosity of the liquid differed substantially from that which obtained for figures 18(*j*) and (*l*), suggesting how dependent the stability limits can be on changes in the various parameters.

As the flow rate was decreased the branch of steady (T) flows lost stability to an unsteady motion at approximate parameter settings of $R = 1.54$, $S = 12.7$, $h = 3.42$ mm, $\nu = 0.791$ St. The photograph shown in figure 19(*d*), which was taken at these conditions, shows the pattern at a reasonably quiescent, and nearly symmetric, phase of its unsteady cycle. The unsteadiness here took the form of mild

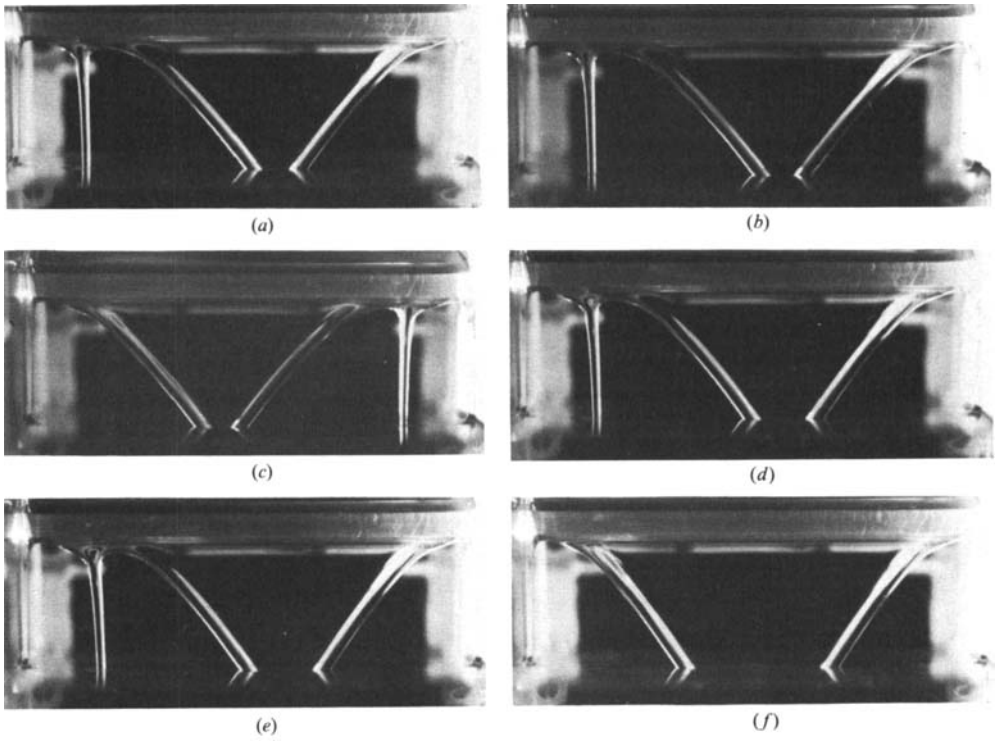

FIGURE 20. Examples of steady (C+T) flows. (*a*) (CT) flow at $R = 1.72$, $S = 11.7$, $h = 3.57$ mm, $\nu = 0.797$ St; (*b*) (CT) flow and (*c*) (TC) flow both at $R = 1.73$, $S = 11.8$, $h = 3.55$ mm, $\nu = 0.789$ St; (*d*) (CT) flow at $R = 1.93$, $S = 10.8$, $h = 3.71$ mm, $\nu = 0.797$ St; (*e*) (CT) flow at $R = 2.05$, $S = 10.4$, $h = 3.78$ mm, $\nu = 0.796$ St; (*f*) the branch of steady (CT) flows lost stability to this (T) flow at $R = 2.16$, $S = 10.1$, $h = 3.84$ mm, $\nu = 0.795$ St.

oscillations (in the plane of the sheet) of the left-hand arm of the sheet; these oscillations built up slowly in amplitude and then died away. At a slightly reduced flow rate, equivalent to $R \approx 1.51$, the unsteadiness was manifested in the form shown in figures 19(*b*, *c*), where a 'blob' of liquid can be seen to have developed near the upper end of the left-hand side of the sheet, as though a separate stream would like to form there. However, this 'blob' would run down the arm, as shown in figure 19(*c*), into the reservoir. Then the left-hand arm might pass through a phase in which it oscillated back and forth and eventually another 'blob' would form. This chaotic type of motion seemed to be quite persistent, being observed for over fifteen minutes before the operating conditions were changed. A further reduction of the flow rate resulted in these unsteady (T) flows losing stability to the steady (7C) flow shown in figure 19(*a*).

4.2.7. (*C*+*T*) *flows*

A class of flows consisting of one continuous jet of liquid and a nearly triangular section, similar in form to that described under the class of (T) flows, was observed at flow rates equivalent to R approximately in the range [1.50, 2.16]. Some examples from the branches of steady (C+T) flows are given in figure 20: (*b*) shows a (CT) flow and (*c*) is a (TC) flow at the same operating conditions as for (*b*); (*d*) and (*e*) show (CT) flows at larger flow rates; and this branch of (CT) flows lost stability at $R = 2.16$,

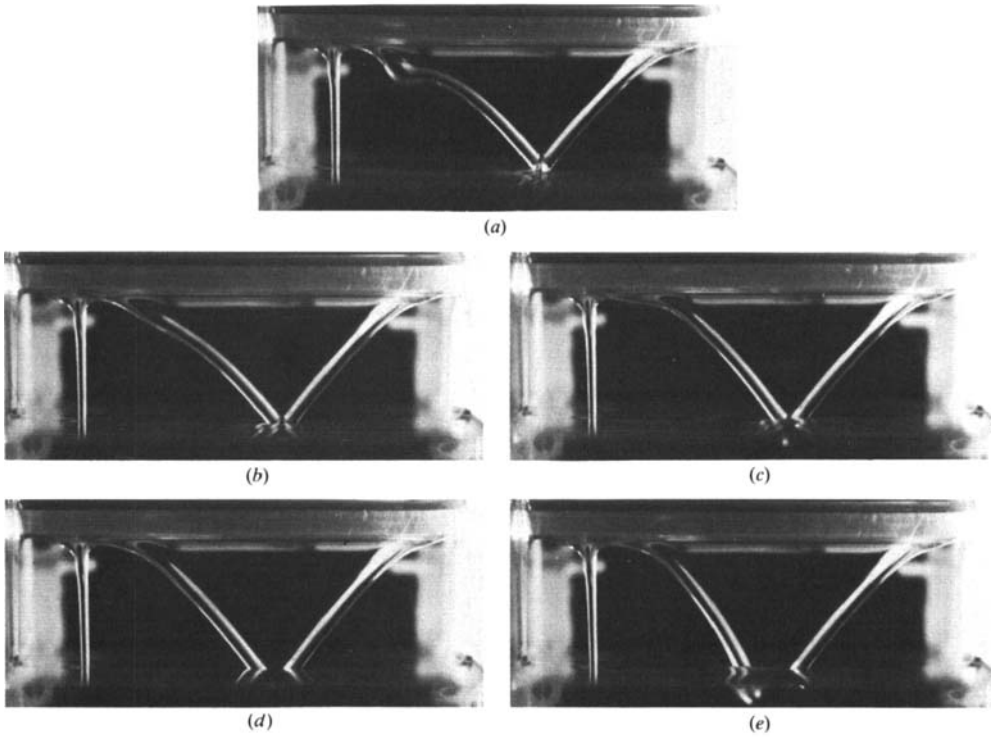

FIGURE 21. Some unsteady (CT) flows. (*a*) $R = 1.57$, $S = 12.4$, $h = 3.46$ mm, $\nu = 0.797$ St; (*b*), (*c*) $R = 1.60$, $S = 12.3$, $h = 3.48$ mm, $\nu = 0.797$ St; (*d*), (*e*) $R = 1.64$, $S = 12.1$, $h = 3.51$ mm, $\nu = 0.797$ St.

$S = 10.1$, $h = 3.84$ mm, $\nu = 0.795$ St to the steady (T) flow shown in (*f*). The flow depicted in figure 20 (*a*) at $R = 1.57, S = 12.4, h = 3.46$ mm, $\nu = 0.797$ St was near the limit of stability for steady (CT) flows, and a further small reduction in the flow rate led to the development of an unsteady (CT) flow, examples of which are given in figure 21. The unsteadiness in (*d*) and (*e*) took the form of the left-hand arm of the T-section oscillating back and forth in the plane of the T, with (*d*) showing the flow in a relatively quiescent phase of its motion and (*e*) in the 'active' phase (as evidenced by the reflection of the left-hand arm of the T-section in the free surface of the reservoir). Still further reductions of the flow rate led to a more vigorous form of the unsteadiness as indicated in (*b*) and (*c*), both of which were taken under the same operating conditions, and in (*a*) where a liquid 'blob', similar to that observed in the unsteady (T) flows, can be seen on the left-hand arm of the T-section. (Note that, in (*a*), (*b*) and (*c*) the two arms at the edges of the T-section came together near the level of the free surface in the reservoir.) The branch of unsteady (CT) flows lost stability to a steady (7C) flow at $R = 1.50$, $S = 12.8$, $h = 3.41$ mm, $\nu = 0.797$ St, corresponding to a flow rate just below that which obtained for figure 21 (*a*).

4.2.8. $(2C+T)$ *flows*

Examples of steady flows from this class are shown in figures 22 (*b–d*). The photograph of figure 22 (*a*) is an oblique view, almost a side elevation, showing how

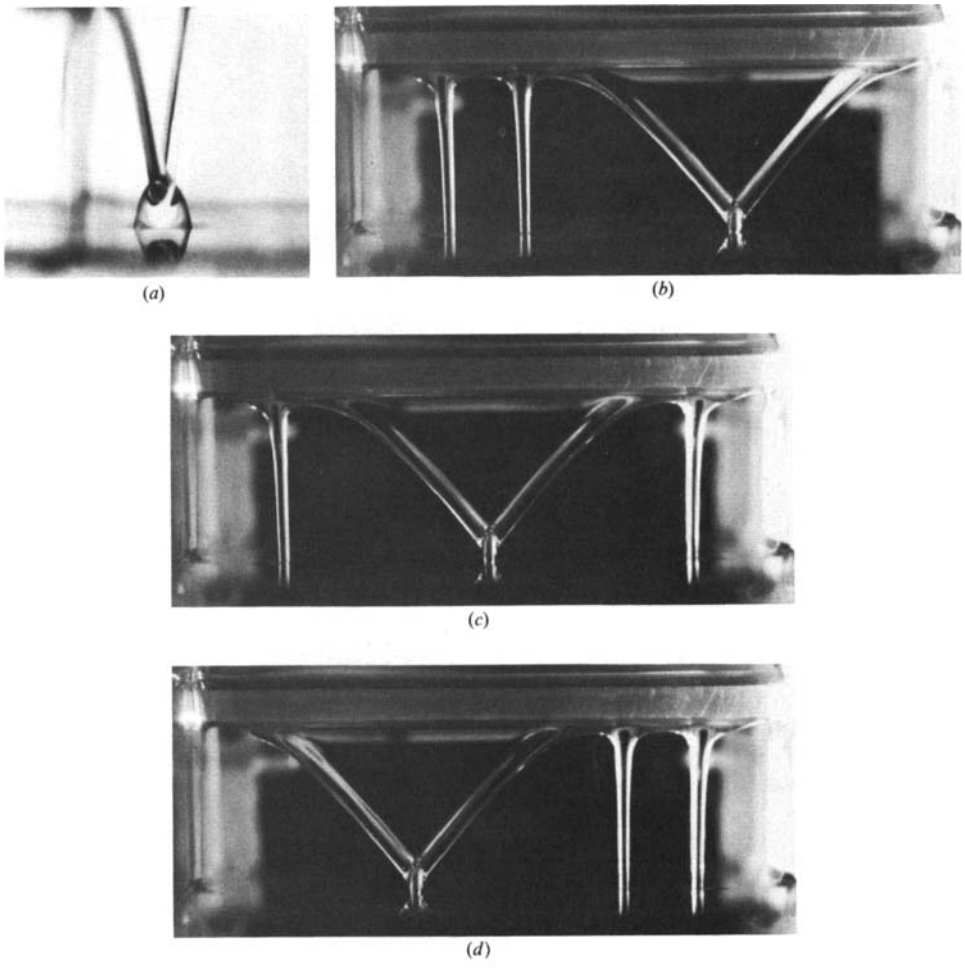

FIGURE 22. Some steady (2C + T) flows. (*a*) A side view of the junction of the two arms of the T-section at $R = 1.67$, $S = 12.1$, $h = 3.51$ mm, $\nu = 0.791$ St; (*b*) is a (CCT) flow, (*c*) is (CTC) flow and (*d*) is a (TCC) flow, all at $R = 1.73$, $S = 11.8$, $h = 3.55$ mm, $\nu = 0.789$ St.

the two arms of the T-section came together to form a kind of fan shape in the plane orthogonal to the plane of the triangular T-section.

Further examples from the branch of steady (CTC) flows are given in figure 23. This branch lost stability with increasing flow rate at $R = 2.06$, $S = 10.4$, $h = 3.79$ mm, $\nu = 0.798$ St to the steady (CT) flow shown in figure 23 (*c*). The branch lost stability with decreasing flow rate at $R = 1.64$, $S = 12.1$, $h = 3.51$ mm, $\nu = 0.798$ St to a branch of unsteady (CTC) flows, an example of which is given in figure 24. Shown there is a sequence of photographs, under fixed operating conditions for the flow, which illustrates the rather violent nature of the gyrations of the central T-section of the pattern, while the C-streams at either side remained essentially unperturbed by the proceedings. This branch of unsteady (CTC) flows collapsed at $R = 1.55$, $S = 12.5$, $h = 3.45$ mm, $\nu = 0.798$ St to an unsteady (CCTC) pattern, and this changed spontaneously after about $2\frac{1}{2}$ min to a steady (7C) flow.

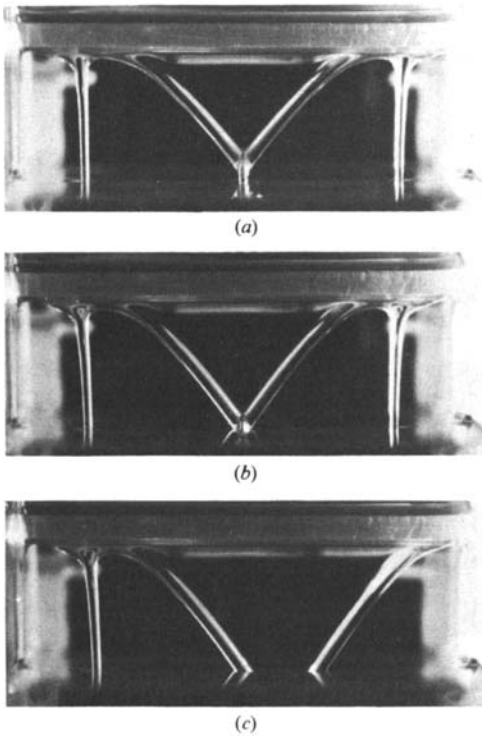

(a)

(b)

(c)

FIGURE 23. Examples from the branch of steady (CTC) flows. (a) $R = 1.71$, $S = 11.7$, $h = 3.56$ mm, $\nu = 0.798$ St; (b) $R = 1.94$, $S = 10.7$, $h = 3.72$ mm, $\nu = 0.799$ St; (c) the steady (CTC) flows lost stability to this steady (CT) flow at $R = 2.06$, $S = 10.4$, $h = 3.79$ mm, $\nu = 0.798$ St.

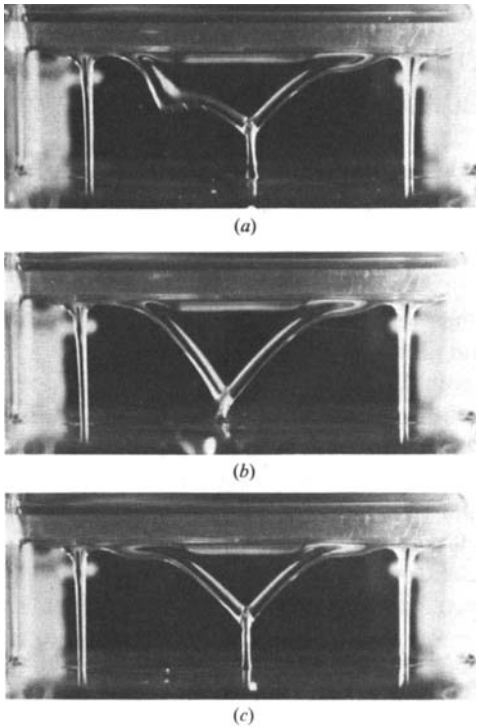

(a)

(b)

(c)

FIGURE 24. A sequence in time of the unsteady (CTC) flow at $R = 1.56$, $S = 12.5$, $h = 3.46$ mm, $\nu = 0.798$ St.

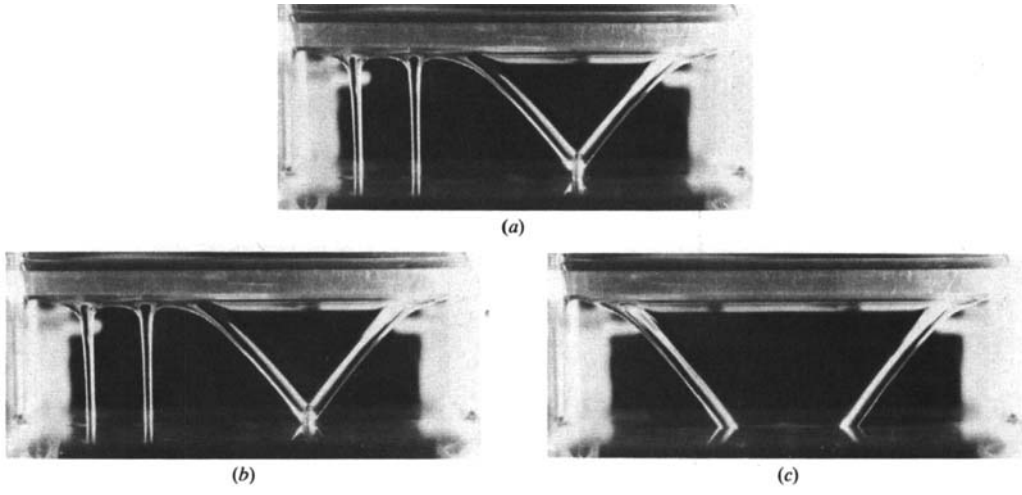

FIGURE 25. Examples from the branch of steady (CCT) flows. (*a*) $R = 1.68$, $S = 11.9$, $h = 3.53$ mm, $\nu = 0.795$ St; (*b*) $R = 1.78$, $S = 11.5$, $h = 3.60$ mm, $\nu = 0.795$ St; (*c*) the branch of flows lost stability to this steady (T) flow at $R = 1.91$, $S = 10.9$, $h = 3.69$ mm, $\nu = 0.796$ St.

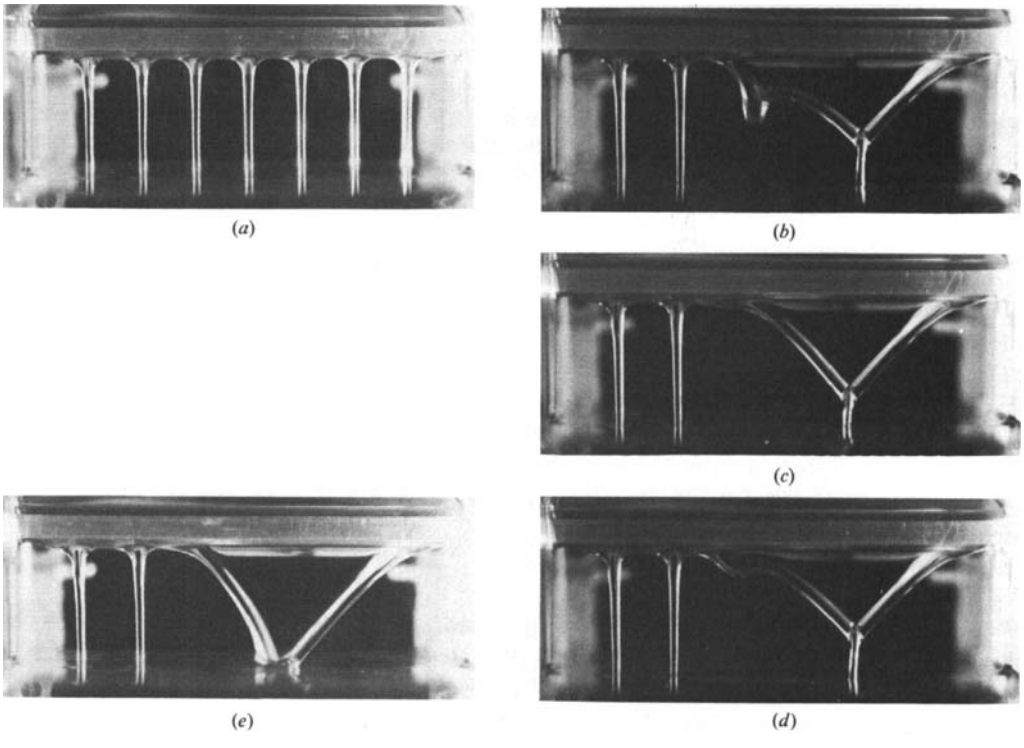

FIGURE 26. Unsteady (CCT) flows. (*a*) Stability was lost to this (7C) flow at $R = 1.59$, $S = 12.3$, $h = 3.47$ mm, $\nu = 0.795$ St; (*b*), (*c*) (*d*) are a sequence in time of an unsteady (CCT) flow at $R = 1.54$, $S = 12.7$, $h = 3.42$ mm, $\nu = 0.792$ St; (*e*) unsteady (CCT) flow at $R = 1.50$, $S = 12.9$, $h = 3.40$ mm, $\nu = 0.794$ St.

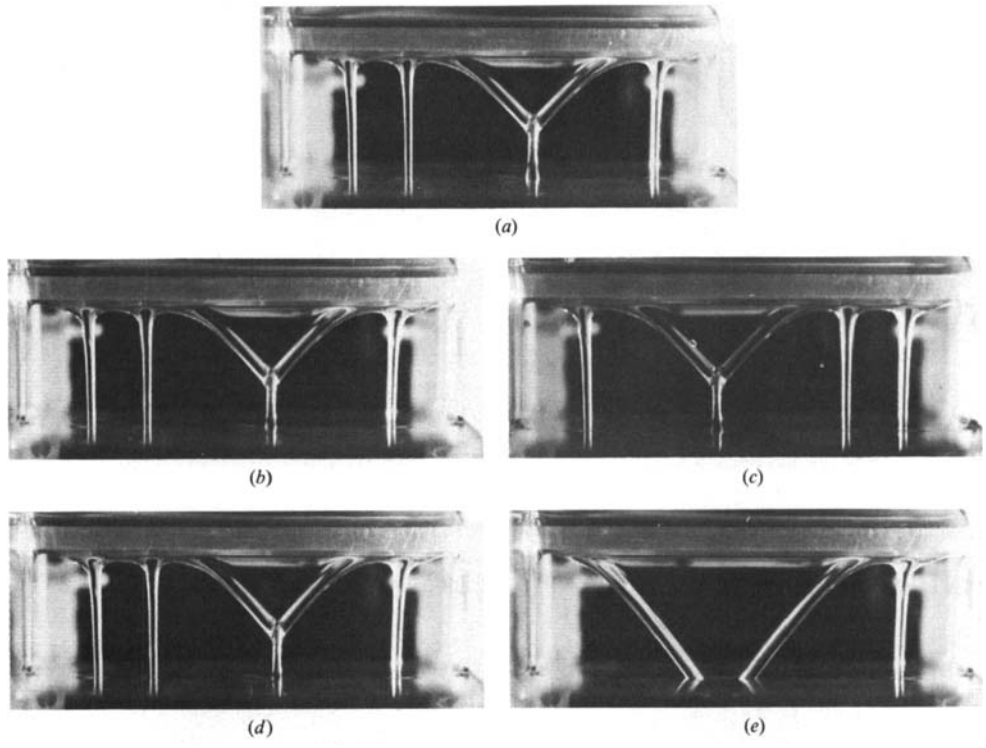

FIGURE 27. Steady (3C+T) flows. (*a*) (CCTC) flow at $R = 1.67, S = 11.9, h = 3.54$ mm, $\nu = 0.801$ St; (*b*) (CCTC) flow at $R = 1.73$, $S = 11.5$, $h = 3.59$ mm, $\nu = 0.802$ St; (*c*) (CTCC) flow at $R = 1.77$, $S = 11.7, h = 3.57$ mm, $\nu = 0.788$ St; (*d*) (CCTC) flow at $R = 1.82, S = 11.2, h = 3.65$ mm, $\nu = 0.802$ St; (*e*) the branch of steady (CCTC) flows lost stability to this steady (TC) flow at $R = 1.86$, $S = 11.0$, $h = 3.68$ mm, $\nu = 0.802$ St.

Flows of the (CCT) kind had similar properties to those just described. The branch of steady (CCT) flows, typified by the photographs of figure 25, lost stability with increasing flow rate at $R = 1.91$, $S = 10.9$, $h = 3.69$ mm, $\nu = 0.796$ St to the steady (T) flow shown in figure 25 (*c*). As the flow rate was decreased the steady (CCT) flow developed into an unsteady motion at $R = 1.59$, $S = 12.3$, $h = 3.47$ mm, $\nu = 0.795$ St (see figure 26*e*). Another example of an unsteady (CCT) flow is shown in figures 26 (*b–d*) in a sequence of photographs taken at a given operating state. The branch of unsteady (CCT) flows lost stability at $R = 1.50$, $S = 12.9$, $h = 3.40$ mm, $\nu = 0.794$ St to the steady (7C) flow shown in figure 26 (*a*).

4.2.9. (3*C*+*T*) *flows*

Flows involving three continuous jets of liquid and one T-section were found to be stable at flow rates equivalent to R lying between about 1.5 and 1.8. Examples of steady (CCTC) flows are given in figure 27 (*a*, *b*, *d*), and an example of a steady (CTCC) flow is shown in figure 27 (*c*). The branch of steady (CCTC) flows lost stability with increasing flow rate at $R = 1.86$, $S = 11.0$, $h = 3.68$ mm, $\nu = 0.802$ St to the steady (TC) flow shown in figure 27 (*e*). On decreasing the flow rate, the branch developed into an unsteady, chaotic type of motion at parameter values near $R = 1.60$, $S = 12.2$, $h = 3.49$ mm, $\nu = 0.801$ St, some examples of the flow at these conditions being given in figure 28 (*e*, *f*). Most of the unsteadiness in this flow was associated with pulsations

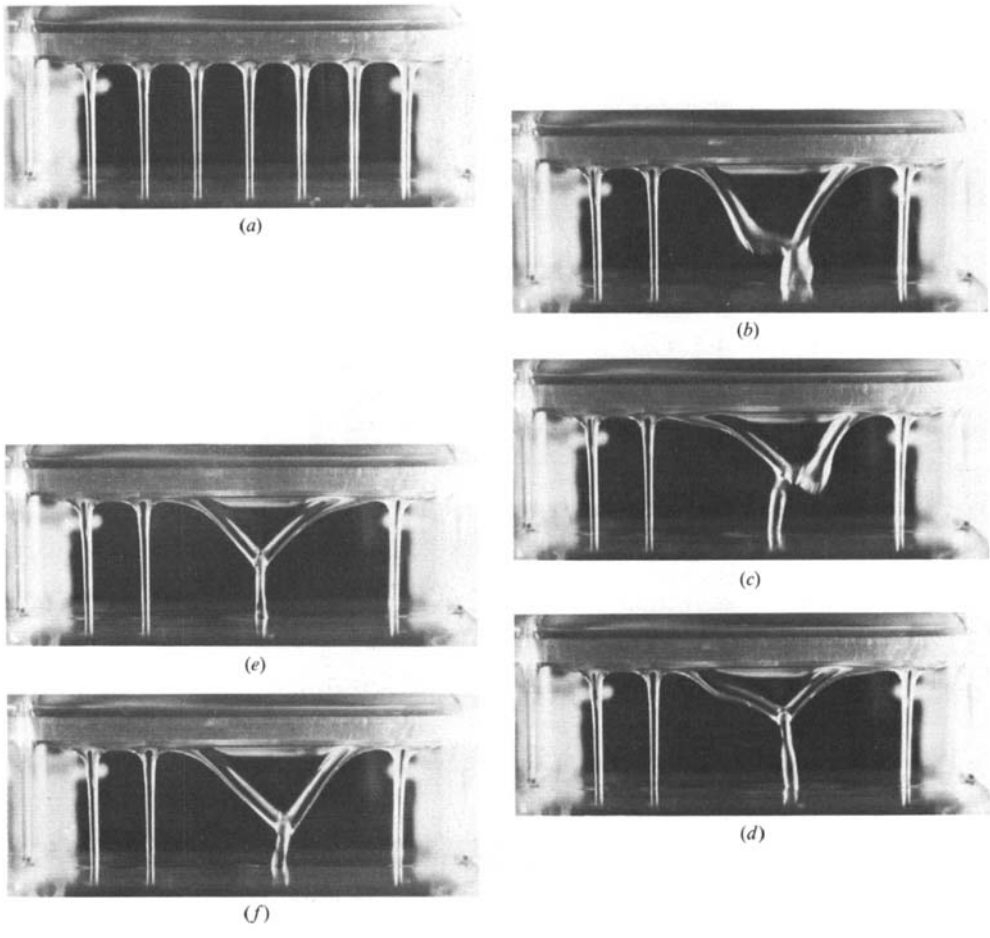

FIGURE 28. Unsteady (CCTC) flows. (*a*) The branch of flows lost stability to this steady (7C) flow at $R = 1.48$, $S = 12.9$, $h = 3.40$ mm, $\nu = 0.799$ St; (*b*), (*c*), (*d*): $R = 1.58$, $S = 12.4$, $h = 3.47$ mm, $\nu = 0.797$ St; (*e*), (*f*): $R = 1.60$, $S = 12.2$, $h = 3.49$ mm, $\nu = 0.801$ St.

of the triangular section or with sideways movements of the 'leg' beneath the triangular section, both features of which are evident in the temporal sequence of photographs shown in figure 28 (*b–d*). In spite of the vigorous motions exhibited by this flow, the pattern, nevertheless, preserved its overall coherence, returning from time to time to a nearly steady (CCTC) flow. This branch of unsteady (CCTC) flows lost stability at $R = 1.48, S = 12.9, h = 3.40$ mm, $\nu = 0.799$ St to the steady (7C) flow shown in figure 28 (*a*).

All attempts to produce a pattern of the form (TCCC) or (CCCT) were unsuccessful.

4.2.10. $(4C+T)$ *flows*

The only flow patterns within this class of flows that I was able to establish were those of the form (CCTCC), some examples of the steady version of this flow being given in figure 29. This branch of flows lost stability, with increasing flow rate, at $R = 1.91$, $S = 11.1$, $h = 3.66$ mm, $\nu = 0.787$ St to the steady (T) flow shown in figure 29 (*d*). On decreasing the flow rate the flow developed an unsteady, chaotic type of motion at values of the parameters near $R = 1.62$, $S = 12.4$, $h = 3.47$ mm,

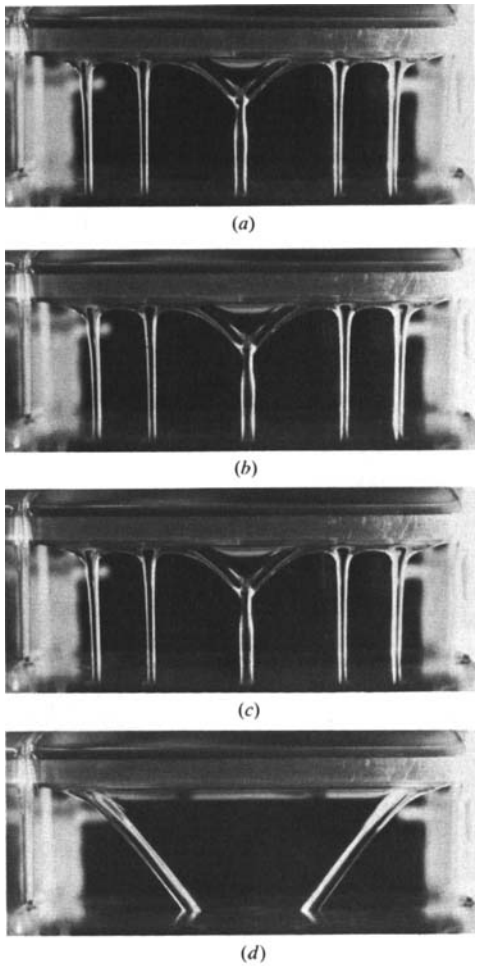

FIGURE 29. Steady (CCTCC) flows. (*a*) $R = 1.70$, $S = 12.0$, $h = 3.53$ mm, $\nu = 0.787$ St; (*b*) $R = 1.80$, $S = 11.5$, $h = 3.59$ mm, $\nu = 0.788$ St; (*c*) $R = 1.84$, $S = 11.3$, $h = 3.62$ mm, $\nu = 0.788$ St; (*d*) the branch of flows lost stability to this steady (T) flow at $R = 1.91$, $S = 11.1$, $h = 3.66$ mm, $\nu = 0.787$ St.

$\nu = 0.787$ St. The nature of the unsteadiness of the pattern at these conditions is indicated in figures 30(*f*, *g*), and a more vigorous form of the unsteadiness is illustrated by the photographs of figures 30(*c*–*e*). This sequence shows how the 'leg' of the triangular section might undergo sideways oscillations, or how the triangular section itself might pulse 'up and down'. This branch of unsteady (CCTCC) flows lost stability at $R = 1.53$, $S = 12.6$, $h = 3.43$ mm, $\nu = 0.798$ St to the steady (7C) flow shown in figure 30(*b*). An early stage in the transition to the steady (7C) flow is shown in figure 30(*a*).

4.2.11. *(TCT) flow*

At flow rates equivalent to R lying between roughly 1.6 and 1.9 there was found a branch of unsteady, chaotic type of flows consisting of two T-portions separated

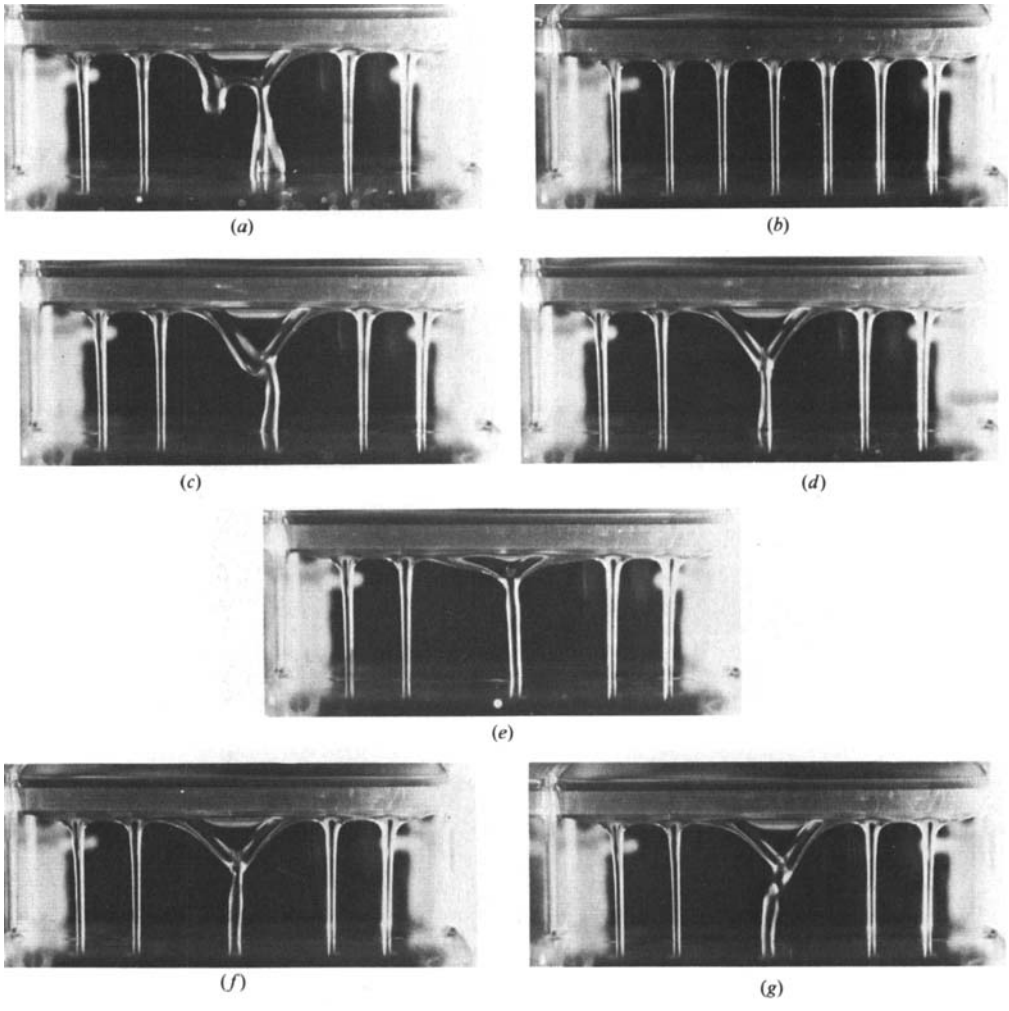

FIGURE 30. Unsteady (CCTCC) flows. (*a*), (*b*): $R = 1.53$, $S = 12.6$, $h = 3.43$ mm, $\nu = 0.798$ St. (*a*) is an early phase in the development of the steady (7C) flow shown in (*b*); (*c*), (*d*), (*e*): $R = 1.56$, $S = 12.5$, $h = 3.46$ mm, $\nu = 0.798$ St; (*f*), (*g*): $R = 1.62$, $S = 12.4$, $h = 3.47$ mm, $\nu = 0.787$ St.

by a continuous jet of liquid. These flows were seen only in an unsteady form and there appeared not to be an associated branch of steady flows of this pattern. Examples of the (TCT) flows are given in figure 31. At each operating condition a pair of photographs is included to indicate the nature of the unsteadiness. Thus, not only did the triangular section pulsate as in previous flows, but the central jet also moved to and fro in the plane of the falling liquid. On increasing the flow rate this branch of flows lost stability at $R = 1.90$, $S = 11.0$, $h = 3.67$ mm, $\nu = 0.793$ St to the steady (T) flow shown in figure 31 (*h*). On reducing the flow rate the (TCT) flows lost stability at $R = 1.54$, $S = 12.7$, $h = 3.43$ mm, $\nu = 0.792$ St to the (CCT) flow shown in figure 31 (*a*), which was also an unsteady motion.

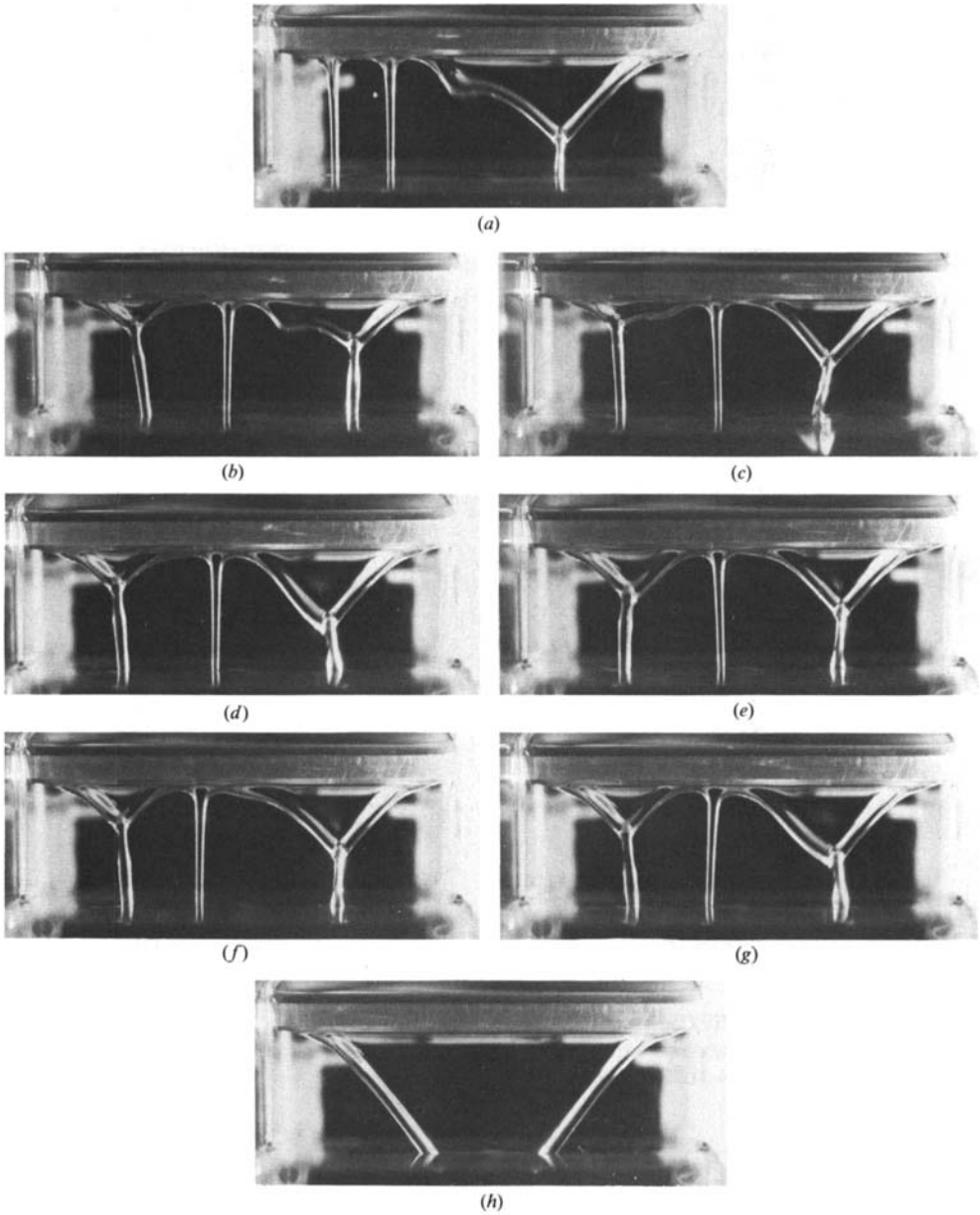

FIGURE 31. Examples from the branch of (TCT) flows. (*a*) The branch of flows lost stability to this unsteady (CCT) flow at $R = 1.54$, $S = 12.7$, $h = 3.43$ mm, $\nu = 0.792$ St; (*b*), (*c*): $R = 1.55$, $S = 12.6$, $h = 3.43$ mm, $\nu = 0.792$ St; (*d*), (*e*): $R = 1.75$, $S = 11.8$, $h = 3.55$ mm, $\nu = 0.786$ St; (*f*), (*g*): $R = 1.86$, $S = 11.2$, $h = 3.65$ mm, $\nu = 0.793$ St; (*h*) the branch of flows lost stability to this steady (T) flow at $R = 1.90$, $S = 11.0$, $h = 3.67$ mm, $\nu = 0.792$ St.

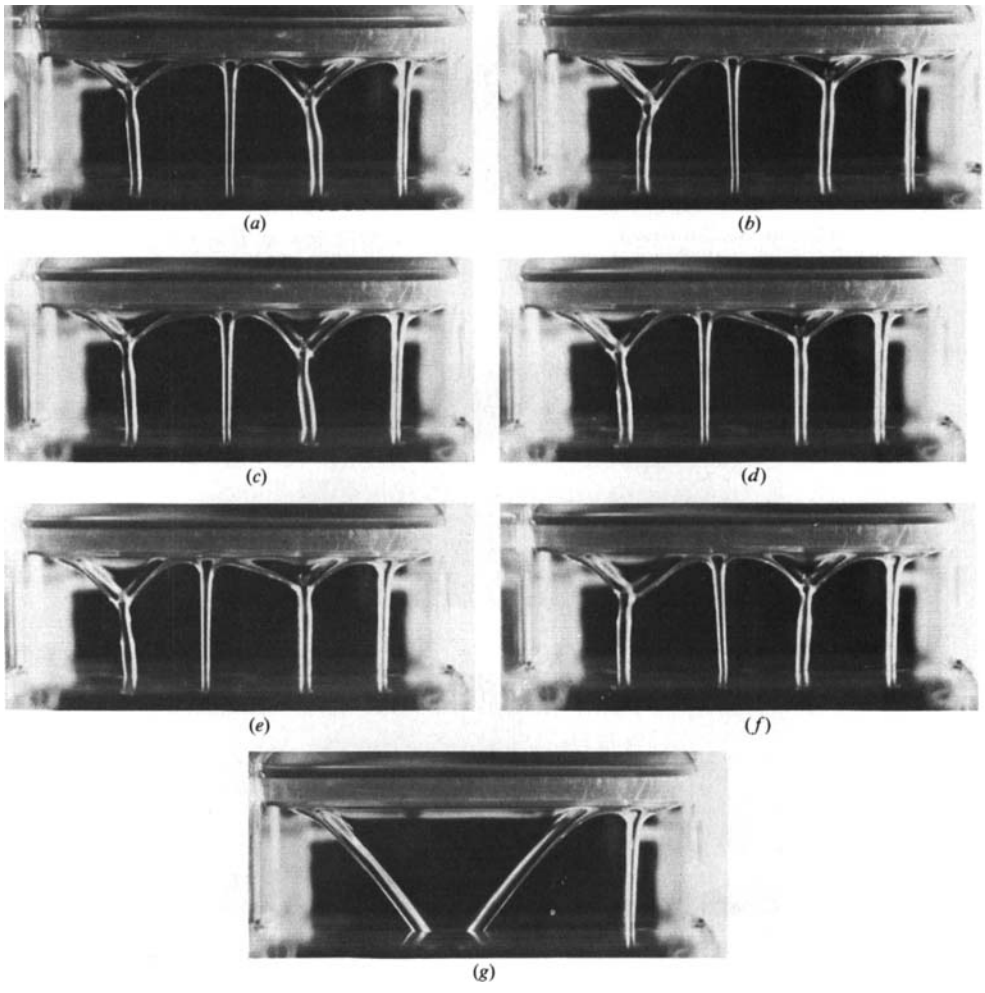

FIGURE 32. Examples from the branch of (TCTC) flows. (*a*), (*b*): $R = 1.68$, $S = 11.9$, $h = 3.54$ mm, $\nu = 0.797$ St; (*c*), (*d*): $R = 1.76$, $S = 11.5$, $h = 3.59$ mm, $\nu = 0.796$ St; (*e*), (*f*): $R = 1.82$, $S = 11.3$, $h = 3.63$ mm, $\nu = 0.795$ St; (*g*) the branch of flows lost stability to this steady (TC) flow at $R = 1.88$, $S = 11.1$, $h = 3.67$ mm, $\nu = 0.795$ St.

4.2.12. $(2T+2C)$ *flows*

As in the case of (TCT) flows, the present class of flows were observed only as unsteady motions. One such flow, a (TCTC) flow, is illustrated in figure 32. The unsteadiness in this flow, which is apparent by comparisons between the pairs of photographs at the same operating conditions, took the form of a pulsation of the two T-sections on a timescale of about 1 s or so, and of a wandering to-and-fro of the C-stream between the two T-sections on a timescale of around 10 to 15 s; the right-hand jet remained relatively unperturbed. This branch of flows lost stability, with increasing flow rate, at $R = 1.88$, $S = 11.1$, $h = 3.67$ mm, $\nu = 0.795$ St to the steady (TC) flow shown in figure 32(*g*). Unfortunately I did not determine how the branch of (TCTC) flows lost stability with decreasing flow rate, but it appeared as

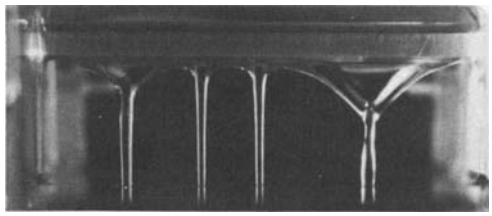

FIGURE 33. An example of an unsteady (TCCT) flow at $R = 1.76$, $S = 11.7$, $h = 3.57$ mm, $\nu = 0.788$ St.

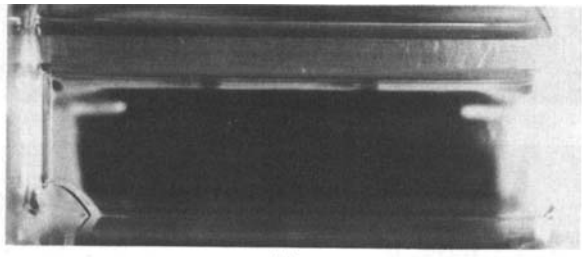

(a)

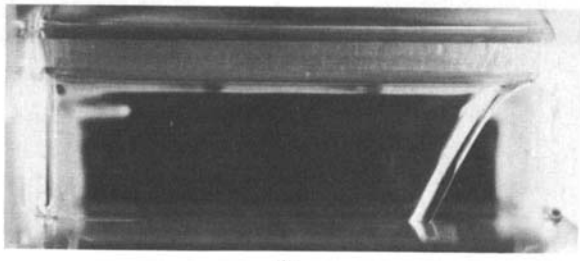

(b)

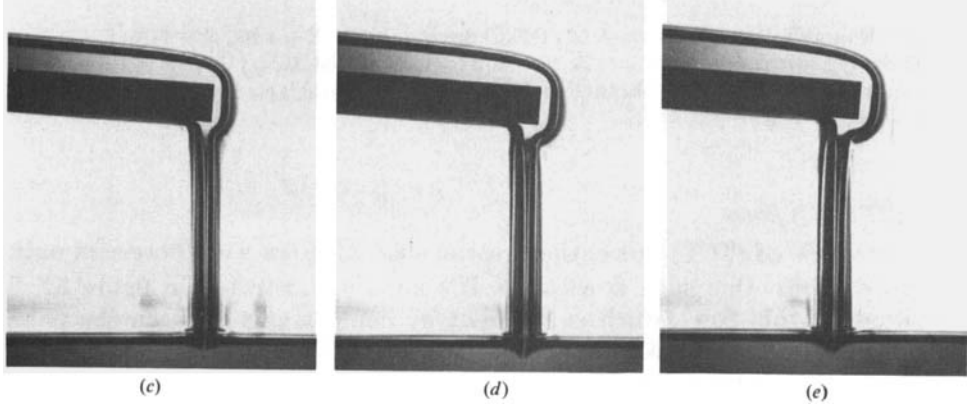

(c) (d) (e)

FIGURE 34. Some partially attached flows. (a) (QA) flow and (b) (A($\frac{1}{2}$T)) flow at $R = 3.95$, $S = 6.73$, $h = 4.70$ mm, $\nu = 0.796$ St. (c), (d) and (e) are side views: (c) (A($\frac{1}{2}$T)) flow at $R = 2.19$, $S = 10.8$, $h = 3.71$ mm, $\nu = 0.748$ St; (d) (($\frac{1}{2}$T)A) flow at $R = 3.50$, $S = 7.94$, $h = 4.33$ mm, $\nu = 0.746$ St; (e) (($\frac{1}{2}$T)A) flow at $R = 4.67$, $S = 6.59$, $h = 4.75$ mm, $\nu = 0.744$ St.

though the branch of (CTCT) flows lost stability to a steady (CCT) pattern at values of the parameters of approximately $R = 1.72$, $S = 11.8$, $h = 3.55$ mm, $\nu = 0.792$ St.

On one occasion I was able to establish a (TCCT) flow but subsequently I was unable to manipulate the conditions to re-establish this flow. The (TCCT) flow that was observed (see figure 33) was an unsteady flow and, in spite of apparently having a small 'domain of attraction', seemed to be quite a stable motion as it persisted for over 15 minutes, at which time a different flow was induced.

4.2.13. *Partially attached flows*

As the flow was increased in this experiment there was a tendency for the fluid more and more to fall as a curtain, or sheet, of liquid. This was apparent with the class of (T) flows described above and is further exemplified in the classes of motions to be described. Indeed, once the flow rate was sufficiently large it was possible to establish a flow with the 'sheet' attached to one wall of the reservoir, but not necessarily to both walls, and at even larger flow rates only those flows with the 'sheet' attached to both walls were possible. States with the 'sheet' attached to one wall only will be referred to as partially attached flows, some examples of which are given in figure 34. The liquid 'curtain' in figure 34(*a*) was attached to the right-hand wall and a small 'quadrant' of the sheet was left open at the corner near the free surface in the reservoir at the left-hand wall; flows of this kind will be referred to as (QA) flows. The photograph in figure 34(*b*), taken at the same parameter settings as for (*a*), shows the liquid curtain attached to the left-hand wall, with the right-hand boundary of the curtain having the appearance of the right-hand half of a (T) flow. Such flows will therefore be denoted as (A($\frac{1}{2}$T)) flows.

Some side views of these kinds of flows are shown in figure 34(*c–e*), from which it is apparent that the attachment line with the plate was on the underside, well behind the lower corner of the plate. Partially attached flows were found over a rather wide range of flow rates, as indicated in figure 13. They were all steady motions.

4.2.14. *Quadrant flows*

The term 'quadrant flow' has been used to indicate those flows in which a free boundary of the liquid curtain attached to a side wall of the reservoir, leaving a 'hole' in the curtain shaped somewhat like a quadrant of a circle. Examples of such flows have already been given under the heading of 'partially attached flows' and three further examples showing a (Q($\frac{1}{2}$T)), a (QQ) and a (($\frac{1}{2}$T)Q) flow, all established at the same operating conditions, are given in figure 35. All the flows observed within this class were steady.

The structure of the branch of (QQ) flows is illustrated in the collection of photographs in figure 36. As the flow rate was increased, the attachment points of the 'quadrants' moved down the side walls leaving increasingly smaller 'holes' in the liquid curtain – only very small holes remained at the conditions for figure 36(*g*) – until eventually a complete, unbroken sheet had formed at a flow rate corresponding approximately to $R = 6.33$, $S = 5.27$, $h = 5.31$ mm, $\nu = 0.755$ St. On decreasing the flow rate the attachment points moved up the sidewalls of the reservoir until, with $R = 4.18$, $S = 6.93$, $h = 4.63$ mm, $\nu = 0.756$ St, the attachment point of the right-hand quadrant had reached the plate (cf. figure 36*a*). It is interesting that a reduction in flow rate of about 10% accounted for the relatively small changes evident between (*c*) and (*b*) of figure 36, whereas the flow rates for (*b*) and (*a*) differed by only about 1.5%. Some side views of (QQ) flows are shown in

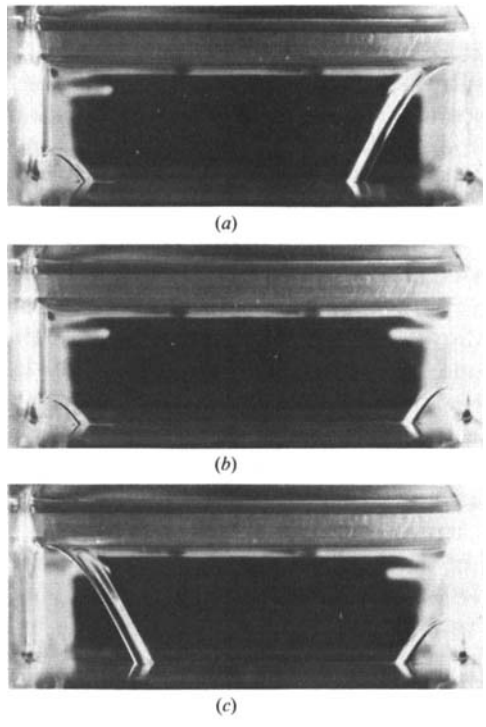

FIGURE 35. Examples of quadrant flows at $R = 3.95$, $S = 6.73$, $h = 4.70$ mm, $\nu = 0.796$ St. (*a*) (Q($\frac{1}{2}$T)) flow; (*b*) (QQ) flow; (*c*) (($\frac{1}{2}$T)Q) flow.

figure 36 (*d* and *e*): in (*d*) the 'quadrant' attached to the near wall at about half way between the plate and the level in the reservoir; in (*e*) the attachment to the near wall was very close to the junction with the free surface.

Examples from the branch of (($\frac{1}{2}$T)Q) flows are given in figure 37. This branch lost stability, with decreasing flow rate, to the steady (T) flow shown in figure 37 (*a*) and, with increasing flow rate at $R = 4.50$, $S = 6.16$, $h = 3.58$ mm, $\nu = 0.796$ St, to a (QQ) flow. The sensitivity of these flows to parameters other than R is indicated by a comparison between figures 37 (*c*) and (*d*), taken at nearly the same value of R but with quite different fluid viscosities.

4.2.15. *Lower-face flows*

As the flow rate was increased a stage was reached, as described above, when the liquid curtain completely spanned the reservoir as an unbroken sheet, disconnecting the region in front of the curtain from that behind. When these circumstances prevailed, the cavity behind the curtain, which was bounded by the walls of the reservoir, the plate, the free surface in the reservoir and the curtain itself, was vented to the atmosphere to equalize the pressure on either side of the curtain. This was done by bending a piece of 1 cm-bore copper tubing in the form of a 'U' so that it hugged the front and rear walls and the bottom of the reservoir. Being well away from the zone at which the liquid sheet penetrated the free surface of the reservoir, this tube had negligible effect on the flow field in the reservoir.

The view looking towards the end of the plate revealed very little for this class

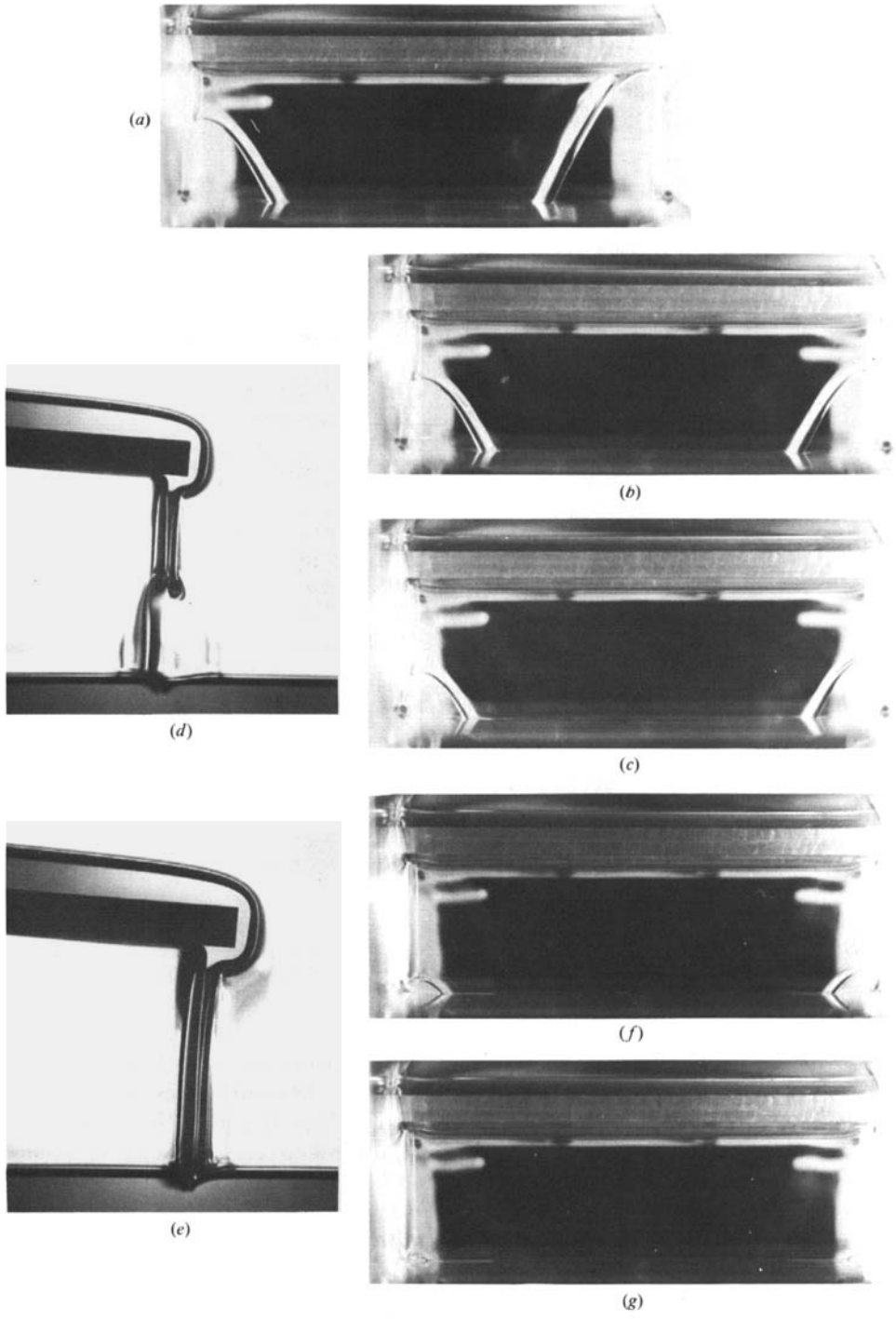

FIGURE 36. The branch of steady (QQ) flows. (*a*) The (QQ) flows lost stability to this (Q($\frac{1}{2}$T)) flow at $R = 4.18$, $S = 6.93$, $h = 4.63$ mm, $\nu = 0.756$ St; (*b*) $R = 4.24$, $S = 6.84$, $h = 4.66$ mm, $\nu = 0.758$ St; (*c*) $R = 4.65$, $S = 6.42$, $h = 4.81$ mm, $\nu = 0.759$ St; (*d*) side view at $R = 4.67$, $S = 6.59$, $h = 4.75$ mm, $\nu = 0.744$ St; (*e*) side view at $R = 5.54$, $S = 5.65$, $h = 5.13$ mm, $\nu = 0.766$ St; (*f*) $R = 5.61$, $S = 5.71$, $h = 5.10$ mm, $\nu = 0.755$ St; (*g*) $R = 6.12$, $S = 5.39$, $h = 5.25$ mm, $\nu = 0.755$ St.

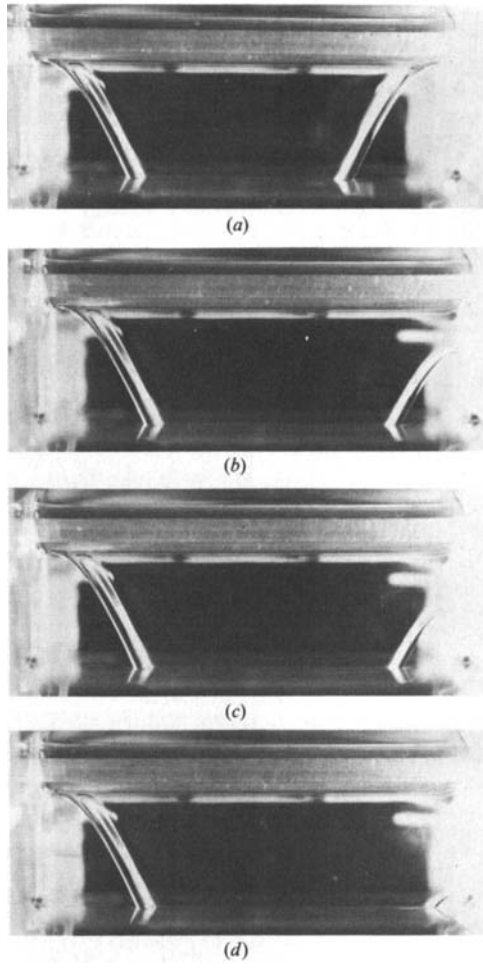

FIGURE 37. The branch of steady ($(\frac{1}{2}$T)Q) flows. (*a*) The ($(\frac{1}{2}$T)Q) flows lost stability to this (T) flow at $R = 4.15$, $S = 6.93$, $h = 4.63$ mm, $\nu = 0.759$ St; (*b*) $R = 4.25$, $S = 6.81$, $h = 4.67$ mm, $\nu = 0.760$ St; (*c*) $R = 4.46$, $S = 6.59$, $h = 4.75$ mm, $\nu = 0.761$ St; (*d*) $R = 4.47$, $S = 6.20$, $h = 4.90$ mm, $\nu = 0.796$ St.

of flows, and so we shall try to characterize them from their appearance from the side, using the position of the attachment line of the free surface on the underside of the plate as a distinguishing feature of the flow. Thus, the term 'lower-face flow' is used to refer to those flows for which a falling, unbroken sheet of liquid completely spanned the reservoir and for which the line of attachment of the free surface with the plate was on the lower face of the plate. One such branch of flows, to be denoted (LF1) flows, is illustrated in figure 38. This branch of flows arose naturally from the class of 'quadrant flows' at around a flow rate equivalent to $R = 6.3$. Once established, however, the branch of (LF1) flows was stable down to a flow rate approximately equivalent to $R = 2.59$, $S = 9.10$, $h = 4.04$ mm, $\nu = 0.784$ St. Unfortunately I do not have any photographs of side views of (LF1) flows at values of R smaller than that applying to figure 38(*a*), namely $R = 3.50$, but the appearance of these flows was not very different from the photographs shown in figures 34(*c*, *d*) for 'partially attached flows'.

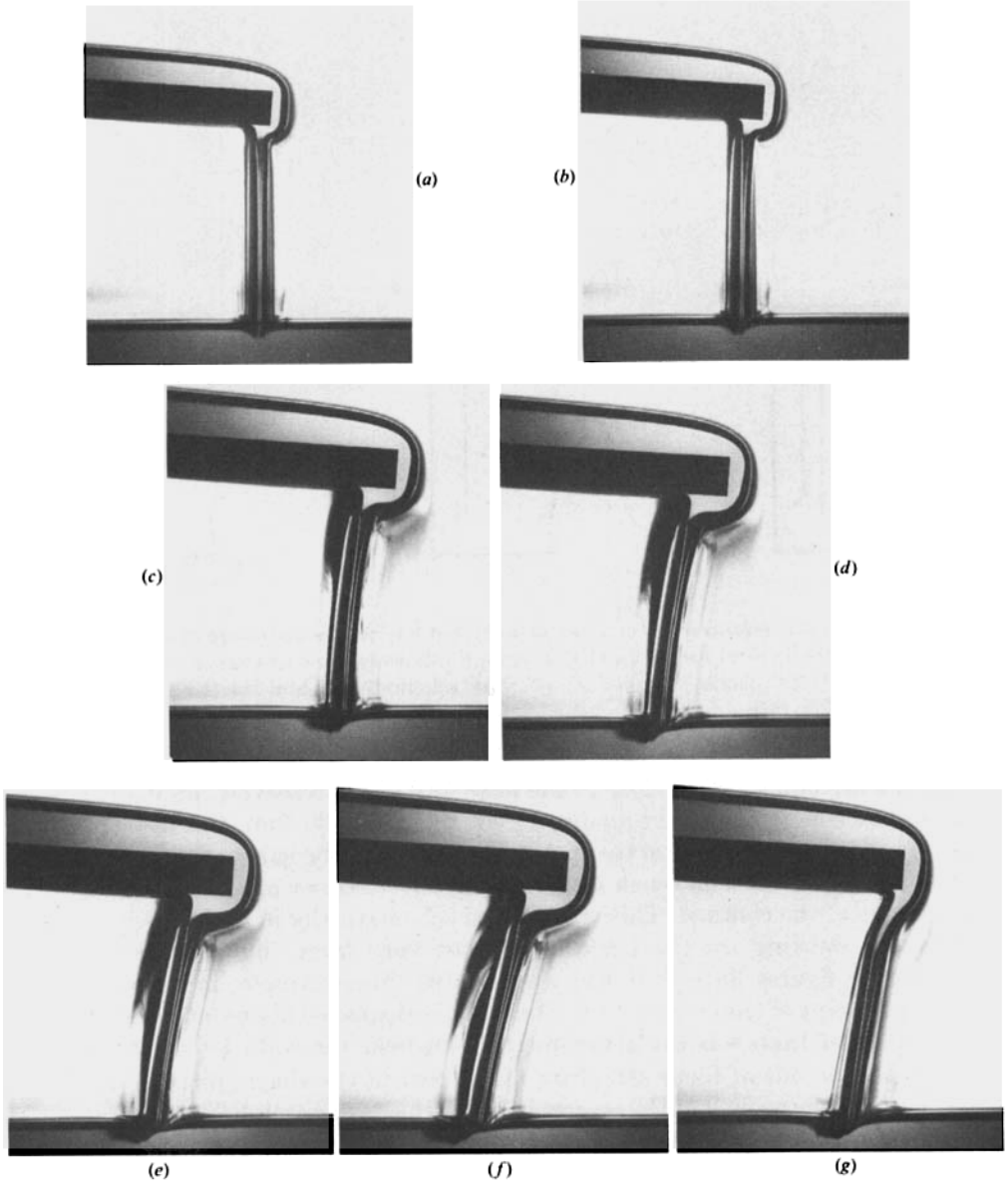

FIGURE 38. The branch of lower-face flows (LF1). (*a*) $R = 3.50, S = 7.94, h = 4.33$ mm, $\nu = 0.746$ St; (*b*) $R = 4.67$, $S = 6.59$, $h = 4.75$ mm, $\nu = 0.744$ St; (*c*) $R = 6.61$, $S = 5.07$, $h = 5.42$ mm, $\nu = 0.761$ St; (*d*) $R = 7.73$, $S = 4.63$, $h = 5.67$ mm, $\nu = 0.753$ St; (*e*) $R = 8.49$, $S = 4.37$, $h = 5.84$ mm, $\nu = 0.751$ St; (*f*) $R = 9.66$, $S = 4.03$, $h = 6.07$ mm, $\nu = 0.747$ St; (*g*) the branch of (LF1) flows lost stability to this (LF2) flow at $R = 10.1, S = 3.93, h = 6.15$ mm, $\nu = 0.745$ St. (Note: the magnifications for (*a*) and (*b*) differ slightly from those for (*c*)–(*g*).)

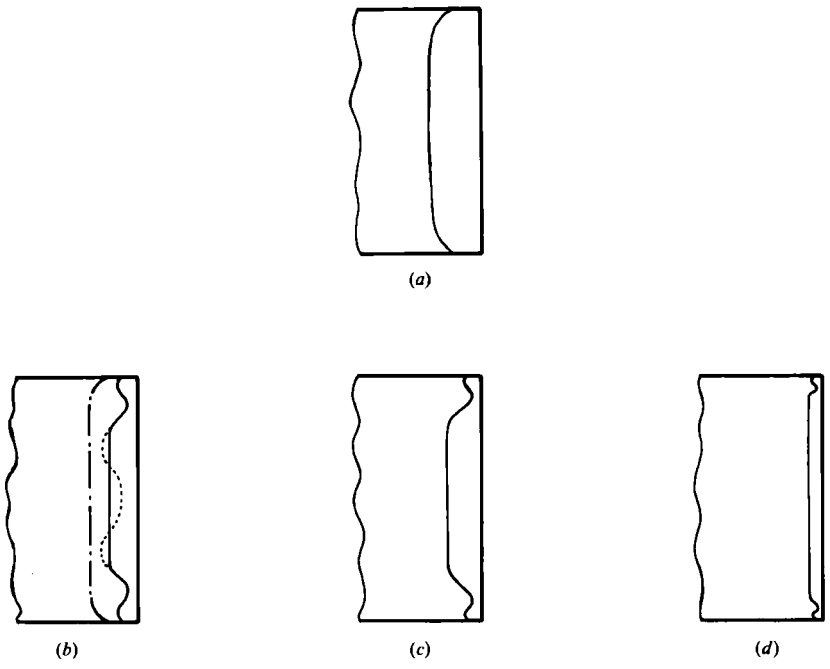

FIGURE 39. Schematic representation of the attachment line on the underside of the plate for (LF1) and (LF2) flows. (*a*) Typical profile for (LF1) flows; (*b*) showing the transition (-----) from an (LF2) profile (—) to an (LF1) profile (–·–). (*b*), (*c*), (*d*) show schematically how the (LF2) profiles changed with increasing flow rate.

Being focused on a region close to the near wall of the reservoir, photographs such as those shown in figure 38 give an incomplete picture of the flow. For these particular flows the liquid curtain was actually bowed, and near the sidewalls the attachment point of the meniscus was much closer to the lower corner of the plate than it was in the centre of the channel. This is indicated schematically in figure 39(*a*). In figure 38(*a*, *b*) the 'bowing' of the curtain was not very large, but for the conditions obtaining for figures 38(*c–f*) it was appreciable. For example, in figure 38(*d*) the attachment point at the centre of the channel was displaced about 0.6*a* to 0.7*a* further from the corner than was the attachment point near the wall. It is this effect that accounts for the out-of-focus structure to the rear of the sharp, focused lines of the meniscus on the near wall of the reservoir. Also, the dark patch below the free surface in the reservoir corresponds to the indentation of the free surface near the entry region for the curtain, and the lateral extent of this patch (note that, being out of focus, it too appears blurred) is indicative of the amount of bowing in the curtain.

FIGURE 40. The branch of lower-face flows (LF2). (*a*) The (LF2) flows lost stability at $R = 8.32$, $S = 4.49$, $h = 5.76$ mm, $\nu = 0.743$ St to this (LF1) flow; (*b*) $R = 8.67$, $S = 4.37$, $h = 5.83$ mm, $\nu = 0.742$ St; (*c*) $R = 9.57$, $S = 4.09$, $h = 6.03$ mm, $\nu = 0.743$ St; (*d*) $R = 11.5$, $S = 3.64$, $h = 6.39$ mm, $\nu = 0.741$ St; (*e*) $R = 13.1$, $S = 3.33$, $h = 6.69$ mm, $\nu = 0.741$ St; (*f*) $R = 15.4$, $S = 3.00$, $h = 7.04$ mm, $\nu = 0.739$ St; (*g*) $R = 17.3$, $S = 2.78$, $h = 7.31$ mm, $\nu = 0.738$ St; (*h*) $R = 19.7$, $S = 2.55$, $h = 7.63$ mm, $\nu = 0.737$ St; (*i*) $R = 21.9$, $S = 2.36$, $h = 7.94$ mm, $\nu = 0.742$ St; (*j*) $R = 25.3$, $S = 2.18$, $h = 8.26$ mm, $\nu = 0.733$ St; (*k*) $R = 27.8$, $S = 2.05$, $h = 8.52$ mm, $\nu = 0.732$ St; (*l*) the (LF2) flows lost stability to this (VF) flow at $R = 28.3$, $S = 2.02$, $h = 8.57$ mm, $\nu = 0.732$ St.

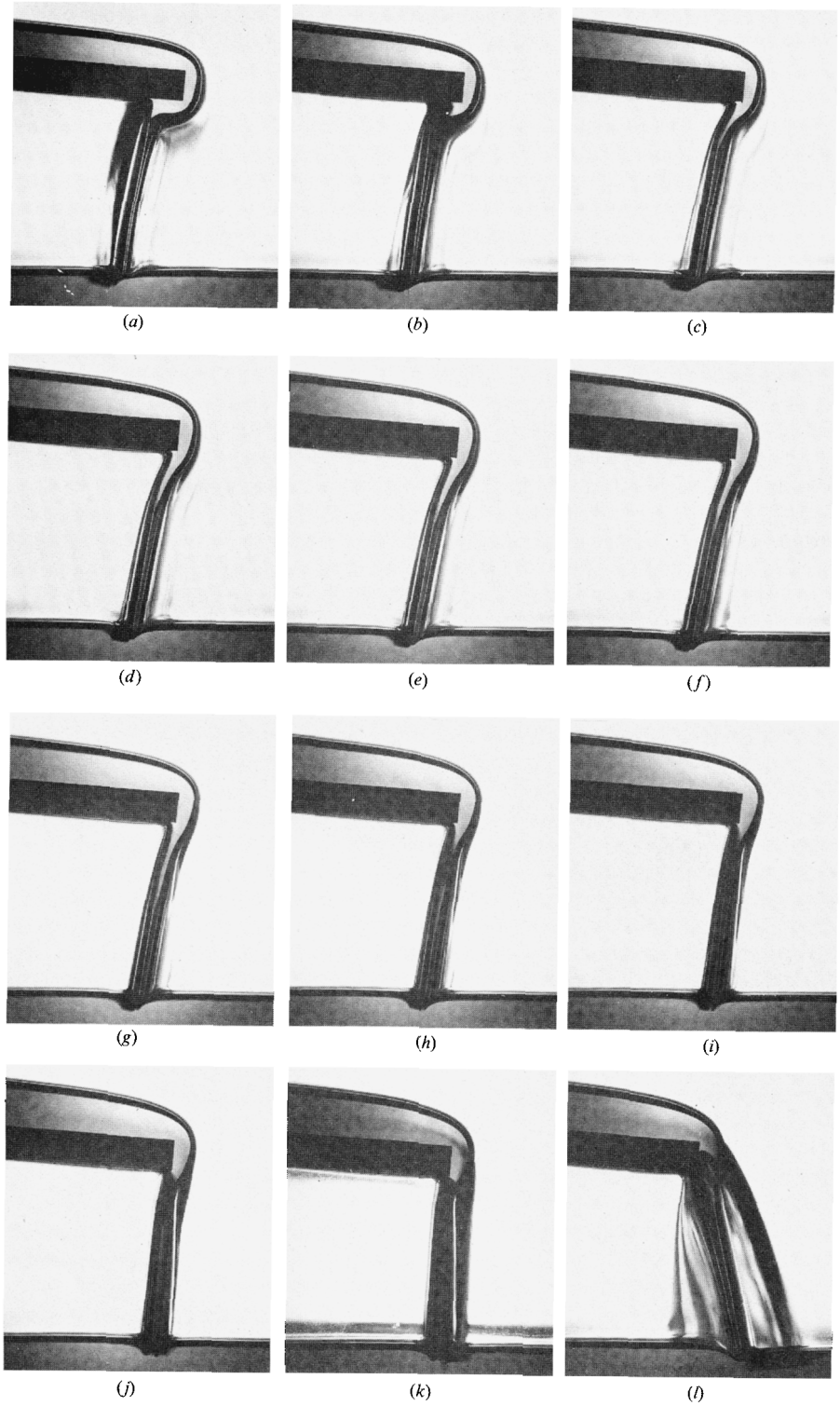

FIGURE 40. For description see facing page.

The attachment point of the free surface in the zone near the walls of the reservoir was approximately $0.57a$ from the corner of the plate when $R = 3.50$, as in figure 38(*a*). With $R = 4.67$, as for figure 38(*b*), this attachment point had moved to a distance of approximately $0.75a$ from the corner and, with $R = 6.61$, the distance had increased to about $0.98a$ (cf. figure 38*c*). Near the stability boundary for the branch of (LF1) flows, the attachment point close to the walls of the reservoir (see figure 38*f*) was about $1.15a$ from the corner of the plate. A small increase in the flow rate from the conditions obtaining for figure 38(*f*) brought about a major change in the flow structure, as indicated by figure 38(*g*), with the attachment point moving forward to a position only about $0.27a$ from the lower corner of the plate. This new branch of flows will be referred to as the (LF2) branch.

Examples of the (LF2) branch of flows are given in figure 40, the photographs being ordered by increasing flow rate (or equivalently by increasing R, since ν was nearly constant for the sequence). The (LF1) branch of flows lost stability to the (LF2) branch at $R = 10.1$, $S = 3.93$, $h = 6.15$ mm, $\nu = 0.745$ St, corresponding to operating conditions lying between (*c*) and (*d*) in the ordering of figure 40. As indicated above, the free surface attached much closer to the corner of the plate for the (LF2) flow shown in figure 38(*g*) than was the case for the (LF1) flow of figure 38(*f*). Another difference between (LF1) and (LF2) flows was the shape of the attachment line on the underside of the plate, a difference which is represented schematically in figure 39. Thus, the curvature of the profile of the attachment line for (LF1) flows was one-signed, whereas the profile for (LF2) flows had five local extrema (on an appropriate open interval). This difference accounts for an apparent slight 'fuzziness' of the free surface attaching to the underside of the plate in figure 38(*g*), and in the photographs of figure 40, compared with the sharp outline evident in figure 38(*f*), say. (*Aside*. My notes and my recollection of the experiment are consistent with the above description, but the texture of the curtain in figure 38(*f*) raises the possibility that the attachment profile of the (LF1) flow may have developed more 'structure' than I have indicated above, as the stability boundary was approached, 'anticipating' the transition to an (LF2) flow.)

After the (LF2) flow shown in figure 38(*g*) had been established, reductions in the flow rate brought about changes typified by figure 40(*c*, *b*), and represented schematically in figure 39 with regard to the attachment profile. When the flow rate was adjusted slightly below that obtaining for figure 40(*b*) the liquid curtain first developed an extra pair of corrugations, as indicated by the dashed 'attachment profile' shown in figure 39(*b*), and then the motion evolved into the (LF1) flow shown in figure 40(*a*).

Changes in the structure of the branch of (LF2) flows with increasing flow rate are exemplified in figure 40 (and cf. figure 39*b–d*). In particular, the attachment line on the underside of the plate moved closer and closer to the (lower) corner of the plate and the liquid curtain became more nearly vertical, until at the conditions obtaining for figure 40 (*k*) the attachment line was located very nearly at the corner of the plate. Then, a slight increase, of less than 2 %, in the flow rate resulted in a dramatic change in flow structure to that shown in figure 40(*l*), with the meniscus now attached to the (nearly) vertical face of the plate. This new class of flows will be referred to as (VF) flows.

4.2.16. *Vertical-face flows*

The transition from the branch of (LF2) flows to the (VF) flow shown in figure 40(*l*) is illustrated in figure 41. Here the end view of the flow shows the profile of the meniscus line on the (nearly) vertical face of the plate. When the branch of (LF2)

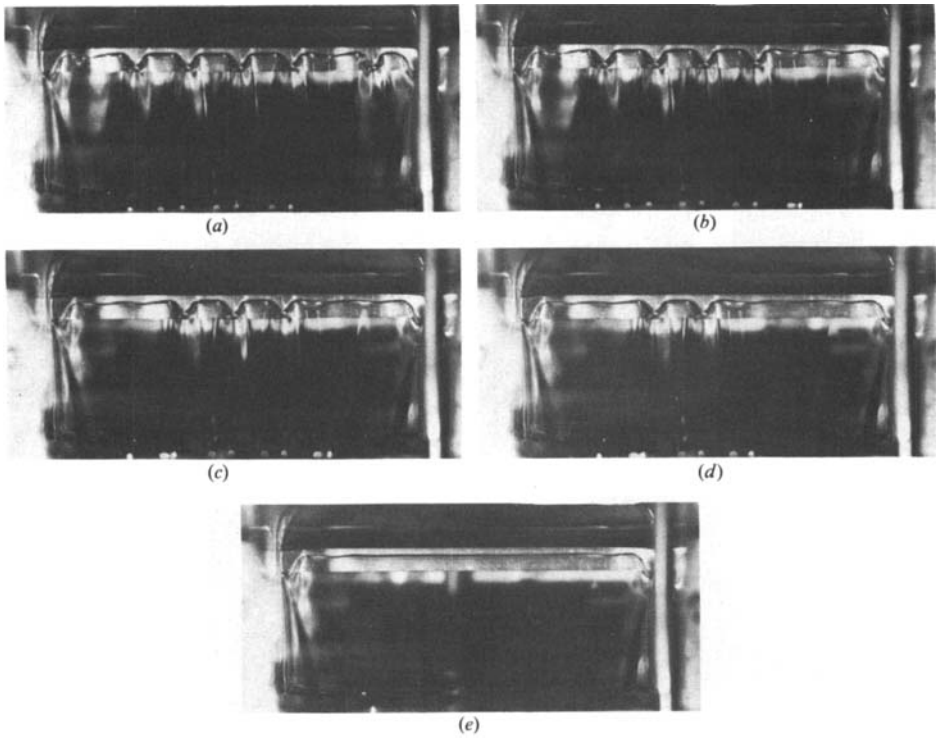

FIGURE 41: Phases in the transition from an (LF2) flow to a (VF) flow, as seen from an end view, at $R = 27.9$, $S = 1.94$, $h = 8.75$ mm, $\nu = 0.760$ St. (*a*) Flow with five corrugations; (*b*) photograph taken 140 s after (*a*), with four corrugations remaining; (*c*) photograph taken 190 s after (*b*), with three corrugations remaining; (*d*) photograph taken 60 s after (*c*), with two corrugations remaining; (*e*) photograph of steady VF(0) flow, taken 80 s after (*d*), shortly after all corrugations had disappeared.

flows lost stability, the meniscus line on the plate moved onto the end surface of the plate and developed a number of corrugations, as shown in figure 41 (*a*). But this corrugated structure evidently was not an equilibrium configuration, and the corrugation near the right-hand wall of the reservoir moved slowly towards this wall. On reaching the sharp gradient in the meniscus line near the wall of the reservoir, the corrugation disappeared, leaving a pattern of the form shown in figure 40 (*b*). Surface-tension forces precluded the flow of figure 40 (*b*) from being an equilibrium state, and slowly the corrugation near the left-hand wall moved sideways and disappeared in the same manner as above, leaving the pattern shown in figure 41 (*c*). The corrugation on the right-hand side was then lost in the same way (see figure 41 *d*). Finally the two remaining corrugations disappeared, not by moving to the edges of the reservoir but by diminishing in amplitude while remaining fixed horizontally, to leave the equilibrium pattern shown in figure 41 (*e*). The latter flow will be referred to as a (VF(0)) flow, the zero indicating that the attachment line on the end of the plate was not corrugated. (*Note*: the vertical tube, somewhat out of focus, in the foreground on the right-hand side of the photographs is part of the 'U-tube' used to equalize the pressure on the two sides of the liquid curtain.)

Further examples of the VF(0) branch of flows are given in figure 42. The photographs shown in figures 42 (*b–d*) are different views of the same flow: (*b*) is a side view showing how the meniscus attached to the plate and (*d*) indicates the shape of the meniscus line on the end of the plate; the way the meniscus attached to the plate

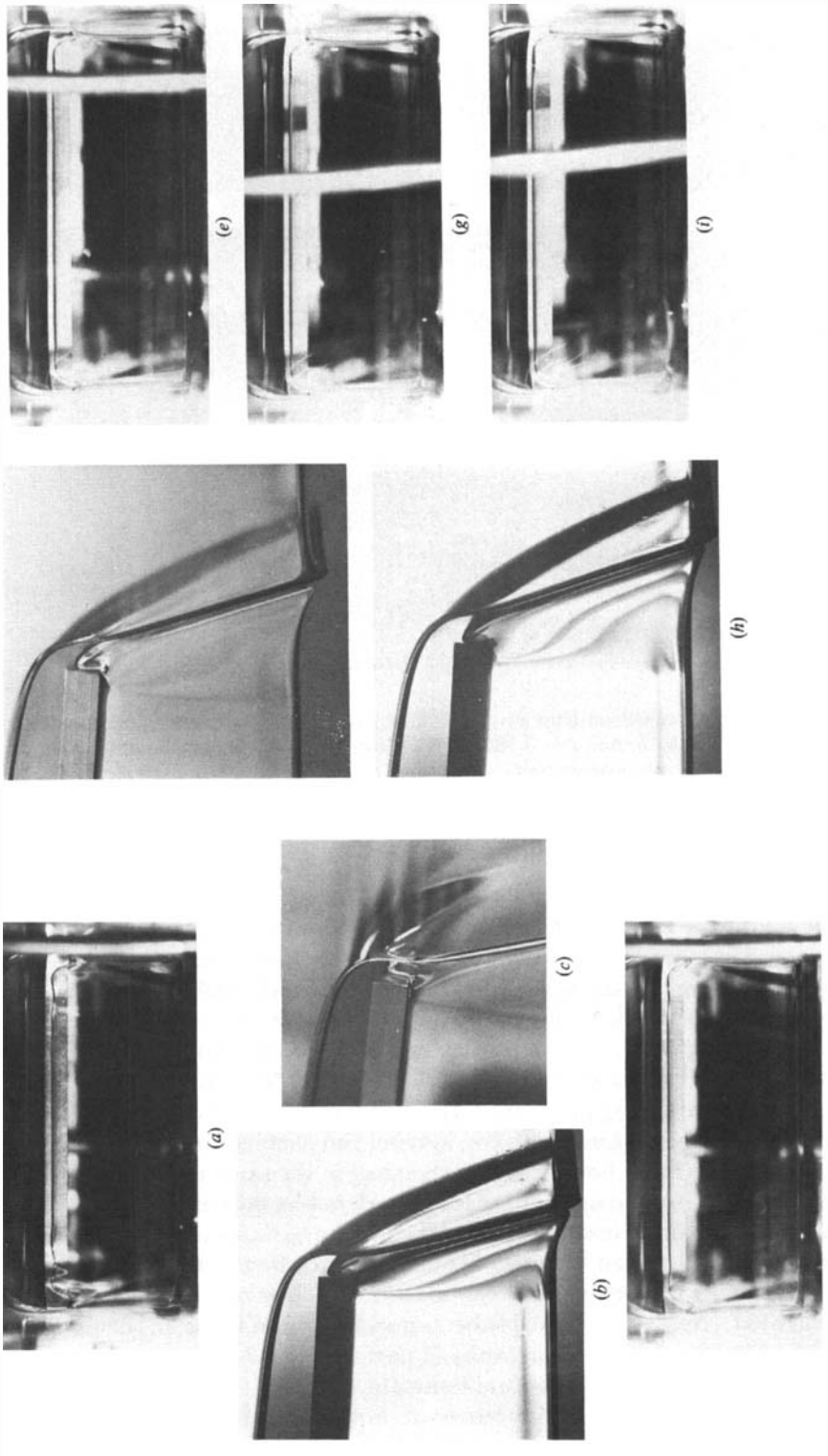

FIGURE 42. Examples from the branch of steady (VF(0)) flows. (*a*) End view at $R = 27.3$, $S = 2.00$, $h = 8.63$ mm, $\nu = 0.753$ St; (*b*) side view, (*c*) oblique view showing the contact line near the junction between the plate and the sidewall, and (*d*) end view, all at: $R = 29.7$, $S = 1.93$, $h = 8.77$ mm, $\nu = 0.740$ St; (*e*) end view at $R = 31.1$, $S = 1.87$, $h = 8.91$ mm, $\nu = 0.740$ St; (*f*) side view and (*g*) end view at: $R = 34.0$, $S = 1.78$, $h = 9.14$ mm, $\nu = 0.735$ St; (*h*) side view and (*i*) end view at: $R = 36.8$, $S = 1.69$, $h = 9.37$ mm, $\nu = 0.734$ St.

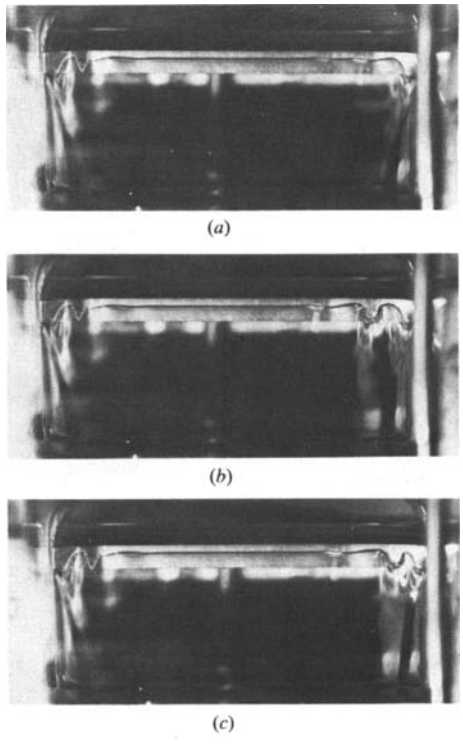

FIGURE 43. A sequence of photographs illustrating the unsteady (VF(0, 1)) flow at $R = 26.9$, $S = 2.01$, $h = 8.59$ mm, $\nu = 0.754$ St. (*a*) No corrugations present; (*b*) one corrugation present; (*c*) the corrugation in (*b*) has moved towards the sidewall.

in the zone near the sidewalls of the reservoir is indicated in (*c*), where it is seen that the attachment line of the free surface passed from the end face of the plate to its lower face. As the flow rate was increased this transition point moved closer to the sidewalls (cf. figure 42*e*, *g*, *i*).

Whereas for (LF2) flows the falling curtain was nearly vertical (cf. figure 40), it extended, in the case of (VF) flows, well beyond the end of the plate. The location of the meniscus on the sidewall of the reservoir is evident in figure 42(*b*), and the spatial location of the curtain near the central region of the channel is indicated by the dark band at the front of the photographs (cf. also figure 42(*f*) taken under different lighting conditions). Thus, the curtain was quite strongly curved in the regions near the walls of the reservoir.

At the smaller flow rates associated with this branch of flows the meniscus line on the end of the plate rose to a maximum height and then dropped slightly to a local minimum (cf. figure 42(*a*), where there is also evidence, on the left-hand half of the plate, of a second pair of local extrema). As the flow rate was increased this local minimum became less pronounced and in figure 42(*i*) is nearly indiscernible. The flow shown in figure 42(*i*) was at the maximum flow rate achievable with the pump used for these experiments.

Following the loss of stability of the (LF2) flows and the formation of a (VF(0)) flow, the flow rate could then be reduced with the (VF(0)) flow maintaining stability. In one experiment, for example, the (VF(0)) flow formed at $R = 28.0$, $S = 1.95$,

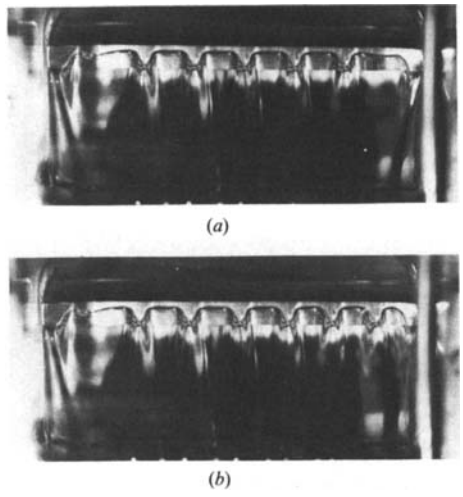

(a)

(b)

FIGURE 44. An example of the unsteady (VF(5, 6)) flow at $R = 26.0$, $S = 2.06$, $h = 8.50$ mm, $\nu = 0.754$ St. (a) Showing five corrugations; (b) showing six corrugations.

$h = 8.74$ mm, $\nu = 0.758$ St, and this branch of flows was stable on reduction of the flow rate until $R = 27.0$, $S = 2.01$, $h = 8.59$ mm, $\nu = 0.752$ St, at which stage a different kind of (VF) motion developed. Another realization of the same sequence is illustrated in figures 42 and 43: the flow shown in figure 42 (a) was near the stability margin for (VF(0)) flows and a small reduction in flow rate led to the unsteady (VF(0, 1)) flow shown in figure 43. The latter flow is so designated because, as shown in figure 43 (a), at a certain phase of the motion the meniscus line on the endplate was free of corrugations, whereas at a later phase the meniscus line developed a single corrugation near the right-hand wall of the reservoir (see figure 43b). This corrugation then moved towards the side wall, as shown in figure 43 (c), eventually losing its identity and allowing the pattern shown in (a) to re-establish itself. The overall motion was nearly periodic in time, on a timescale of about 8 s.

As the flow rate was reduced the (VF(0, 1)) flow persisted until the conditions were such that $R = 26.0$, $S = 2.06$, $h = 8.50$ mm, $\nu = 0.754$ St, at which stage the flow illustrated in figure 44 developed. This, too, was a nearly periodic motion involving either five or six corrugations and will be referred to as a (VF(5, 6)) flow. That phase of the motion where there were five corrugations is illustrated in figure 44 (a) and the phase involving six corrugations is illustrated in figure 44 (b). It is seen that the sixth corrugation formed at the right-hand side of the pattern. Once it had formed, the new corrugation moved slowly towards the right-hand wall of the reservoir, losing its identity when it reached the sharp gradient of the meniscus line near the wall. The approximate period of this motion was about 40 s and it was observed for approximately 16 minutes before the flow rate was changed. (Note that the corrugating of the free surface increases the mean curvature, enabling it to support a greater load than would otherwise be possible.) The presence of the corrugations caused the upper and lower surfaces of the liquid curtain to become wrinkled, some of which structure can be seen in figure 44 from reflections from the free surface (and cf. figure 42 where the free surface was much less wrinkled).

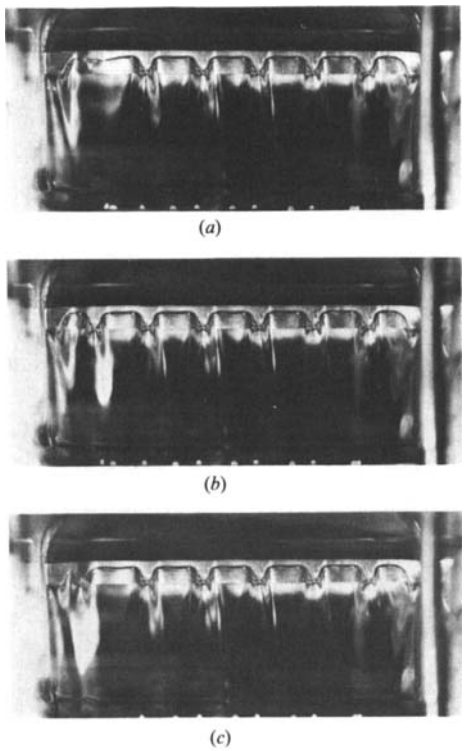

FIGURE 45. An unsteady (VF(6, 5)) flow at $R = 25.6$, $S = 2.09$, $h = 8.43$ mm, $\nu = 0.751$ St. (*a*) Showing five corrugations; (*b*) a sixth corrugation has formed near the left-hand wall; (*c*) the sixth corrugation has nearly disappeared at the left-hand side.

A small reduction in the flow rate from that obtaining for figure 44, giving operating conditions of $R = 25.6, S = 2.09, h = 8.43$ mm, $\nu = 0.751$ St, initiated a change of flow structure to the (VF(6, 5)) flow illustrated in figure 45. As for the (VF(5, 6)) flow this motion also was nearly periodic in time, but the approximate period was much smaller, taking a value of about 4 s. In addition the sixth corrugation now formed on the left-hand side of the pattern (cf. figure 45*a*, *b*) and proceeded leftwards (cf. figure 45*c*), losing its identity near the left-hand wall. The flow shown in figure 45 was observed for 20 minutes before the flow rate was reduced. Further small reductions in the flow rate had little effect on the general features of the flow illustrated in figure 45, except that the 'period' of the motion increased slightly, reaching a value of about 6 s when $R = 24.6$, $S = 2.18$, $h = 8.25$ mm, $\nu = 0.741$ St. Then a small reduction in flow rate, to the conditions $R = 24.3$, $S = 2.21$, $h = 8.21$ mm, $\nu = 0.741$ St, increased the 'period' of the motion to a value of about 40 s. With a further small reduction in flow rate, such that $R = 23.9$, $S = 2.23$, $h = 8.16$ mm, $\nu = 0.740$ St, the 'period' increased to around 100 s and the sixth corrugation seemed to have considerable difficulty in forming: the meniscus line 'dimpled' as though the corrugation would form, but it did not and the line straightened out again; however, after about 30 to 40 such attempts the sixth corrugation would finally become established and then it would translate slowly towards the left-hand wall.

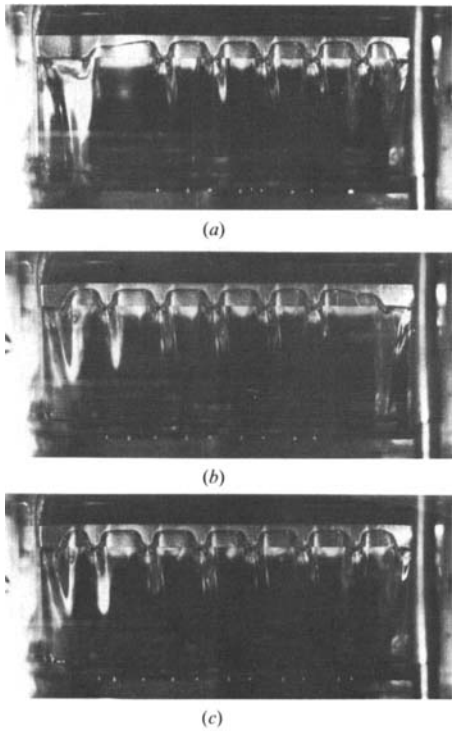

FIGURE 46. An unsteady (VF) flow at $R = 23.7$, $S = 2.25$, $h = 8.12$ mm, $\nu = 0.738$ St. (*a*) Five corrugations accumulated near the right-hand wall; (*b*) five corrugations accumulated near the left-hand wall; (*c*) a phase when six corrugations were present.

When the flow rate was then reduced to a value such that $R = 23.7$, $S = 2.25$, $h = 8.12$ mm, $\nu = 0.738$ St, a qualitative change occurred in the flow structure, as indicated in figure 46. In this flow a new corrugation would develop near one wall and the corrugation near the opposite wall would 'slip away'. So, for example, a new corrugation would form in the long, flat section of the meniscus line on the left-hand side of figure 46(*a*) and a corrugation would slip off the right-hand side leaving a pattern of the kind shown in figure 46(*b*). Figure 46(*c*) shows an intermediate stage where a new corrugation has formed on the right, and the corrugation at the extreme left is in the process of 'slipping away'. Unfortunately I observed this flow only for a 20 minute period and, on reflection, it is feasible that eventually it might have evolved into another kind of motion.

A further small reduction in flow rate brought about another structural change with the flow settling into a steady (VF(5)) motion. The evolution to this state is depicted in figure 47: first a corrugation 'slipped away' at the right, as shown in figure 47(*a*, *b*); at this stage it seemed (cf. figure 47*c*) as though the vertical-face structure would collapse in favour of a lower-face flow; but, as seen in figure 47(*d*), a fifth corrugation developed and eventually the pattern equilibrated itself forming the steady motion seen in (*e*). (A side view of this particular flow has already been shown in figure 4(*d*).) An interesting feature of the steady (VF(5)) patterns was that the meniscus line at

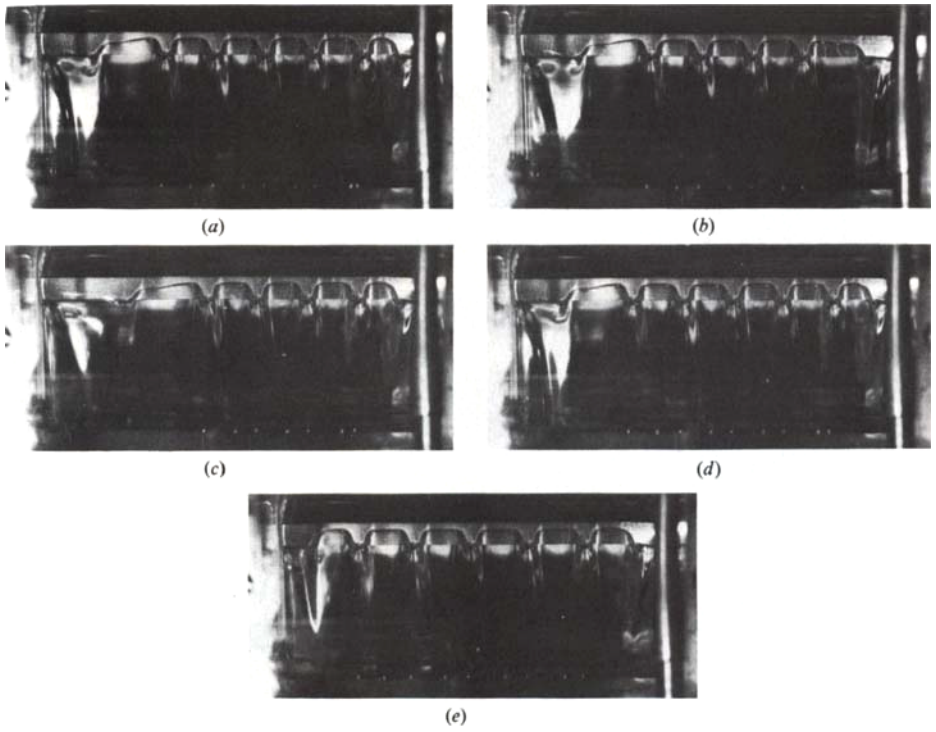

FIGURE 47. A sequence showing the transition to a steady (VF(5)) flow at $R = 23.3$, $S = 2.29$, $h = 8.05$ mm, $\nu = 0.735$ St. (*a*) Five corrugations accumulated near the right-hand wall; (*b*) photograph 60 s after (*a*) with only four corrugations; (*c*) photograph 140 s after (*b*) with four corrugations present; (*d*) a photograph 30 s after (*c*) showing a new, fifth corrugation; (*e*) the steady five-corrugated flow.

the troughs of the corrugations passed round the lower corner onto the underside of the plate, giving the appearance of a buttressing of the rear face of the liquid sheet. The branch of steady (VF(5)) flows was stable to further reductions of the flow rate until the conditions $R = 21.5, S = 2.33, h = 7.98$ mm, $\nu = 0.754$ St were reached. The steady (VF(5)) flow was observed for about 15 minutes at this setting, and appeared to be stable, but a further small reduction in flow rate brought about a loss of stability of the flow and the eventual formation of a steady (LF2) flow. The evolution to the (LF2) flow was a slow process, taking over 1 hour to complete. Shortly after the flow rate was changed, a corrugation 'slipped off' the left-hand side of the pattern, leaving a flow of the form shown in figure 48(*a*), with five 'lobes' of air protruding onto the end face. Then each of the end lobes disappeared and the three remaining air pockets spread sideways (see figure 48*b*). Eventually the extreme right-hand lobe disappeared, leaving the pattern shown in figure 48(*c*) and then the flow quickly reverted to the lower-face flow shown in figure 48(*d*).

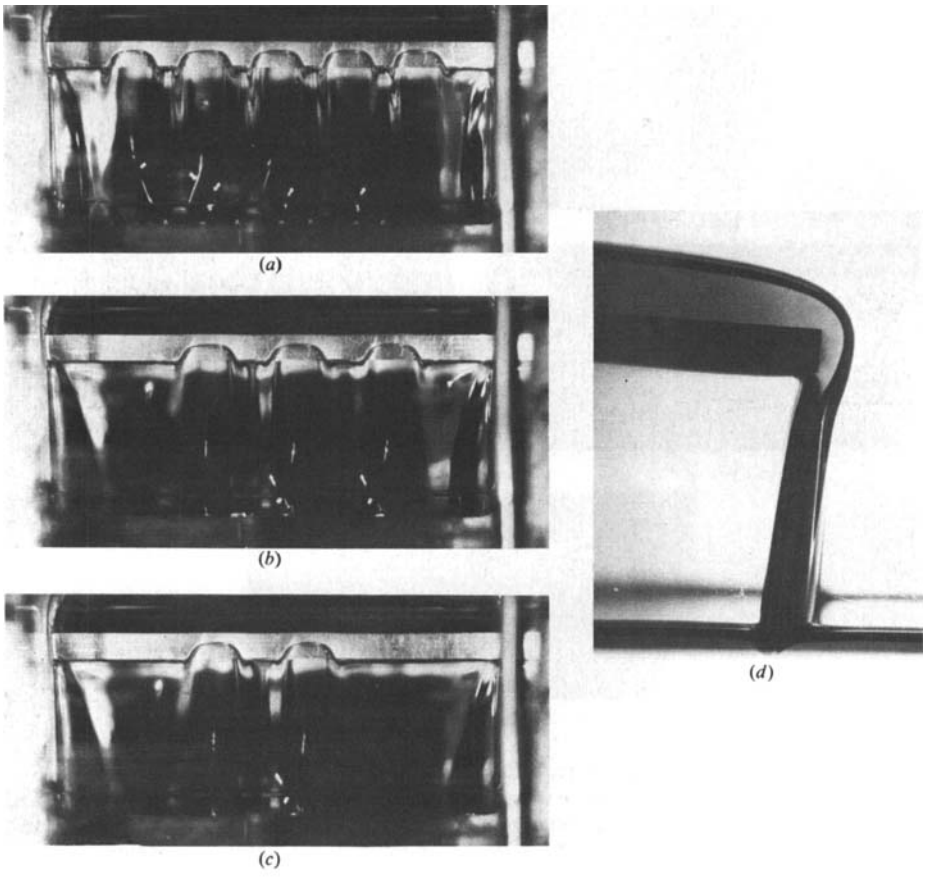

FIGURE 48. A sequence showing the transition from a (VF) flow to an (LF2) flow at $R = 20.8$, $S = 2.37$, $h = 7.92$ mm, $\nu = 0.758$ St. (*a*) Five lobes present; (*b*) photograph 15 minutes after (*a*) showing three lobes; (*c*) photograph 47 min after (*b*) showing two lobes; (*d*) photograph 1 min after (*c*) showing the (LF2) flow.

5. Comments

(i) No attempt has been made here to provide a mathematical description of the observed phenomena and, in general, this would appear to be a daunting task. It may, however, be possible to give a mathematical account of some of the phenomena by studying a related abstraction of the more complete model outlined in §3. For example, the main characteristics of the steady (VF(0)) flow, in the zone near the centre of the channel, should be well represented by a two-dimensional abstraction of the more complete model. In particular, the apparent uniqueness of the (VF(0)) flow at the larger flow rates of the experiment suggests that such a model could have considerable relevance to the observed flow. Moreover, should such a flow exist, it would be interesting to examine its stability properties with decreasing flow rate, to look for bifurcation to a spatially periodic flow similar to the 'corrugated' flows described above.

(ii) The experiments suggested that, at sufficiently small flow rates, all the observed motions were time dependent. It was only at larger flow rates that steady

motions were observed. This suggests the theoretical question of whether there are any steady flows in the limit that obtains as the flow rate is reduced to zero.

(iii) Many unsteady flows were observed, of which a large proportion were nearly periodic in time.

Some of these were the 'drip flows' found at the smaller flow rates. These flows had the appearance of a basic periodic motion, modulated over a larger timescale because the period for droplet formation differed slightly from site to site. For the 'periodic' part of this motion it seemed empirically as though the relative phase of formation of the droplets could be fixed in any desired order and, moreover, it seemed as though the phase at one drip site could take any value within some interval, relative to that at another site.

Note that a mathematical representation of the dripping process involves the consideration not only of domains which are time dependent, but also of domains whose connectivity is a function of time.

Many of the 'corrugated' (VF) flows had a nearly periodic structure in time. The time-dependent properties of these flows seemed to be intimately linked to the presence of the sidewalls of the reservoir, since any asymmetries in the pattern of corrugations meant an unbalanced distribution of surface-tension forces, resulting in one of the corrugations moving to a sidewall and losing its identity. The only corrugated flow that appeared to be steady was the one in which the meniscus line extended to the underside of the plate at the trough of each of the corrugations.

(iv) No attempt was made in this work to study the dependence of the flows on changes of the geometric parameters a, b, d and α. It was, however, evident in the course of the experiments that the flow structures were strongly dependent on d, the distance of the plate above the free-surface level in the reservoir.

(v) At sufficiently large flux rates there is a potential long-wave instability of the free surface in the main channel. Theoretically (e.g. see Yih 1969, p. 502) this is possible at flow rates such that $R \geqslant \frac{5}{6}\cot\alpha$, i.e. when R exceeded approximately 11.3 for the channel slope used in the present experiments. Thus, any unsteadiness in the approaching flow from this source would have influenced only the (LF2) flows and the vertical-face flows. Moreover, from monitoring the depth of the stream, the influence of this instability was not noticeably evident above the level of the depth variations observed at much smaller flow rates.

(vi) Several of the observed unsteady flows had a temporal structure much less regular than the nearly periodic flows mentioned above in (iii). They all had a certain recurrence property associated with them, but the period of the 'cycle' could be dramatically different from cycle to cycle, and the motion realized during one cycle often differed significantly from that which evolved during the next cycle. Nevertheless, the flow would eventually return to a structure that appeared to be only marginally unstable. In some cases, (e.g. the (T), (C+T), ... flows) the recurring structure was one for which, at slightly different parameter settings, there was a steady, stable flow. Thus, the question arises as to whether or not the related mathematical problem, subject to steady flux conditions, has unsteady solutions of the kind observed experimentally. For it is quite conceivable that, near the margin of stability of a flow, temporal imperfections could move the flow parameters back and forth between the basin of attraction of one steady solution and that of another, resulting in a forced unsteady motion, driven by imperfections in the boundary data. Whatever the source was for these unsteady flows they would appear to be of considerable importance, for such unsteadiness could well arise in other flow situations where there is a large degree of multiplicity. Note that several of the

observed unsteady flows (e.g. the (TCT), (TCTC), ... flows) apparently had no associated steady 'base' patterns; and one of these flows, namely the (TCT) flow, lost stability to yet another unsteady motion.

I am greatly indebted to Mr J. K. Bartington for constructing the apparatus, for much helpful advice during the course of the experiment, and for printing all the photographs.

This work was sponsored by the United States Army under Contract No. DAAG29-80-C-0041.

REFERENCES

CUVELIER, C. 1981 On the numerical solution of a capillary free boundary problem governed by the Navier–Stokes equations. *Seventh Intl Conf. on Num. Methods in Fluid Dynamics* (ed. W. C. Reynolds & R. W. MacCormack). Lecture Notes in Physics, vol. 141. Springer.

DUTTA, A. & RYAN, E. 1982 Dynamics of a creeping Newtonian jet with gravity and surface tension: a finite difference technique for solving steady free-surface flows using orthogonal curvilinear coordinates. *AIChE J.* **28**, 220.

JEAN, M. 1980 Free surface of the steady flow of a Newtonian fluid in a finite channel. *Arch. Rat. Mech. Anal.* **74**, 197.

JEAN, M. & PRITCHARD, W. G. 1980 The flow of fluids from nozzles at small Reynolds numbers. *Proc. R. Soc. Lond.* A **370**, 61.

KISTLER, S. 1983 The fluid mechanics of certain coating and related viscous free-surface flows with contact lines. Ph.D. dissertation, University of Minnesota.

NICKELL, R. E., TANNER, R. I. & CASWELL, B. 1974 The solution of viscous incompressible jet and free-surface flows using finite-element methods. *J. Fluid Mech.* **65**, 189.

OMODEI, B. J. 1980 On the die swell of an axisymmetric Newtonian jet. *Computers and Fluids* **8**, 275.

SAITO, H. & SCRIVEN, L. E. 1981 Study of coating flow by the finite element method. *J. Comp. Phys.* **42**, 53.

SILLIMAN, W. J. & SCRIVEN, L. E. 1978 Slip of liquid inside a channel exit. *Phys. Fluids* **21**, 2115.

SOLONNIKOV, V. A. 1980 Solvability of a problem on the plane motion of a heavy viscous incompressible capillary liquid partially filling a container. *Math. USSR Izvestia* **14**, 193.

TANNER, R. I., LAM, H. & BUSH, M. B. 1984 On the separation of viscous jets. *Phys. Fluids* **28**, 23.

YIH, C.-S. 1969 *Fluid Mechanics: A Concise Introduction to the Theory.* McGraw-Hill.